FLORIDA DEPARTMENT OF TRANSPORTATION

BRIDGE SCOUR MANUAL

MAY 2005

TABLE OF CONTENTS

TABLE OF CONTENTS i

LIST OF FIGURES iii

LIST OF TABLES vi

LIST OF SYMBOLS vii

UNITS CONVERSION TABLE xi

CHAPTER 1 INTRODUCTION 1-1

CHAPTER 2 BRIDGE SCOUR 2-1
2.1. General Scour 2-2
2.2. Long Term Aggradation and Degradation 2-5
2.3. Contraction Scour 2-5
2.3.1 Steady, uniform flows 2-7
2.3.1.1. Live bed contraction scour equation 2-7
2.3.1.2. Clear water contraction scour equation 2-9
2.3.2 Unsteady, complex flows 2-10
2.4. Bed Forms 2-10
2.5. Local Scour 2-13

CHAPTER 3 LOCAL SCOUR AT A SINGLE PILE 3-1
3.1. Introduction 3-1
3.2. Description of the Flow Field Around a Single Pile 3-1
3.3. Equilibrium Scour Depths in Steady Flows 3-3

CHAPTER 4 SCOUR AT PIERS WITH COMPLEX GEOMETRIES 4-1
4.1. Introduction 4-1
4.2. Methodology for Estimating Local Scour Depths at Complex Piers 4-1
4.2.1 Complex Pier Local Scour Depth Prediction - Case 1 Piers (Pile Cap above the Bed) 4-6
4.2.1.1. Effective Diameter of the Column 4-6
4.2.1.2. Effective Diameter of Pile Cap 4-10
4.2.1.3. Effective Diameter of the Pile Group 4-11
4.2.1.4. Equilibrium Local Scour Depth at a Case 1 Complex Pier 4-16
4.2.1.5. Case 1 Example Problem 4-16
4.2.2 Complex Pier Local Scour Depth Prediction - Case 2 Piers (Partially Buried Pile Cap) 4-23
4.2.2.1. Effective Diameter of the Column 4-23
4.2.2.2. Effective Diameter of the Pile Cap 4-25
4.2.2.3. Effective Diameter of the Pile Group 4-30
4.2.2.4. Complex Pier Effective Diameter 4-32

4.2.2.5. Equilibrium Local Scour Depth at a Case 2 Complex Pier 4-33
4.2.2.6. Case 2 Example Problem 4-33
4.2.3.....Complex Pier Local Scour Depth Prediction - Case 3 Piers (Fully Buried Pile Cap) 4-42
4.2.3.1. Effective Diameter of the Column 4-42
4.2.3.2. Effective Diameter of the Pile Cap 4-44
4.2.3.3. Effective Diameter of the Pile Group 4-50
4.2.3.4. Complex Pier Effective Diameter 4-52
4.2.3.5. Equilibrium Local Scour Depth at a Case 3 Complex Pier 4-53
4.2.3.6. Case 3 Example Problem 4-53
4.3. Predicted versus Measured Laboratory Data 4-67
4.3.1.....Laboratory Experiments 4-67
4.3.1.1. Jones' Experiments 4-67
4.3.1.2. Coleman's Experiments 4-70
4.3.1.3. Sheppard's Experiments 4-76

CHAPTER 5 CONSERVATISM IN APPROACH TO SCOUR ESTIMATION..... 5-1
5.1. Sediment Size Distribution 5-1
5.2. Fine Sediment Suspensions 5-2
5.3. Time Dependency of Local Scour 5-2
5.4. Geometric Considerations 5-3

BIBLIOGRAPHY B-1

LIST OF FIGURES

Figure 1-1 Effects of Local Scour on a Bridge Pier 1-3

Figure 2-1 Aerial view of the Lower Mississippi River 2-3

Figure 2-2 Ft. George Inlet 1992 2-3

Figure 2-3 Ft. George Inlet 1994 2-4

Figure 2-4 Ft. George Inlet 1998 2-4

Figure 2-5 Two manmade features that create a contracted section in a channel. 2-6

Figure 2-6 An example of manmade causeway islands that create a channel contraction..... 2-6

Figure 2-7 Fall Velocity of Sediment Particles having Specific Gravity of 2.65 (taken from HEC-18, 2001) 2-9

Figure 2-8 Critical bed shear stress as a function of sediment particle diameter, Shields (1936). 2-13

Figure 3-1 Schematics of the vortices around a cylinder 3-2

Figure 3-2 Equilibrium Scour Depth Dependence on the Aspect Ratio, y_0/ D^* (V/V_c =1 and D^*/D_{50} =46)..... 3-8

Figure 3-3 Equilibrium Scour Depth Dependence with Flow Intensity, V/V_c (for $y_0/D^*>3$ and constant values of D^*/D_{50})..... 3-8

Figure 3-4 Equilibrium Scour Depth Dependence on D^*/D_{50} for $y_0/ D^* > 3$ and V/V_c=1. 3-9

Figure 3-5 Predicted versus Measured Scour Depth (Equations 3.4-3.6). 3-11

Figure 3-6 Scour Depth Prediction using Measured Peak Tidal Flows at the West Channel Pier on the Existing Tacoma Narrows Bridge in Tacoma, Washington. 3-13

Figure 4-1 Complex pier configuration considered in this analysis. The pile cap can be located above the water, in the water column or below the bed... 4-2

Figure 4-2 Schematic drawing of a complex pier showing the 3 components, column, pile cap and pile group..... 4-3

Figure 4-3 Definition sketches for the effective diameters of the complex pier components, column (D^*_{col}), pile cap (D^*_{pc}) and pile group (D^*_{pg}). 4-4

Figure 4-4 Definition sketch for total effective diameter for a complex pier. 4-5

Figure 4-5 Examples of Case 1, Case 2 and Case 3 Complex Piers. 4-5

Figure 4-6 Nomenclature definition sketch. 4-6

Figure 4-7 Graph of K_f versus f/b_{col} for the column. 4-8

Figure 4-8 Graph of effective diameter of the column versus $H_{col}/y_{o(max)}$. 4-9

Figure 4-9 Graph of normalized pile cap effective diameter. 4-11

Figure 4-10 Diagram illustrating the projected width of a pile group, W_p. 4-13

Figure 4-11 Graph of K_h versus $H_{pg}/y_{0(max)}$. 4-15

Figure 4-12 Elevation and plan view of the complex pier used in the Case 1 example scour calculation. 4-16

Figure 4-13 The Projected Width of the Pile Group. 4-21

Figure 4-14 Definition sketch for T' and H'_{pc} 4-26

Figure 4-15 Definition sketch showing datum for pile group effective diameter, D^*_{pg} , computations. 4-30

Figure 4-16 Elevation and plan view of the complex pier used in the Case 2 example scour calculation 4-34

Figure 4-17 The Projected Width of the Pile Group. 4-39

Figure 4-18 Graph of the A coefficient in Equation 4.64 4-46

Figure 4-19 Graph of the B coefficient in Equation 4.64 4-46

Figure 4-20 Graph of the buried pile cap's coefficient, $K_{bpc.}$ 4-46

Figure 4-21 Elevation and plan view of the complex pier used in the Case 3 example scour calculation 4-54

Figure 4-22 The Projected Width of the Pile Group. 4-64

Figure 4-23 Structures used in Sterling Jones' experiments. 4-68

Figure 4-24 Position of the structures in Sterling Jones' experiments. 4-68

Figure 4-25 Scour predictions of Jones' laboratory complex pier local scour experiments using the current scour prediction procedures (HEC-18) and using the revised procedures (UF). 4-70

Figure 4-26 Plan and elevation view of model complex pier 1 (Type A, All dimensions are in feet). 4-71

Figure 4-27 Plan and elevation view of model complex pier 2 (Type B, All dimensions are in feet). 4-71

Figure 4-28 Plan and elevation view of model complex pier 3 (Type C, All dimensions are in feet). 4-71

Figure 4-29 Scour predictions of laboratory complex pier local scour experiments (non-buried complex piers) using the current scour prediction procedures (HEC-18) and using the revised procedures (UF). 4-74

Figure 4-30 Scour predictions of laboratory buried or partially buried complex pier local scour experiments using the current scour prediction procedures (HEC-18) and using the revised procedures (UF). 4-75

Figure 4-31 Position of the piers in Sheppard's experiments. 4-76

Figure 4-32 Scour predictions of Sheppards' laboratory complex pier local scour experiments using the current scour prediction procedures (HEC-18) and using the revised procedures (UF). 4-77

Figure 5-1 Effects of sediment size distribution, σ, on equilibrium scour depths..... 5-2

LIST OF TABLES

Table 2-1 Determination of Exponent, K_1 2-8

Table 2-2 Bed Classification for determining Bed Forms 2-11

Table 2-3 Bed Form Length and Height (van Rijn, 1993) 2-12

Table 3-1 Effective Diameters for Common Structure Cross-sections. 3-6

Table 4-1 Flow and sediment inputs for the example calculation. 4-17

Table 4-2 Flow and sediment inputs for the example calculation. 4-34

Table 4-3 Flow and sediment inputs for the example calculation. 4-53

Table 4-4 Flow conditions for Jones' experiments. 4-69

Table 4-5 Pier information for Jones' experiments. 4-69

Table 4-6 Flow conditions during the laboratory scour experiments. 4-72

Table 4-7 Scale model geometrical information for the laboratory scour experiments. 4-73

Table 4-8 Flow conditions for Sheppard's experiments. 4-76

Table 4-9 Pier information for Sheppard's experiments. 4-77

LIST OF SYMBOLS

b	pile width (diameter)
b_{col}	column width
b_m	model pile width
b_p	prototype pile width
b_{pc}	pile cap width
d^*	dimensionless particle diameter
D^*_{col}	effective diameter of the column
$D^*_{col(min)}$	minimum value for the column effective diameter when the base of the column is buried
$D^*_{col(max)}$	maximum value for the column effective diameter when the base of the column is buried
$D^*_{col(f)}$	attenuated effective diameter for the column
D^*_m	effective diameter of the model pier tested
D^*_p	effective diameter of the prototype pier
D^*_{pc}	effective diameter of the pile cap
D^*_{pg}	effective diameter of the pile group
D_{16}	sediment size for which 16 percent of bed material is finer
D_{50}	median sediment diameter
D_{84}	sediment size for which 84 percent of bed material is finer
D_{90}	sediment size for which 90 percent of bed material is finer
f	weighted average value for the pile cap extension, $(3f_1+f_2)/4$
f_1	distance between the leading edge of the column and the leading edge of the pile cap
f_2	distance between the side edge of the column and the side edge of the pile cap

Fr	Froude number, $V / \sqrt{gy_0}$
Fr_c	critical Froude number = $V_c / \sqrt{gy_0}$
g	acceleration of gravity = 32.17 ft/s^2
H_{col}	distance between the bed (adjusted for general scour, aggradation/degradation, and contraction scour) and the bottom of the column
H_{pc}	distance between the bed (adjusted for general scour, aggradation/degradation, contraction scour, and column scour) and the bottom of the pile cap
H'_{pc}	distance from the original bed and the sand water interface
H_{pg}	distance between the bed (adjusted for general scour, aggradation/degradation, contraction scour, column scour, and pile cap scour) and the top of the pile group
$\bar{H}_{pg}$	distance from the bed to the top of the pile group after adjusting the bed for the scour caused by the column and pile cap, $y_{s(col+pc)}$
k	bed roughness height
K_{bpc}	buried pile cap attenuation coefficient
K_{bpg}	buried pile group attenuation coefficient
K_{cp}	peak value of normalized clearwater scour depth
K_d	sediment-size factor
K_h	coefficient that accounts for the height of the pile group above the adjusted bed
K_I	flow intensity factor
K_{lp}	dimensionless scour depth magnitude at the live bed peak scour
K_m	number of piles in the direction of unskewed flow
K_s	shape factor
K_{sp}	pile spacing coefficient
$K_{s(pile)}$	individual pile group pile shape factor
$K_{s(pile\ group)}$	pile group shape factor

K_1	factor for shape of pier nose
K_2	factor for angle of attack of flow
K_α	flow skew angle coefficient
K_σ	factor for the gradation of sediment
L	length of pier
l_{col}	column length
L_m	model scale length
L_p	prototype scale length
l_{pc}	pile cap length
q	discharge per unit width
RR	relative roughness of the bed, k/D_{50}
Re_p	pier Reynolds number, $Vb\rho/\mu$
s	distance between centerlines of adjacent piles in a pile group
s_m	distance between centerlines of adjacent piles in line with the flow in a pile group
s_n	distance between centerlines of adjacent piles perpendicular to the flow in a pile group
sg	ratio of sediment density to the density of water ρ_s/ρ
T	pile cap thickness
T'	exposed pile cap thickness
T_r	dimensionless parameter in van Rijn's bed form equations
T_{90}	time required to reach 90% of the equilibrium scour depth
V	mean depth averaged velocity
V_c	critical depth averaged velocity
V_{lp}	depth averaged velocity at the live bed peak scour depth
V_0	depth averaged velocity upstream of the pier

W_p	projected width of the piles in the pile group
W_{pi}	projected width of a single unobstructed pile
$y_{o(max)}$	limiting value for the effective diameter calculation
y_s	equilibrium scour depth
$y_{s\,m}$	model equilibrium scour depth
$y_{s\,p}$	prototype equilibrium scour depth
$y_{s(col)}$	scour due to the column in a complex pier
$y_{s(pc)}$	scour due to the pile cap in a complex pier
$y_{s(pg)}$	scour due to the pile group in a complex pier
y_o	water depth adjusted for general scour, aggradation/degradation, and contraction scour
$\overline{y}_o$	water depth adjusted for general scour, aggradation/degradation, contraction scour and scour caused by the column and pile cap, $y_{s(col+pc)}$
α	flow skew angle in degrees
μ	dynamic viscosity of water
ν	kinematic viscosity of water
ρ	mass density of water
ρ_s	mass density of sediment
σ	measure of the gradation of sediment, $\sqrt{D_{84} / D_{16}}$
τ	bed shear stress
τ_c	critical bed shear stress
τ_u	upstream bed shear stress
τ_0	maximum bed shear stress in local scour hole
ϕ	factor for pier shape
$\equiv$	symbol for “identically equal to” (or “defined as”)

UNITS CONVERSION TABLE

1 meter (m) = 3.28 ft

1 Newton (N) = 1 x 10^5 dynes = 0.22481 pounds force (lb_f)

1 Pascal (Pa) = 1 N/m^2 = 1.45 x 10^{-4} lb_f/in^2

1 kilometer (km) = 1000 m = 3280.83 ft = 0.62137 statute miles (miles)

1 m/s = 3.28 ft/s = 1.9438 (nautical miles/hr (knots) = 2.2369 miles/hr

1 watt = 1.341 x 10^{-3} horsepower (hp)

1 poise = 1 stoke = 1 gm/(cm s) = 6.7197 x 10^{-2} lb_m/ft s = 2.0886 x 10^{-3} slugs/ft s

1 kg/m^3 = 1 x 10^{-3} gm/cm^2 = 6.249 x 10^{-2} pounds mass/ft^3 (lb_m/ft^3)

= 1.942 x 10^{-3} slugs/ft^3

CHAPTER 1 INTRODUCTION

The lowering of the streambed at bridge piers is referred to as bridge sediment scour or simply bridge scour. Bridge scour is the biggest cause of bridge failure in the United States and a major factor that contributes to the total construction and maintenance costs of bridges in the United States. Under prediction of design scour depths can result in costly bridge failures and possibly in the loss of lives; while over prediction can result in wasting millions of dollars on a single bridge. For these reasons, proper prediction of the amount of scour anticipated at a bridge crossing during design conditions is essential.

Sediment scour occurs when the amount of sediment transport leaving an area is greater then the amount of sediment entering the area. Sediment transport is divided into two categories: 1) bed load and 2) suspended load. Bed load refers to sediment particles that roll and slide in a thin layer, two sediment particle diameters, near the bed. Sediment particles suspended in the water column by turbulent fluctuations and transported with the flow is suspended load. Sediment movement is initiated when the forces acting on the particles reaches a threshold value that exceeds the forces keeping them at rest. Flows over a sediment bed exert lift and drag forces on the sediment particles. When these forces per unit area tangent to the bed (bed shear stress) exceed a critical value (critical shear stress) the sediment bed begins to move. For cohesionless sediments (e.g., sand), the critical shear stress depends on the mass density and viscosity of the water, the sediment mass density, the size and shape of the sediment particle, the bed roughness, and the local water velocity. For cohesive sediments (e.g., muds and clays) and erodible rock, additional water and sediment properties associated with the bonding of the particles also play a role. The local velocity of the water depends on many quantities including the sediment that forms the boundaries of the flow. A change in the sediment boundaries (e.g., deposition or erosion) results in a change in the flow and vice versa. Man-made or natural obstructions to the flow can also change flow patterns and create secondary flows. Any change in the flow can impact sediment transport and thus the scour at a bridge site.

For engineering purposes, sediment scour at bridge sites is normally divided into four categories: 1) general, 2) aggradation and degradation, 3) contraction and 4) local. Local scour is further divided into pier and abutment scour. General scour refers to mechanisms such as river meanders, tidal inlet instability, etc. Aggradation and degradation refer to the raising or lowering of the streambed due to changes taking place up and/or downstream of the bridge (i.e., an overall lowering or rising of the stream bed). Contraction scour results from a reduction in the channel cross-section at the bridge site. This reduction is usually attributed to the encroachment by the bridge abutments and/or the presence of large bridge piers (large relative to the channel cross-section). Local abutment scour results from the obstruction to the flow at the bridge abutments at the edges of the waterway. Local pier scour is likewise the result of a flow obstruction, but one located within the flow field. Figure 1-1 shows the effect of local scour on a bridge pier. An additional mechanism, bed form propagation through the bridge site, may also play a role. Bed forms refer to the pattern of regular or irregular waves that may result from water flow over a sediment bed. These forms may propagate either in the same or in the opposite direction of the flow. Since these undulations in the sediment bed may have large amplitudes, one must also take into account their contribution to the lowering of the bed near the bridge piles. Additionally, their presence contributes to the calculation of the overall roughness of the bed, and hence the vertical structure of the flow over the bed.

The main mechanisms of local scour are: (1) increased mean flow velocities and pressure gradients in the vicinity of the structure; (2) the creation of secondary flows in the form of vortices; and (3) the increased turbulence in the local flow field. Two kinds of vortices may occur: 1) wake vortices, downstream of the points of flow separation on the structure; and 2) horizontal vortices at the bed and free surface due to stagnation pressure variations along the face of the structure and flow separation at the edge of the scour hole. These phenomena, although relatively easy to observe, are difficult to quantify mathematically. Some researchers (Shen et al., 1969) have attempted to describe this complex flow field mathematically, but with little success. A number of numerical solutions have also been attempted, but again with limited success.

Local scour is divided into two different scour regimes that depend on the flow and sediment conditions upstream of the structure. **Clear-water scour** refers to the local scour that takes place under the conditions where sediment is not in motion on a flat bed upstream of the structure**.** If sediment upstream of the structure is in motion, then the local scour is called **live-bed scour**.

Figure 1-1 Effects of Local Scour on a Bridge Pier

Most scour prediction formulae, such as the Colorado State University (CSU) equation [currently used in the U.S. Federal Highway Administration (FHWA) Hydraulic Engineering Circular Number 18 (HEC-18)], and those published by Sheppard et al. (2004), Melville (2000), and Breusers (1977) are empirical and based on laboratory-scale data. Many of these equations yield similar results for laboratory-scale structures, but differ significantly in their predictions for prototype scale structures. The over prediction of many of these equations for large structures in fine sands is well documented and is referred to as the "Wide Pier" problem. Sheppard (2004) believes this problem results from the exclusion of the pier width to sediment diameter ratio in many of these

equations as well as to the wrong functional dependence of this parameter in those equations that do include it. He presents a possible explanation for why equilibrium scour depth depends on this ratio as well as why this dependence diminishes with increased values of this parameter. The limited field data that exist support his conclusions. Additionally, the field data confirm the functional relationship of this parameter in his equations, thus eliminating the "wide pier problem."

This manual is organized as follows. Chapter 2 discusses total scour at a bridge crossing as well as presents summaries of and references to more detailed treatments of general scour, aggradation/degradation and contraction scour. Chapter 3 details the calculation of local scour at a single simple structure under both clear-water and live-bed scour flow conditions. Chapter 4, outlines the procedure for calculation of local scour at bridge piers with complex geometries including those with buried or partially buried pile caps. Finally, Chapter 5 discusses the conservatism in the methods and equations presented in Chapters 3 and 4.

CHAPTER 2 BRIDGE SCOUR

When water flows through a bridge opening with sufficient velocity the bed, in general, will change in elevation. This change in elevation is more significant near the abutments and piers. The magnitude of these changes depends on many factors including the flow and sediment parameters, structure size and shape, local and global channel characteristics, etc. A net loss of sediment at the site is referred to as sediment scour or simply scour. Knowledge of the maximum scour that will occur at the abutments and piers during the life of the bridge is required for the design of the bridge foundation. Under prediction of these values could result in catastrophic failure and possible loss of life while over prediction can result in over design of the structure, and thus prove costly and economically inefficient. Accurate prediction of scour is therefore of the utmost importance. The methods and equations presented in this chapter are the result of 15 years of research on this topic at the University of Florida.

For analysis purposes, it is convenient to divide bridge scour into the following categories: 1) general scour, 2) long term aggradation/degradation, 3) contraction scour, and 4) local structure-induced pier and abutment scour. An additional mechanism, bed form propagation through the bridge site, may also play a role. The combined sum of all five components determines the total scour at a bridge pier or abutment. Even though most of these processes take place simultaneously, for purposes of local scour calculation, the equations presented herein were developed under the assumption that the first three categories plus bed form amplitudes have occurred prior to the start of local and abutment scour. **Therefore, general scour, aggradation/degradation, contraction scour and bedform amplitudes must be computed and the bed elevation adjusted prior to calculating local and abutment scour**. Sections 2.1 through 2.5 present outlines and summaries of procedures, equations, and methods used to analyze each of the scour components along with references to more detailed treatments of these topics.

2.1. General Scour

For the purposes of this document, general scour refers to the bed elevation changes that result from lateral instability of the waterway. This horizontal shifting is divided in two classes. Bridge sites are often classified according to the nature of the flows encountered. Sites that are far removed from the coasts where the flows are not significantly influenced by astronomical tides are referred to as "riverine" sites while those near the coast are called "tidal" sites. The flows at both sites are unsteady but, in general, the time scales of the temporal variation are significantly different in the two cases. Additionally, tidal flows often reverse flow direction. In the riverine environment, general scour refers to the natural meandering process as illustrated in Figure 2-1. Meanders in rivers result from transverse oscillation of the thalweg (the deepest part of the channel) within a straight channel. This oscillation initiates formation of self-perpetuating bends. Although the literature contains relatively little research regarding river meandering, observations indicate characteristics associated with flow in bends. These characteristics include: (1) super-elevation of the water at the outside of the bend, (2) strong downward currents causing potential erosion at the outside of the bend, (3) scour at the outside and deposition of sediment on the inside of the bend that moves the channel thalweg toward the outside of the bend, and (4) a spiral secondary current that directs the bottom current toward the inside of the bend. The overall effect of these mechanisms is to accentuate existing bends in rivers. If a bridge crossing is located near one of these meanders, the horizontal migration of the stream can result in an overall rising or lowering of the bed. Therefore this process is treated as a component of sediment scour. For more information on this topic the reader is referred to the US Federal Highway Administration's Hydraulic Engineering Circular Number 20 (HEC-20).

In coastal waters, tidal inlet instability is similar in that the channel migrates laterally to affect a change in bed elevation at piers located in the vicinity of the inlet. Unimproved inlets (inlets without jetties) are, in general, much less stable and are prone to larger and more frequent lateral shifts. Inlet stability depends on several variables including the magnitude and variability of longshore sediment transport, incident waves, the tidal prism, other inlets in the system, coastal structures in the vicinity, etc. Figure 2-2 through

Figure 2-4 contain aerials that illustrate channel migration at Ft. George Inlet in Jacksonville, Fl from 1992 to 1998. The channel cross section at the bridge has seen significant change over the six year period as seen in photographs. For more information on inlet instability the reader is referred to Dean and Dalrymple (2002).

Figure 2-1 Aerial view of the Lower Mississippi River

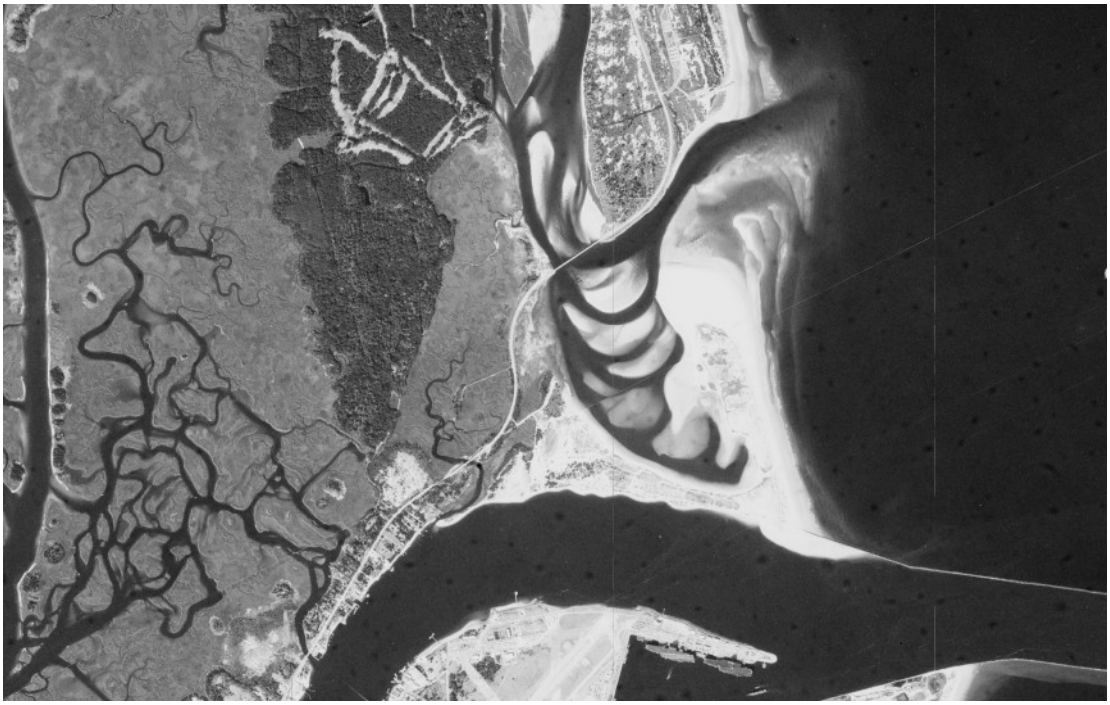

Figure 2-2 Ft. George Inlet 1992

Figure 2-3 Ft. George Inlet 1994

Figure 2-4 Ft. George Inlet 1998

2.2. Long Term Aggradation and Degradation

Whereas general scour refers to bed elevation changes that result from lateral instability, aggradation and degradation is associated with the overall vertical stability of the bed. Long term aggradation and degradation refers to the change in the bed elevation over time over an entire reach of the water body. For riverine conditions, manmade or natural changes in the system may produce erosion or deposition time over the entire reach of the water body. Anything that changes the sediment supply of a river reach can impact the bed elevation at the bridge site. Examples of these changes include the erection of a dam, changes in upland drainage basin characteristics (e.g., land use changes), upstream mining in the channel, etc. For information on aggradation/degradation in riverine environments, the reader is referred to the US Federal Highway Administration's Hydraulic Engineering Circular Number 18 and its references.

Similar processes exist in tidal waters. However, in general, prediction of these processes is more difficult due to the complex geometry of the flow boundaries, reversing flows, wave climate, etc. As with riverine locations, historical information about the site and the quantities that impact the sediment movement in the area are very useful in estimating future changes in bed elevation at the site. For more information refer to the US Army Corps of Engineers' Coastal Engineering Manual (2002).

2.3. Contraction Scour

Contraction scour occurs when a channel's cross-section is reduced by natural or manmade features. Possible constrictions include the construction of long causeways to reduce bridge lengths (and costs), the placement of large (relative to the channel cross-section) piers in the channel, abutment encroachment, and the presence of headlands (see Figure 2-5 and Figure 2-6). The reduction of cross sectional area results in an increase in flow velocity due to conservation of flow. This may cause the condition of more sediment leaving than entering the area and thus an overall lowering of the bed in the contracted area. This process is known as "contraction scour."

For design flow conditions that have long durations, such as those created by stormwater runoff in rivers and streams in relatively flat country, contraction scour can reach near equilibrium depths. Equilibrium conditions exist when the sediment leaving and entering a section of a stream are equal. Laursen's contraction scour prediction equations were developed for these conditions. A summary of Laursen's equations is presented below. For more information and discussion the reader is referred to HEC-18.

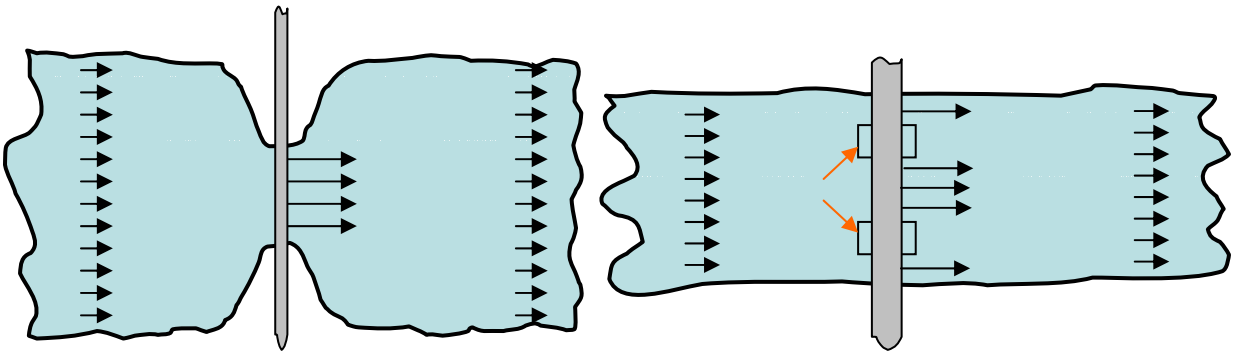

Figure 2-5 Two manmade features that create a contracted section in a channel.

Figure 2-6 An example of manmade causeway islands that create a channel contraction.

2.3.1. Steady, uniform flows

For steady, uniform flow situations one-dimensional computer flow models are usually adequate for estimating design flow velocities. If, in addition, the design flow event is of long duration, such as a riverine storm water runoff event in relatively flat terrain, equilibrium contraction scour equations can estimate design contraction scour depths. Laursen's contraction scour equations [Laursen (1960)] were developed for these situations. However, predictions using these equations tend to be conservative, even for long duration flows, since the rate of erosion decreases significantly with increased contraction scour depth. That is, unless the flow duration is extremely long, equilibrium depths are not achieved. Laursen developed different equations for clear-water and live-bed scour flow regimes. Both equations are designed for situations with relatively simple flow boundaries to facilitate determination of meaningful values for the terms in the equations. A brief summary of the equations are presented herein. The reader is referred to HEC-18 for more information.

2.3.1.1. Live bed contraction scour equation

The live-bed scour equation assumes that the upstream flow velocities are greater than the sediment critical velocity, V_c .

$$\frac{y_2}{y_1} = \left(\frac{Q_2}{Q_1}\right)^{\frac{6}{7}} \left(\frac{W_1}{W_2}\right)^{K_1} \qquad 2.1$$

$$y_s = y_2 - y_o = \text{average contraction scour} \qquad 2.2$$

where,

y_1	=	Average depth in the upstream channel, ft (m)
y_2	=	Average depth in the contracted section after scour, ft (m)
y_0	=	Average depth in the contracted section <u>before scour</u>, ft (m)
Q_1	=	Discharge in the upstream channel transporting sediment, ft^3/s (m^3/s)

Q_2 = Discharge in the contracted channel, ft^3/s (m^3/s)

W_1 = Bottom width of the main upstream channel that is transporting bed material, ft (m)

W_2 = Bottom width of the main channel in the contracted section less pier widths, ft (m)

K_1 = Exponent listed in Table 2-1 below

Table 2-1 Determination of Exponent, K_1

$\frac{V_*}{\omega}$	K_1	Mode of Bed material Transport
<0.50	0.59	Mostly contact bed material discharge
0.50 to 2.0	0.64	Some suspended bed material discharge
>2.0	0.69	Mostly suspended bed material discharge

V_* = $(\tau_o/\rho)^{0.5}$, shear velocity in the upstream section, ft/s (m/s)

ω = Fall velocity of bed material based on the D_{50}, ft/s (m/s) (Figure 2-7)

g = Acceleration of gravity, 32.17 ft/s^2 (9.81 m/s^2)

τ_o = Shear stress on the bed, lb_f/ft^2 (Pa (N/m^2))

ρ = Density of water, $slugs/ft^3$ (kg/m^3)

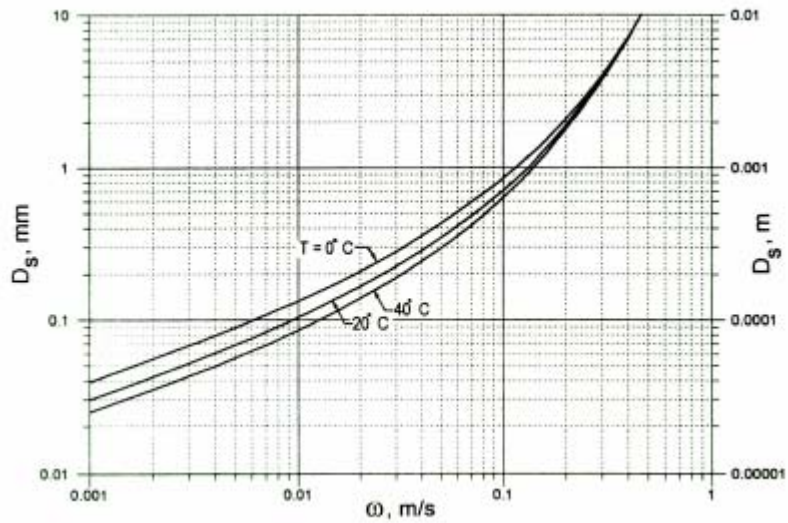

Figure 2-7 Fall Velocity of Sediment Particles having Specific Gravity of 2.65 (taken from HEC-18, 2001)

2.3.1.2. Clear water contraction scour equation

The clear-water scour equation assumes that the upstream flow velocities are less than the sediment critical velocity.

$$y_2 = \left[\frac{K_u Q^2}{D_m^{\frac{2}{3}} W^2} \right]^{\frac{3}{7}} \qquad 2.3$$

$$y_s = y_2 - y_o = \text{average contraction scour} \qquad 2.4$$

where,

y_2	=	Average equilibrium depth in the contracted section after contraction scour, ft (m)
Q	=	Discharge through the bridge or on the set-back overbank area at the bridge associated with the width W, ft^3/s (m^3/s)
D_m	=	Diameter of the smallest non-transportable particle in the bed material (1.25 D_{50}) in the contracted section, ft (m)

D_{50}	=	Median diameter of bed material, ft (m)
W	=	Bottom width of the contracted section less pier widths, ft (m)
y_o	=	Average existing depth in the contracted section, ft (m)
K_u	=	0.0077 (when using English units)

For a more detailed discussion of these equations, the reader is referred to the HEC-18.

2.3.2. Unsteady, complex flows

There are many situations where Laursen's contraction scour equations are not appropriate including cases where: 1) the flow boundaries are complex, 2) the flows are unsteady (and/or reversing), and 3) the duration of the design flow event is short, etc. These situations usually require the application of two-dimensional, flow and sediment transport models for estimating contraction scour depths. For example, the US Army Corps of Engineers' RMA2 hydraulics model and SED2D sediment transport model. Just what constitutes a short or long duration flow event is not well defined, but is dependent on several factors including site conditions, design flows, and sediment parameters. As such, one must rely on engineering judgment and experience when making these determinations. As a general rule of thumb, if the situation requires a 2D model for the hydraulics it will most likely require a 2D model for computing contraction scour.

2.4. Bed Forms

When cohesionless sediments are subjected to currents and/or surface waves, bed forms can occur. These bed features are divided into several categories (ripples, mega ripples, dunes, sand waves, antidunes, etc.) according to their size, shape, method of generation, etc. Since some of these wave-like features can have large amplitudes, they must be accounted for by those responsible for establishing design scour depths. This is particularly true for structures with buried pile caps that may be uncovered by these bedforms. There are a number of predictive equations for estimating bed form height and length in the literature [Tsubaki-Shinohara (1959), Ranga Raju-Soni (1976), Allen (1968), Fredsoe (1980), Yalin (1985), van Rijn (1993]. One of these formulations is presented below.

The following methods and equations for estimating bed form heights and lengths were developed by Leo C. van Rijn. The details of this work and the work of other researchers can be found in van Rijn (1993).

The first step in van Rijn's procedure establishes the type of bed form that will exist for the flow and sediment conditions of interest. This is accomplished by computing the values of the dimensionless parameters T and D^* and then referring to Table 2.2. The equations in Table 2.3 estimate the bed form height and length given the bed form type.

Table 2-2 Bed Classification for determining Bed Forms

Transport Regime		Particle Size $1 \le d_* \le 10$	Particle Size $d_* > 10$
Lower	$0 \le T_r \le 3$	Mini-Ripples	Dunes
	$3 \le T_r \le 10$	Mega-Ripples and Dunes	Dunes
	$10 \le T_r \le 15$	Dunes	Dunes
Transition	$15 \le T_r \le 25$	Washed-Out Dunes, Sand Waves	
Upper	$T_r \ge 25,\ Fr < 8$	(Symmetrical) Sand Waves	
	$T_r \ge 25,\ Fr > 8$	Plane Bed and/or Anti-Dunes	

The expressions for T_r, d_* and Fr are as follows:

$$T_r = \frac{\tau' - \tau_c}{\tau_c} \qquad 2.5$$

where the critical bed shear stress, τ_c, can be estimated from Shield's Diagram in Figure 2-8.

$$\tau' \equiv \rho g \left(\frac{V}{C'} \right)^2,$$

$$C' \equiv 32.6 \ \frac{ft^{1/2}}{s} \ \log_{10}\left(\frac{12y_0}{3D_{90}} \right) = 18 \ \frac{m^{1/2}}{s} \ \log_{10}\left(\frac{12y_0}{3D_{90}} \right),$$

$$d_* \equiv D_{50} \left[\frac{(sg-1)g}{\nu^2} \right]^{1/3},$$

$sg \equiv \frac{\rho_s}{\rho}$ = mass density of sediment divided by mass density of water,

$\nu \equiv \frac{\mu}{\rho}$ = kinematic viscosity of water,

$g \equiv$ acceleration of gravity = 32.17 ft/s^2,

$y_0 \equiv$ water depth just upstream of structure,

$D_{90} \equiv$ grain diameter of which 90% of sediment has a smaller value, and

$Fr \equiv$ Froude Number $= \frac{V}{\sqrt{gy_0}}$.

Table 2-3 Bed Form Length and Height (van Rijn, 1993)

Bed Form Classification	Bed Form Height (Δ)	Bed Form Length (λ)
Mega- Ripples[1]	$0.02\ y_0\left[1-exp\left(-0.1\ T\right)\right]\left(10-T\right)$	$0.5y_o$
Dunes	$0.11\ y_0\left(\frac{D_{50}}{y_0}\right)^{0.3}\left[1-exp\left(-0.5\ T\right)\right]\left(25-T\right.$	$7.3y_o$
Sand Waves	$0.15\ y_0\ \left(1\text{-}Fr^2\right)\left\{1-exp\left[-0.5\left(T-15\right)\right]\right\}$	$10y_o$

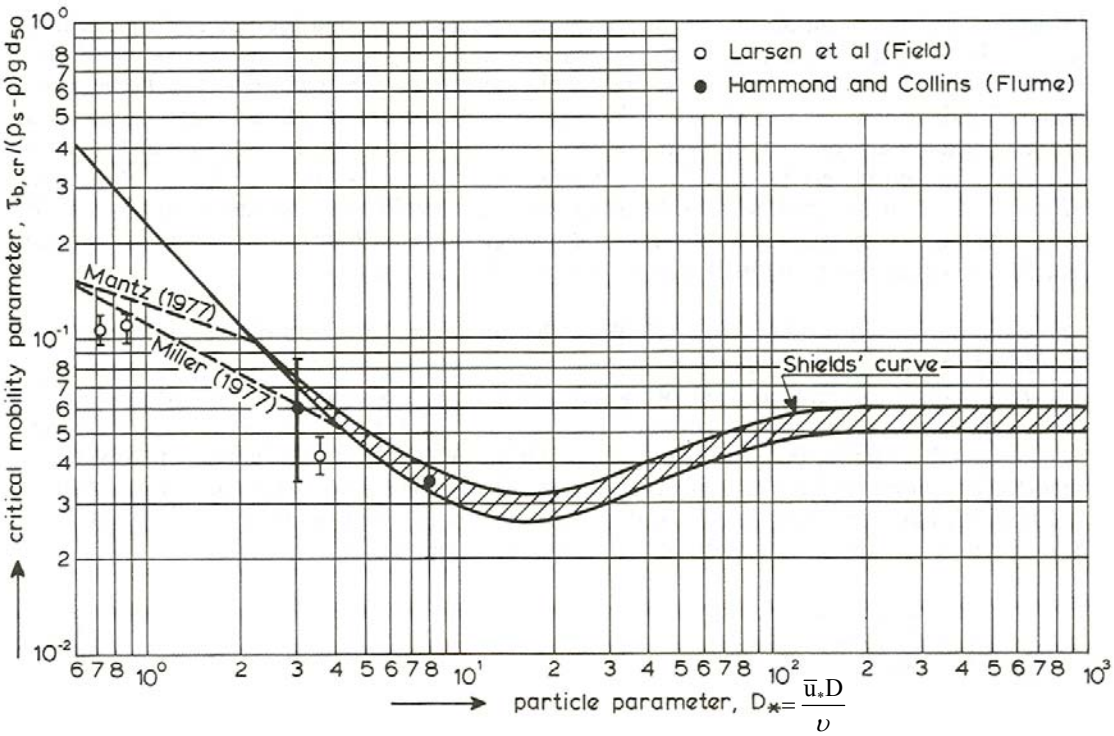

Figure 2-8 Critical bed shear stress as a function of sediment particle diameter, Shields (1936).

2.5. Local Scour

When water flows around a structure located in or near an erodible sediment bed, the increased forces on the sediment particles near the structure may remove sediment from the vicinity of the structure. This erosion of sediment is referred to as structure-induced sediment scour (local scour or pier scour). For cohesionless sediments, the scour hole usually takes the form of an inverted cone with a slope approximately equal to the angle of repose for the sediment in water. The deepest depth of the scour hole is of greatest interest to the structural engineer designing a new (or analyzing the stability of an existing) structure. Therefore, scour hole depth, or more simply scour depth, refers to the maximum depth within the scour hole. For a given steady flow velocity and water depth, the scour depth increases with time until it reaches a maximum value known as the equilibrium scour depth, y_s. The integrity of the structure supported by the sediment is often highly dependent on the depth of the scour hole. Much research devoted to local scour over the last few decades has revolved around scour around a single circular pile. As a result, methods and equations for estimating scour at more complex structures are

based on the knowledge and understanding of local scour at single, circular structures. Chapter 3 is devoted to methods for computing equilibrium scour depths at singular pile structures. Chapter 4 presents methods and equations for complex bridge pier structures.

CHAPTER 3 LOCAL SCOUR AT A SINGLE PILE

3.1. Introduction

There are many local scour depth prediction equations in the literature as well as a number of review papers that compare the various equations and methodologies [e.g., Breusers et al. (1977), Jones (1983), Landers, and Mueller (1996)]. Most of these equations are empirical and based primarily on small scale laboratory data. While many of these equations yield reasonable results for laboratory scale structures and sediments, they can differ significantly in their prediction of scour depths at large, prototype scale structures. This chapter discusses the formulation of equilibrium local scour depth prediction equations for single pile structures developed by D. Max Sheppard and his students at the University of Florida. The FDOT and FHWA have both accepted these equations for use in design scour predictions in Florida and they have also been used for a number of bridges in other states throughout the United States. These equations were first published in 1995 [Sheppard et al. (1995)] but have been modified and updated over the years as more laboratory data became available. The data from which these equations are based cover a wide range of structure, flow and sediment parameters. Clearwater scour tests with prototype scale structures were performed in a 20 ft wide, 21 ft deep by 126 ft long flume in the USGS-BRD Conte Laboratory in Turners Falls, Massachusetts. Live-bed tests with velocities up to six times the sediment critical velocity were conducted in a 5 ft wide, 4 ft deep by 148 ft long flume in the Hydraulics Laboratory at the University of Auckland in Auckland, New Zealand. Finally, the chapter concludes with two example problems that help illustrate the use of the equations.

3.2. Description of the Flow Field Around a Single Pile

This section discusses the flow field near a cylindrical pile in a steady flow, as described by various researchers. The flow field in the immediate vicinity of a structure is quite complex, even for simple structures such as circular piles. One of the dominant features of the local flow field is the formation of secondary flows in the form of vortices. Many investigators (e.g. Shen et al., 1966, Melville, 1975) believe that these vortices are the

most important mechanisms of local scour (at least during certain phases of the scour evolution).

Vortices, with near horizontal axes are formed at the bed and near the water surface on the upstream edge of the structure. These are referred to as the "horseshoe" and "surface" vortices respectively. The term "horseshoe" is derived from the shape that the vortex takes as it wraps around the pile and trails downstream when viewed from above (Figure 3.1). Shen et al. (1966) describes the horseshoe vortex system in detail. The horseshoe vortex is initiated by the stagnation pressure gradient on the leading edge of the structure resulting from the bottom boundary layer of the approaching flow. That is, the variation in flow velocity from zero at the bed to the value at the surface causes a variation in stagnation pressure on the leading edge of the structure. The largest stagnation pressure occurs at the elevation of the highest velocity. In its simplest form, the horseshoe vortex system is composed of two vortices, a large one next to the structure and one adjacent small counter rotating vortex. For more complex flows and structure shapes, multiple unsteady vortices are formed which periodically shed and are swept downstream. Clearly, the geometry of the structure is important in determining the strength of the vortex system. Blunt nosed structures create the most energetic vortex systems.

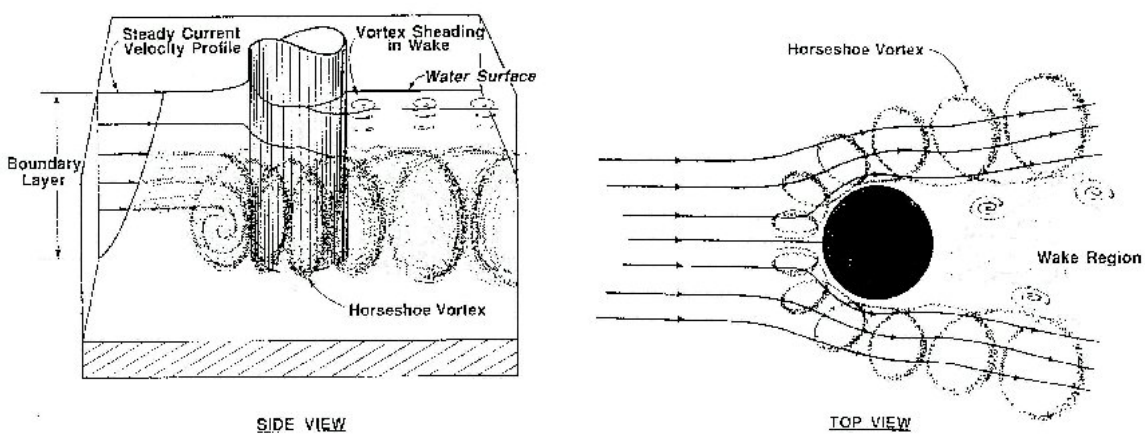

Figure 3-1 Schematics of the vortices around a cylinder

Melville (1975) measured mean flow directions, mean flow magnitude, turbulent flow fluctuations, and computed turbulent power spectra around a circular pile for flatbed, intermediate and equilibrium scour holes. He found that a strong vertical downward flow

developed ahead of the cylinder as the scour hole enlarged. The size and circulation of the horseshoe vortex increased rapidly and the velocity near the bottom of the hole decreased as the scour hole was enlarged. As the scour hole develops further, the intensity of the vortex decreases and reaches a constant value at the equilibrium stage.

Although the horseshoe vortex is considered the most important scouring mechanism for steady flows, the wake vortex system is also important. Wake vortices are created by flow separation on the structure. Large scour holes may also develop downstream from piers under certain circumstances (e.g. Shen et al., 1966). With their vertical component of flow, wake vortices act somewhat like a tornado. They put the bed material in suspension, where it is carried downstream by the mean flow.

More recently another potential scour mechanism was identified [Sheppard (2004)]. This mechanism results from the pressure gradient field generated by the presence of the structure in the flow. The pressure field near the bed is, for the most part, determined by the pressure field in the main body of flow. Potential flow theory shows that there are significant variations in pressure in the flow field near the structure. These pressure gradients impose pressure forces on the sediment grains that can be much larger than the drag forces due to the flow around the grains. The pressure gradients reduce in magnitude with increasing structure size; therefore, they are more important for laboratory scale than for prototype scale structures. The results of the analysis presented in Sheppard (2004) help explain the dependence of equilibrium scour depth on the various dimensionless groups discussed in the next section.

3.3. Equilibrium Scour Depths in Steady Flows

There is usually a distinction made between local scour that occurs at flow velocities less than and greater than the sediment critical velocity (the velocity required to initiate sediment movement on a flat bed upstream of the structure). If the velocity is less than the sediment critical velocity, the scour is known as “clear-water scour”. If the velocity is greater than the sediment critical velocity, the scour is called “live-bed scour”. The following discussion is limited to sediments that are cohesionless, such as sand. For

sediments such as silts, muds, clays, and rock additional parameters must be considered to account for the forces that bond the particles together.

For most structures in a steady flow, the local scour depth varies in magnitude around the structure. In this discussion the term local scour depth (or just local scour) refers to the depth of the deepest point in the local scour hole.

Equilibrium local scour depth depends on a number of fluid, sediment and structure parameters. Equation 3.1 expresses this mathematically as

$$y_s \equiv f\left(\rho, \mu, g, D_{50}, \sigma, \rho_s, y_0, V, D^*, \Theta\right), \qquad 3.1$$

where

y_s ≡ the equilibrium scour depth (maximum local scour depth after the flow duration is such that the depth is no longer changing),

f ≡ symbol meaning "function of ",

ρ and ρ_s ≡ density of water and sediment respectively,

μ ≡ dynamic viscosity of water (depends primarily on temperature),

g ≡ acceleration of gravity,

D_{50} ≡ median diameter of the sediment,

σ ≡ gradation of sediment,

y_o ≡ depth of flow upstream of the structure,

V ≡ depth average velocity upstream of the structure,

D^* ≡ effective diameter of structure, i.e. the diameter of circular pile that would experience the same scour depth as the structure for the same sediment and flow conditions. For a circular pile D^* is simply the diameter of the pile.

Θ ≡ parameter quantifying the concentration of fine sediments in suspension .

The most important dimensionless groups for local scour can be obtained from the quantities given in Equation 3.1. These eleven quantities can be expressed in terms of three fundamental dimensions: force, length and time. According to the Buckingham π

theorem, eight (11 variables - 3 fundamental dimensions) independent dimensionless groups exist for this situation. An example of these eight groups is given in Equation 3.2

$$\frac{y_s}{D^*} = f\left(\frac{y_0}{D^*}, \frac{V}{\sqrt{g\,y_0}}, \frac{\rho_s}{\rho}, \frac{VD^*\rho}{\mu}, \frac{V}{V_c}, \frac{D_{50}}{D^*}, \sigma, \Theta\right) \qquad 3.2$$

where V_c is the critical depth-averaged velocity (the velocity required to initiate sediment motion on a flat bed).

The large number of variables (and therefore dimensionless groups) affecting local scour processes has resulted in researchers presenting their data in a wide variety of ways. This has made it difficult to compare results from different investigations and to some extent has slowed progress in local scour research. As with any complex problem, some of the groups are more important than others. It is impractical (if not impossible) to include all of the groups in an analysis of the problem. The question becomes "which of the groups are most important for local scour processes?"

Based on the importance of Froude Number ($V/\sqrt{gy_0}$) in open channel flows some of the earlier researchers chose to employ this group to account for flow intensity and water depth. For example, the equation referred to as the CSU (Colorado State University) equation, which is presented in the current version of the FHWA Hydraulic Engineering Circular Number 18 (HEC-18), includes the Froude Number. A wide variety of groups and combinations of groups have been proposed over the years, each working reasonably well for at least the range of (mostly laboratory) data used in their development. Some researchers (including the authors of this manual) have found that the parameters in Equation 3.3 can describe equilibrium scour depths for a wide range of conditions.

$$\frac{y_s}{D^*} = f\left(\frac{y_0}{D^*}, \frac{V}{V_c}, \frac{D^*}{D_{50}}, \sigma, \Theta\right) \qquad 3.3$$

If the sediment is near uniform in size $(\sigma \leq 1.5)$ the effect of σ is small and can be neglected. If the size distribution is large, the equilibrium scour depth can be

significantly reduced due to natural armoring as the finer grains are removed leaving only the larger grains which require more energy for their removal.

The suspended fine sediment in the water column (often referred to as washload) has been shown to reduce equilibrium scour depths in laboratory tests. However, more research is needed before the level of scour reduction can be quantified. The effects of both σ and Θ are discussed further in Chapter 5.

The discussion thus far in this chapter has been limited to single circular piles (or single circular piles that represent a more complex structure shape). As indicated above, scour at single structures with other shapes can be analyzed using their "effective diameter", D^*. The effective diameter is the diameter of a water surface penetrating circular pile that will experience the same equilibrium scour depth as the structure of interest under the same sediment and flow conditions.

Table 3-1 presents effective diameters for several common shapes which have been determined using Equations 3.4-3.6 and laboratory data.

Table 3-1 Effective Diameters for Common Structure Cross-sections.

Structure Cross-section	Projected Width	Effective Diameter D^*
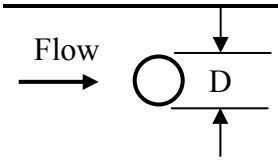	$W = D$	$D^* = D$
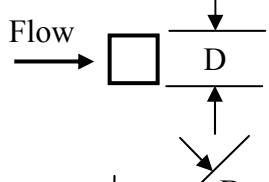	$W = D$	$D^* = 1.23W$ $= 1.23D$
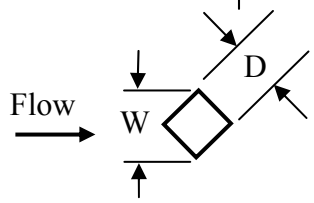	$W = 1.4D$	$D^* = W$ $= 1.2D$

The following equilibrium local scour depth equations were developed by Sheppard and his graduate students at the University of Florida. They are empirical and based

primarily on laboratory data obtained by Sheppard in four different Laboratories (University of Florida in Gainesville, Florida, Colorado State University in Fort Collins, Colorado, University of Auckland in Auckland, New Zealand and the Conte USGS-BRD Laboratory in Turners Falls, Massachusetts).

In the clear-water scour range ($0.47 < V/V_c < 1$)

$$\frac{y_s}{D^*} = 2.5\, tanh\left[\left(\frac{y_0}{D^*}\right)^{0.4}\right]\left\{1-1.75\left[ln\left(\frac{V}{V_c}\right)\right]^2\right\}\left[\frac{D^*/D_{50}}{0.4\left(D^*/D_{50}\right)^{1.2}+10.6\left(D^*/D_{50}\right)^{-0.13}}\right] \qquad 3.4$$

In the live-bed scour range up to the live-bed peak ($1 < V/V_c < V_{lp}/V_c$)

$$\frac{y_s}{D^*} = tanh\left[\left(\frac{y_0}{D^*}\right)^{0.4}\right] \times \left[2.2\left(\frac{V/V_c - 1}{V_{lp}/V_c - 1}\right) + 2.5\left\{\frac{D^*/D_{50}}{0.4\left(D^*/D_{50}\right)^{1.2}+10.6\left(D^*/D_{50}\right)^{-0.13}}\right\}\left(\frac{V_{lp}/V_c - V/V_c}{V_{lp}/V_c - 1}\right)\right], \qquad 3.5$$

and in the live-bed scour range above the live-bed peak ($V/V_c > V_{lp}/V_c$)

$$\frac{y_s}{D^*} = 2.2\, tanh\left[\left(\frac{y_0}{D^*}\right)^{0.4}\right], \qquad 3.6$$

The variations of normalized equilibrium scour depth, y_s/D^*, with the three dimensionless groups, y_0/D^*, V/V_c, and D^*/D_{50} are shown graphically in Figure 3-2 through Figure 3-4.

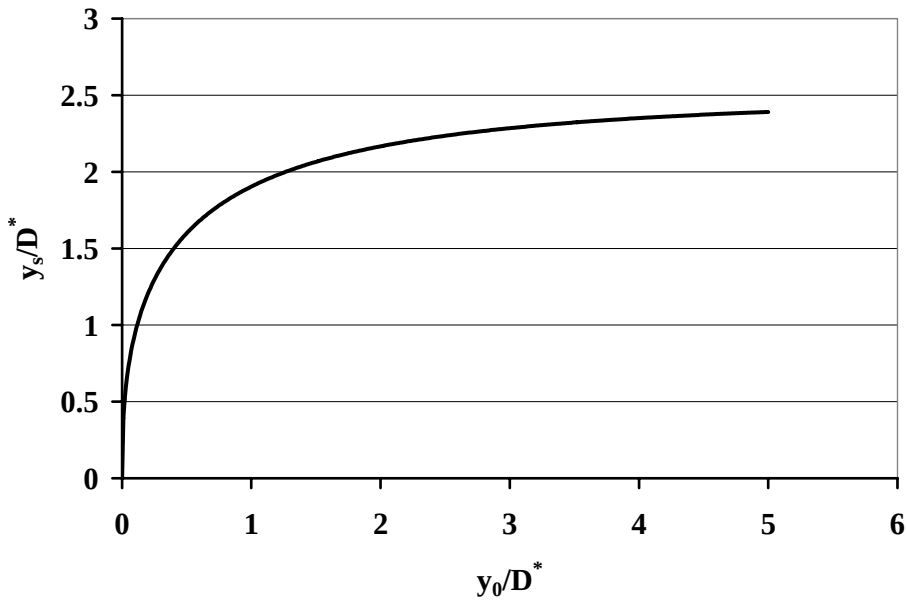

Figure 3-2 Equilibrium Scour Depth Dependence on the Aspect Ratio, y_0/D^* (V/V_c =1 and D^*/D_{50} =46).

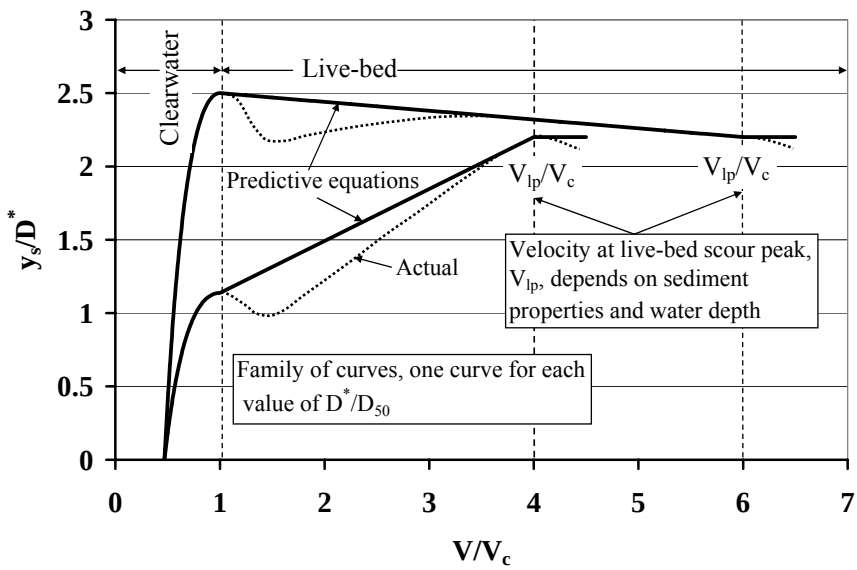

Figure 3-3 Equilibrium Scour Depth Dependence with Flow Intensity, V/V_c (for y_0/D^*>3 and constant values of D^*/D_{50}).

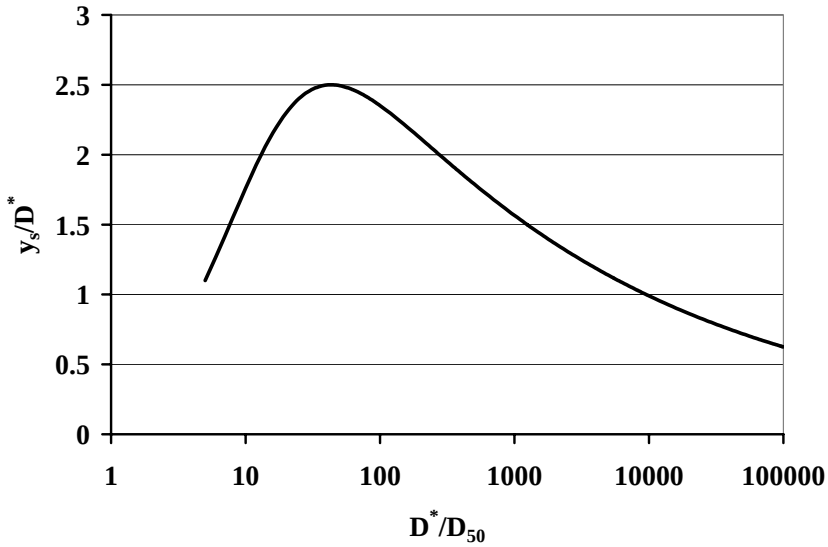

Figure 3-4 Equilibrium Scour Depth Dependence on D^*/D_{50} for $y_0/D^* > 3$ and $V/V_c=1$.

Figure 3-2 shows the dependence of scour depth on the aspect ratio, y_0/D^* while holding V/V_c and D^*/D_{50} constant. Figure 3-3 shows the variation of scour depth with flow intensity, V/V_c for constant y_0/D^* and D^*/D_{50}. Figure 3-4 shows the dependence of scour depth on D^*/D_{50} for constant y_0/D^* and V/V_c. The data indicates that there are two local maximums in the scour depth versus V/V_c plots. The first local maximum occurs at transition from clear-water to live-bed scour conditions, i.e., at $V/V_c=1$. The second maximum, referred to here as the "live-bed peak" is thought to occur at the flow conditions where the bed forms disappear (i.e., the bed planes out). The velocity that produces the live-bed scour peak is called the live-bed peak velocity and is denoted by V_{lp}.

Data obtained by the author and other researchers clearly show that the equilibrium scour depth decreases with increasing velocity just beyond the transition peak before proceeding to the live-bed peak. Since Equations 3.4-3.6 are intended for design applications, no attempt was made to include this reduction in scour depth in the predictive equations. For slowly varying flows, the structure will experience the transition peak en route to the live-bed design flow condition.

In the clear-water scour range, equilibrium scour depth is very sensitive to changes in the flow intensity, V/V_c. To a lesser extent, scour depth is also sensitive to the magnitude of

the live-bed peak velocity, V_{lp}. It is therefore important to employ the same methods applied during the development of the equations when computing V_c and V_{lp}. The sediment critical velocity, V_c, is calculated using a curve fit to Shield's diagram (Figure 2-8). The live-bed peak velocity, V_{lp}, is computed from van Rijn's (1993) prediction of the conditions under which the bed planes out. The equations for computing V_c and V_{lp} are presented below.

Sediment Critical Velocity, V_c

$$V_c = 2.5\, u_{*c}\, ln_e\left(\frac{y_0}{2.72\, z_0}\right), \tag{3.7}$$

where

$$u_{*c} \equiv \sqrt{\frac{\tau_c}{\rho}} = \text{critical friction velocity} = \sqrt{\Theta_c\,(sg\text{-}1)\,g\,D_{50}} \tag{3.8}$$

$$\Theta_c = \begin{cases} 0.25\text{-}0.1\sqrt{d_*} & 0.01 < d_* < 3, \\ 0.0023 d_* \text{-} 0.000378 d_*\, ln_e(d_*) + 0.23/d_* \text{-} 0.005 & 3 < d_* < 150, \\ 0.0575 & d_* > 150, \end{cases} \tag{3.9}$$

$$d_* = D_{50}\left[(sg\text{-}1)\,g/\nu^2\right]^{1/3}, \tag{3.10}$$

$$z_0 = \begin{cases} \nu/(9\,u_{*c}) & 0 < Re_c \le 5, \\ k_s 10^{-3}\left[-6 + 2.85 Re_c - 0.58 Re_c\, ln_e(Re_c) + 0.002 Re_c^2 + 111/Re_c\right] & 5 < Re_c \le 70, \\ k_s/30 & Re_c > 70, \end{cases} \tag{3.11}$$

$$Re_c = u_{*c} k_s/\nu, \text{ and} \tag{3.12}$$

$$k_s \equiv \begin{cases} 2.5\, D_{50} & \text{for } D_{50} \ge 0.6 \text{ mm}, \\ 5\, D_{50} & \text{for } D_{50} < 0.6 \text{ mm} \end{cases}. \tag{3.13}$$

Live-Bed Scour Peak Velocity, V_{lp} [van Rijn, (1993)]

V_{lp} is the larger of:

$$V_1 = 0.8\sqrt{g\ y_0} \quad \text{or} \tag{3.14}$$

$$V_2 = 29.31\ u_{*c}\ log_{10}\left(4y_0/D_{90}\right). \tag{3.15}$$

where D_{90} is the sediment grain size exceeded by 10% (by weight) of a sediment sample.

That is:

$$V_{lp} = \begin{Bmatrix} V_1 \text{ if } V_1 \geq V_2 \\ V_2 \text{ if } V_1 < V_2 \end{Bmatrix}. \tag{3.16}$$

Figure 3-5 is a plot of predicted (Equations 3.4-3.6) versus measured scour depths for both clear-water and live-bed laboratory scour tests.

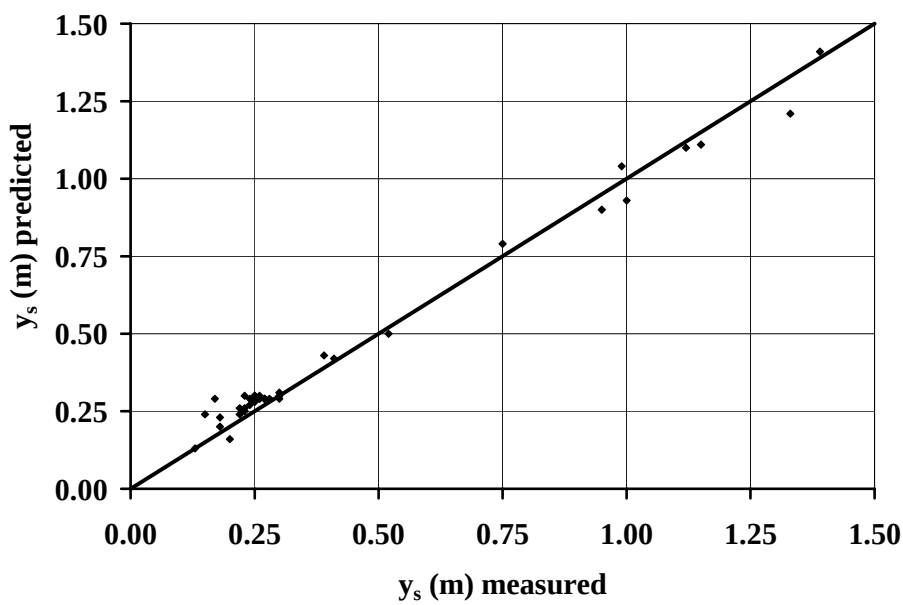

Figure 3-5 Predicted versus Measured Scour Depth (Equations 3.4-3.6).

Over predictions for the live-bed tests are at least partially due to the reduction in scour depths beyond the transition peak (shown in Figure 3-3) that is not accounted for in the equations.

An example application of the equations to a prototype structure is shown in Figure 3-6. Normalized scour depth, y_s/D^* is plotted versus D^*/D_{50} for a range of flow velocities up to the peak tidal velocity at the west channel pier on the existing Tacoma Narrows Bridge in Tacoma, Washington. This pier is 64.5 ft wide, 117.5 ft long, is skewed to the flow approximately 18 degrees, and is located in a water depth of 111 ft. The pier experiences near 100-year design tidal (reversing) flow conditions twice per month during spring tides. The spring tidal velocity is 8.2 ft/s and the effective diameter of the pier is 86.3 ft. This pier, built approximately 64 years ago, is located in sediment with a median diameter of 0.18 mm. The bed material does, however, contain sediment particles larger than the sediment core apparatus (with some sediment diameters exceeding 150 mm). Therefore, the correct sediment diameter standard deviation $\left(\sigma \equiv \sqrt{D_{84}/D_{16}}\right)$ is not available. The predicted scour depth (from Equations 3.4-3.6) is 56.7 ft and the measured depth was 36 ft. The reason for the larger than normal over prediction most likely results from armoring of the bed by the larger sediment particles as the scour progressed. The spring tidal velocities lie within the live-bed scour regime for the 0.18 mm sediment, but clear-water scour conditions exist at this site due to natural armoring of the channel bed by the larger sediment particles. Extensive video images of the bed in the vicinity of the bridge provide evidence that clear water scour conditions exist at the site. Under clear-water conditions the measured scour depth should be the equilibrium depth at the peak spring tidal velocity. For comparison purposes the predicted scour depth for these conditions using the CSU equation [Richardson, E.V. and Davis, S.R. (2001)] is 80.7 ft. This value is also shown in Figure 3-6.

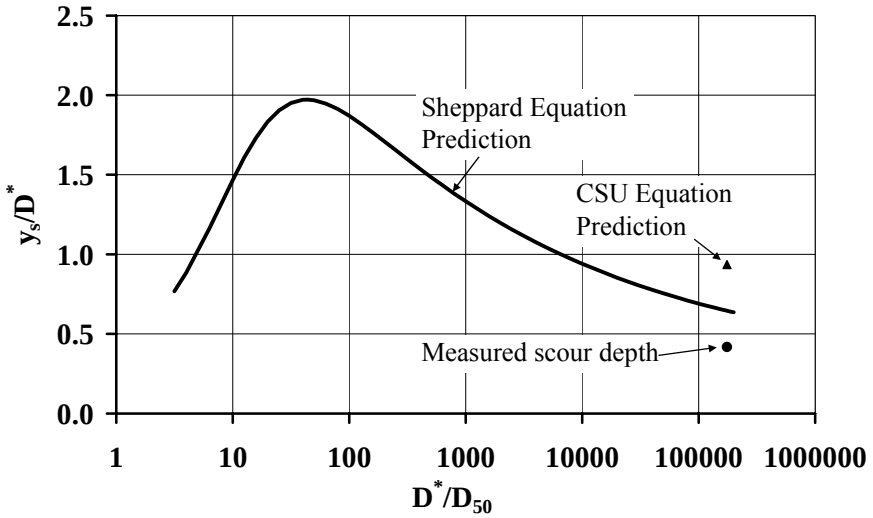

Figure 3-6 Scour Depth Prediction using Measured Peak Tidal Flows at the West Channel Pier on the Existing Tacoma Narrows Bridge in Tacoma, Washington.

CHAPTER 4 SCOUR AT PIERS WITH COMPLEX GEOMETRIES

4.1. Introduction

Most large bridge piers are complex in shape and consist of several clearly definable components. While these shapes are sensible and cost effective from a structural standpoint, they can present a challenge for those responsible for estimating design scour depths at these structures. This chapter presents a methodology for estimating scour depths at a class of structures composed of up to three components. The data used in the development of this methodology were obtained by J. Sterling Jones at FHWA, D. Max Sheppard at the University of Florida, and Steven Coleman at the University of Auckland through numerous laboratory experiments.

4.2. Methodology for Estimating Local Scour Depths at Complex Piers

This section presents a methodology for estimating equilibrium local scour depths at bridge piers with complex pier geometries, located in cohesionless sediment and subjected to steady flow conditions. These methods apply to structures composed of up to three components as shown in Figure 4-1. In this document, these components are referred to as the 1) column, 2) pile cap and 3) pile group.

Most published data and information on local scour is for single circular piles. Likewise, the most accurate predictive equations for equilibrium scour depth are for single circular piles. It seems reasonable then that predictive methods for local scour at more complex structures would build upon and take advantage of this knowledge and understanding. The methods presented in this chapter are based on the assumption that a complex pier can be represented (for the purposes of scour depth estimation) by a single circular (water surface penetrating) pile with an "effective diameter" denoted by D^*. The magnitude of D^* is such that the scour depth at a circular pile with this diameter is the same as the scour depth at the complex pier for the same sediment and flow conditions. The problem of computing equilibrium scour depth at the complex pier is therefore reduced to one of determining the value of D^* for that pier and applying the single pile equations presented in Chapter 3 to this pile for the sediment and flow conditions of interest.

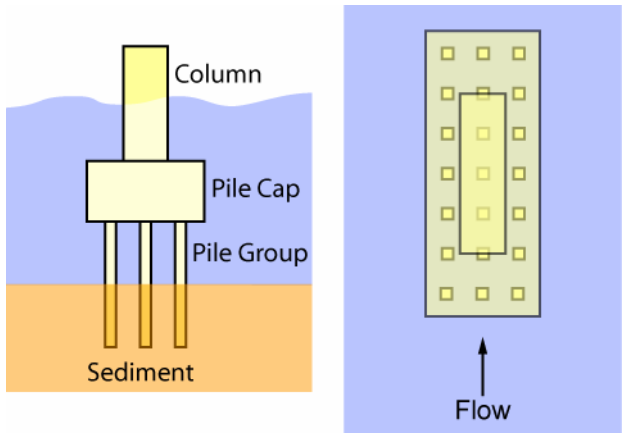

Figure 4-1 Complex pier configuration considered in this analysis. The pile cap can be located above the water, in the water column or below the bed.

The methodology is based on the following assumptions:

1. The structure can be divided into up to three components as shown in Figure 4-2.

2. For scour computation purposes, each component can be replaced by a single, surface penetrating, circular pile with an effective diameter (D^*) that depends on the shape, size and location of the component and its orientation relative to the flow as shown in Figure 4-3. For partially or fully buried pile caps the effective diameter also depends on the flow and sediment conditions.

3. The total D^* for the structure can be approximated by the sum of the effective diameters of the components making up the structure (Figure 4-4). That is,

$$D^* \equiv D^*_{col} + D^*_{pc} + D^*_{pg} , \qquad 4.1$$

where

D^* = effective diameter of the complex pier,

D^*_{col} = effective diameter of the column,

D^*_{pc} = effective diameter of the pile cap,

D^*_{pg} = effective diameter of the pile group.

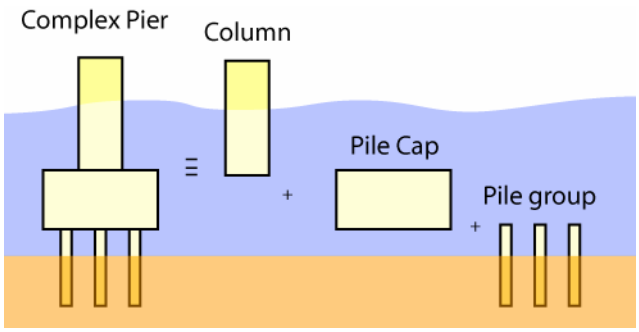

Figure 4-2 Schematic drawing of a complex pier showing the 3 components, column, pile cap and pile group.

The effective diameter for each component is a function of its shape, size and location relative to the bed and water surface. The mathematical relationships for these effective diameters have been established empirically with data from experiments performed by J. Sterling Jones at the FHWA Turner Fairbanks Laboratory in McLean, Virginia, by D. Max Sheppard in flumes at the University of Florida, the Conte USGS-BRD Research Center Hydraulics Laboratory in Turners Falls, Massachusetts and in the Hydraulics Laboratory at the University of Auckland in Auckland, New Zealand and by Steven Coleman at the University of Auckland.

This methodology is for estimating local scour only. General scour, aggradation/degradation, contraction scour, and bed form heights must be established prior to applying this procedure. The information needed to compute local scour depths at complex piers is summarized below:

1. General scour, aggradation/degradation, contraction scour, and bed form heights.

2. External dimensions of all components making up the pier including their vertical positions relative to the pre-local scoured bed.

3. Sediment properties (mass density, median grain diameter and grain diameter distribution).

4. Water depth and temperature and depth-averaged flow velocity just upstream of the structure.

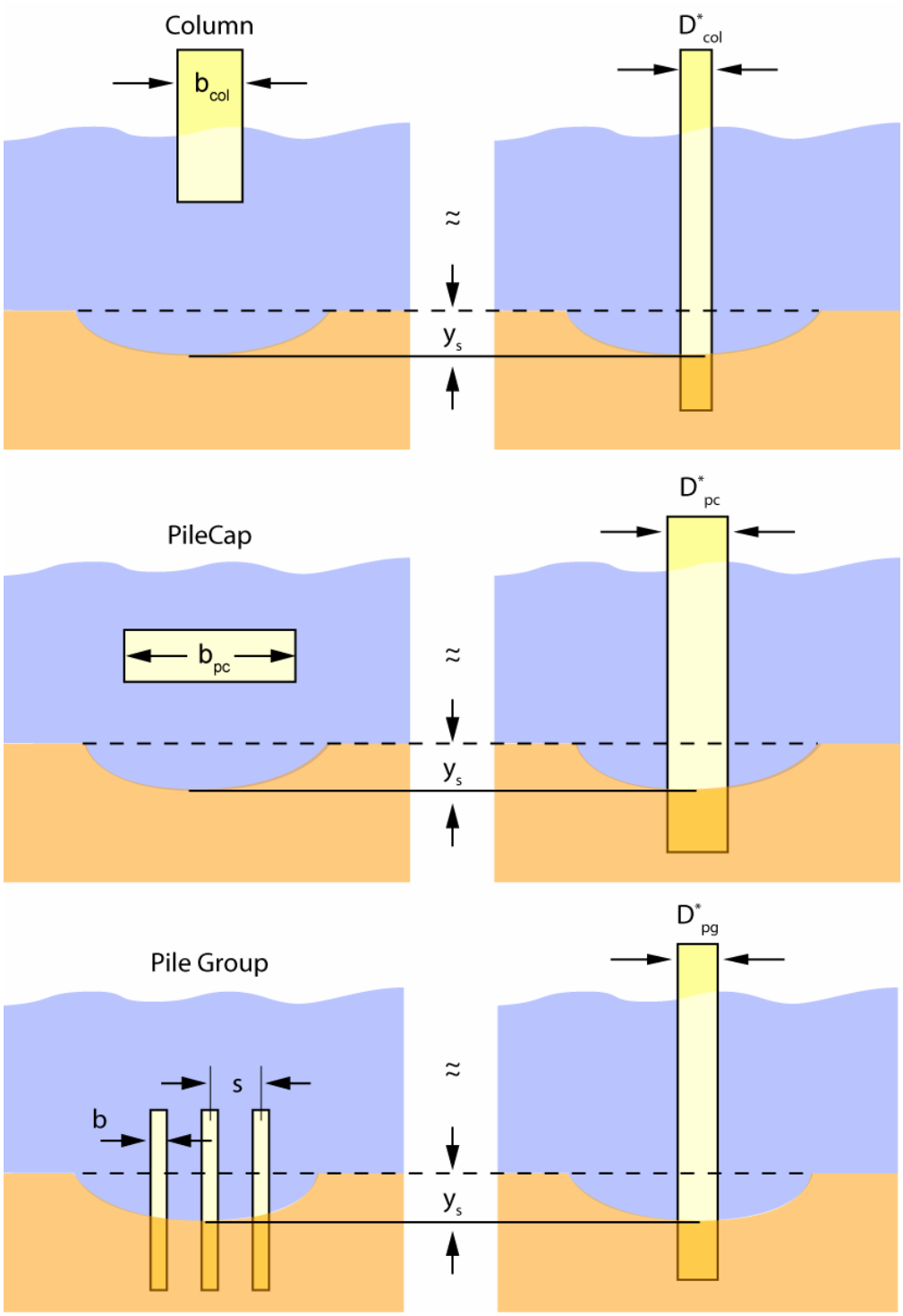

Figure 4-3 Definition sketches for the effective diameters of the complex pier components, column (D^*_{col}), pile cap (D^*_{pc}) and pile group (D^*_{pg}).

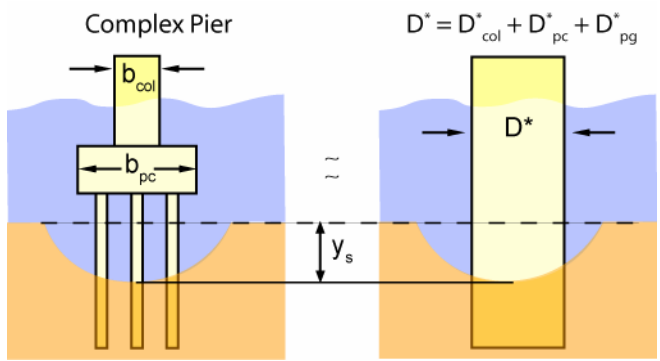

Figure 4-4 Definition sketch for total effective diameter for a complex pier.

For situations where the shape of the structure exposed to the flow changes as local scour progresses (such as complex piers with buried or partially buried pile caps), equilibrium scour depth prediction is more involved. For these cases, the scour depth computation scheme must involve iterative computations and the effective diameter will depend on the flow and sediment conditions as well as the structure parameters. For this reason, the scour computation procedure is divided into three cases,

Case 1 for situations where the structure shape exposed to the flow does not change as local scour progresses (pile cap initially above the bed),

Case 2 for partially buried pile caps, and

Case 3 for completely buried pile caps.

Recall that all components of stream bed scour (i.e. general scour, aggradation/degradation, contraction and bed form height) must be computed and the bed elevation adjusted prior to computing local scour.

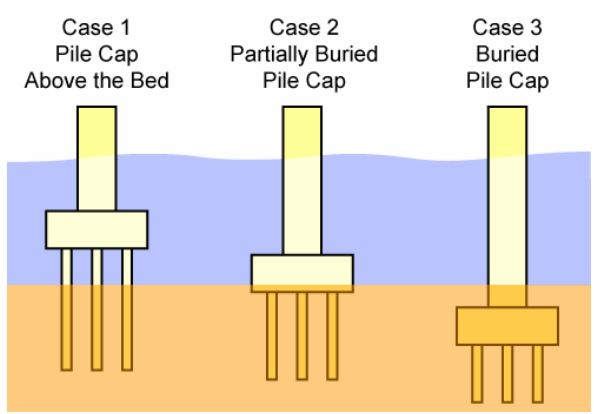

Figure 4-5 Examples of Case 1, Case 2 and Case 3 Complex Piers.

4.2.1. Complex Pier Local Scour Depth Prediction - Case 1 Piers (Pile Cap above the Bed)

The procedure for computing the effective diameter for Case 1 complex piers is described in this section. The procedure begins with the computation of the effective diameter of the uppermost component exposed to the flow and proceeds to the lowest component. The complex pier may be composed of any combination of the three components shown in Figure 4-2. The notation used in this analysis is shown in the definition sketch in Figure 4-6.

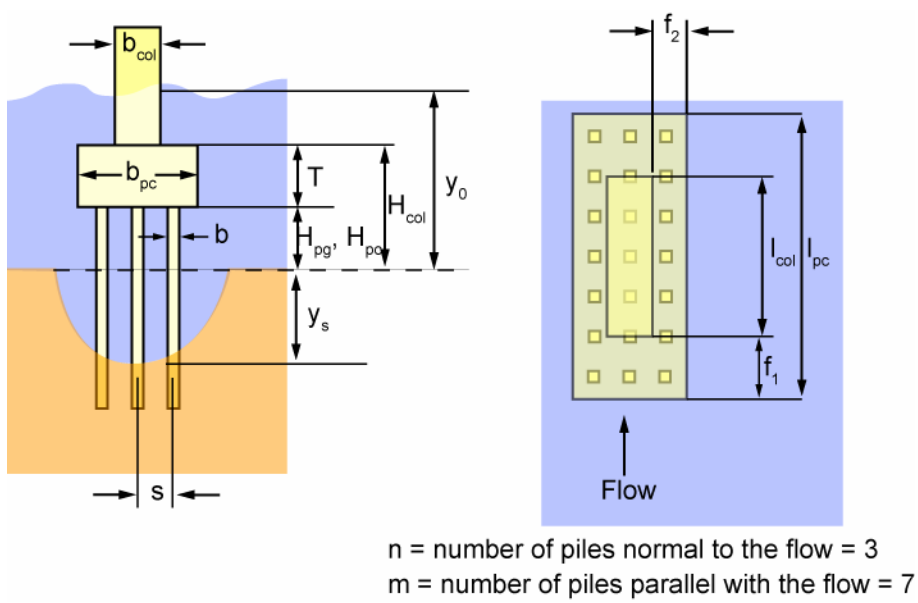

Figure 4-6 Nomenclature definition sketch.

4.2.1.1. Effective Diameter of the Column

The procedure for computing the effective diameter of the column is presented in steps A-F below.

A. Calculate $y_{0(max)}$ for the column. Equilibrium scour depth for a given structure depends on the water depth up to a certain depth. This limiting depth, denoted by $y_{0(max)}$, depends on the structure size and its location relative to the bed and can be estimated using Equation 4.2.

$$y_{0(max)} = \begin{cases} 5\,b_{col} & \text{for } y_o \geq 5\,b_{col} \\ y_o & \text{for } y_o < 5\,b_{col} \end{cases} \qquad 4.2$$

B. Compare the column's base height, H_{col}, to $y_{0(max)}$. If H_{col} is greater than $y_{0(max)}$, set $D^*_{col} = 0$ and proceed to the computation of the effective diameter of the pile cap, D^*_{pc}. The column will not influence the overall structure's effective diameter unless the base of the column lies below $y_{0(max)}$. That is:

$$\text{If} \begin{cases} H_{col} \geq y_{0(max)}, \; D^*_{col} = y_{s(col)} = 0, \text{ proceed to Section 4.2.1.2} \\ H_{col} < y_{0(max)}, \; \text{proceed to step C.} \end{cases} \qquad 4.3$$

C. Compute the column shape coefficient using Equation 4.4

$$K_s = \begin{cases} 1 & \text{for circular columns} \\ 0.86 + 0.97\left|\alpha \dfrac{\pi}{180^o} - \dfrac{\pi}{4}\right|^4 & \text{for rectangular columns} \end{cases} \qquad 4.4$$

where α is the flow skew angle (angle between the column axis and the flow direction, see Figure 4-6). Equation 4.4 is valid for $0^o \leq \alpha \leq 90^o$.

D. Compute the column skew factor using Equation 4.5

$$K_\alpha = \frac{b_{col}\, cos(\alpha) + l_{col}\, sin(\alpha)}{b_{col}} \qquad 4.5$$

E. Using Equation 4.6, compute the weighted average value of the pile cap extension beyond the column, f. The value of f is a function of the front (f_1) and side (f_2) overhangs shown in Figure 4-6. The non-dimensional ratio of f/b_{col} is then used to compute the pile cap extension coefficient, K_f (Equation 4.7 or Figure 4-7). K_f attenuates the column effective diameter as the ratio of f/b_{col} increases. The column contribution to the scour hole is reduced to zero for values of $f/b_{col} > 3$.

$$f = \begin{cases} \dfrac{3f_1 + f_2}{4} & \text{for } \alpha \le 45^o \\ \dfrac{3f_2 + f_1}{4} & \text{for } \alpha > 45^o \end{cases} \qquad 4.6$$

$$K_f = \begin{cases} -0.12\left(\dfrac{f}{b_{col}}\right)^2 + 0.03\left(\dfrac{f}{b_{col}}\right) + 1 & \text{for } 0 \le \left(\dfrac{f}{b_{col}}\right) \le 3 \\ 0 & \text{for } \left(\dfrac{f}{b_{col}}\right) > 3 \end{cases} \qquad 4.7$$

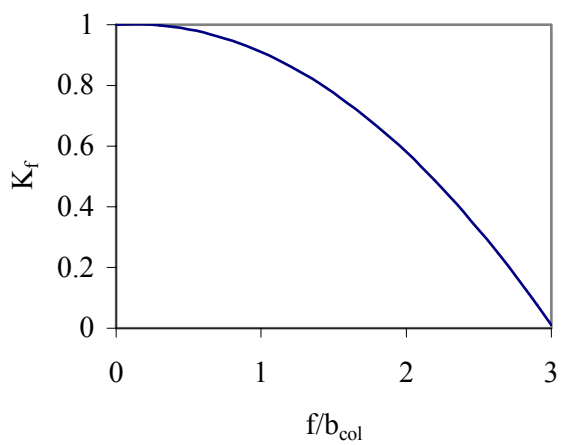

Figure 4-7 Graph of K_f versus f/b_{col} for the column.

F. Once the coefficients K_s, K_α, and K_f are known, the effective diameter of the column can be computed using Equation 4.8 or Figure 4-8.

$$D^*_{col} = \begin{cases} K_s\, K_\alpha\, K_f\, b_{col}\left[0.1162\left(\dfrac{H_{col}}{y_{0(max)}}\right)^2 - 0.3617\left(\dfrac{H_{col}}{y_{0(max)}}\right) + 0.2476\right] & \text{for } 0 \le \dfrac{H_{col}}{y_{0(max)}} \le 1 \\ 0 & \text{for } \dfrac{H_{col}}{y_{0(max)}} > 1 \end{cases} \qquad 4.8$$

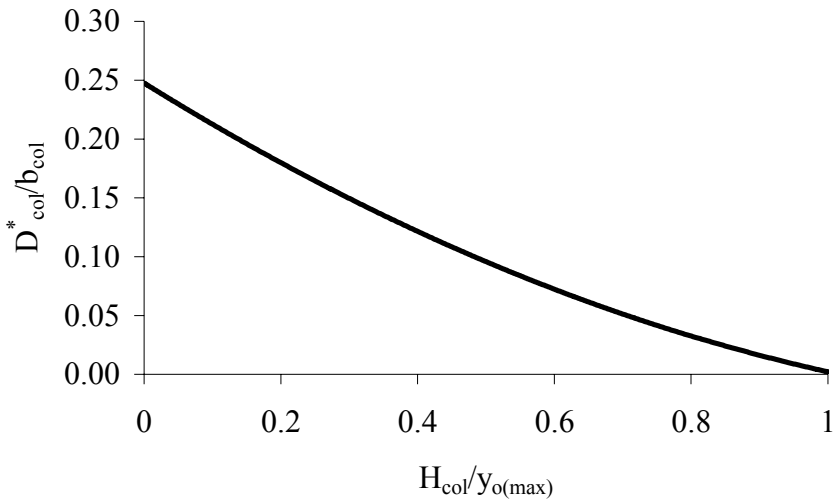

Figure 4-8 Graph of effective diameter of the column versus $H_{col}/y_{o(max)}$.

4.2.1.2. Effective Diameter of Pile Cap

The pile cap's potential for producing scour (and thus the value of D^*_{pc}) increases as its position approaches the bed from above. Its greatest potential occurs at the start of the scour (i.e., the pile cap is closest to the bed at the start of the scour); therefore, the bed is not lowered by the column scour depth when computing D^*_{pc}. The procedure for computing D^*_{pc}, is presented in Steps A through E below.

A. Compute pile cap shape coefficient, K_s using Equation 4.9.

$$K_s = \begin{cases} 1 & \text{for circular pile caps} \\ 0.86 + 0.97\left|\alpha\dfrac{\pi}{180^o} - \dfrac{\pi}{4}\right|^4 & \text{for rectangular pile caps} \end{cases} \qquad 4.9$$

B. Compute the pile cap skew angle coefficient, K_α, using Equation 4.10.

$$K_\alpha = \frac{b_{pc}\cos(\alpha) + l_{pc}\sin(\alpha)}{b_{pc}} \qquad 4.10$$

where α is the angle between the column axis and the flow direction. Equation 4.10 is valid for $0^o \le \alpha \le 90^o$.

C. Compute $y_{0(max)}$ for the pile cap using Equation 4.11.

$$y_{0(max)} = \begin{cases} 1.64\left(T\left(K_s b_{pc}\right)^{\frac{5}{2}}\right)^{\frac{2}{7}} & y_o \ge 1.64\left(T\left(K_s b_{pc}\right)^{\frac{5}{2}}\right)^{\frac{2}{7}} \\ y_o & y_o < 1.64\left(T\left(K_s b_{pc}\right)^{\frac{5}{2}}\right)^{\frac{2}{7}} \end{cases} \qquad 4.11$$

D. Determine if the pile cap contributes to the complex pier total effective diameter.

$$\text{If } \begin{cases} H_{pc} \ge y_{0(max)},\ D^*_{pc}=0,\ \text{proceed to Section 4.2.1.3} \\ \text{otherwise proceed to Step E} \end{cases} \qquad 4.12$$

E. Compute the effective diameter of the pile cap, D^*_{pc}, using Equation 4.13 and noting that $-1 \le H_{pc} / y_{o(max)} \le 1$ and $0 \le T / y_{o(max)} \le 1$.

$$D^*_{pc} = K_s K_\alpha b_{pc} \, exp\left[-1.04 - 1.77 \, exp\left(\frac{H_{pc}}{y_{0(max)}} \right) + 1.695 \left(\frac{T}{y_{0(max)}} \right)^{\frac{1}{2}} \right] \qquad 4.13$$

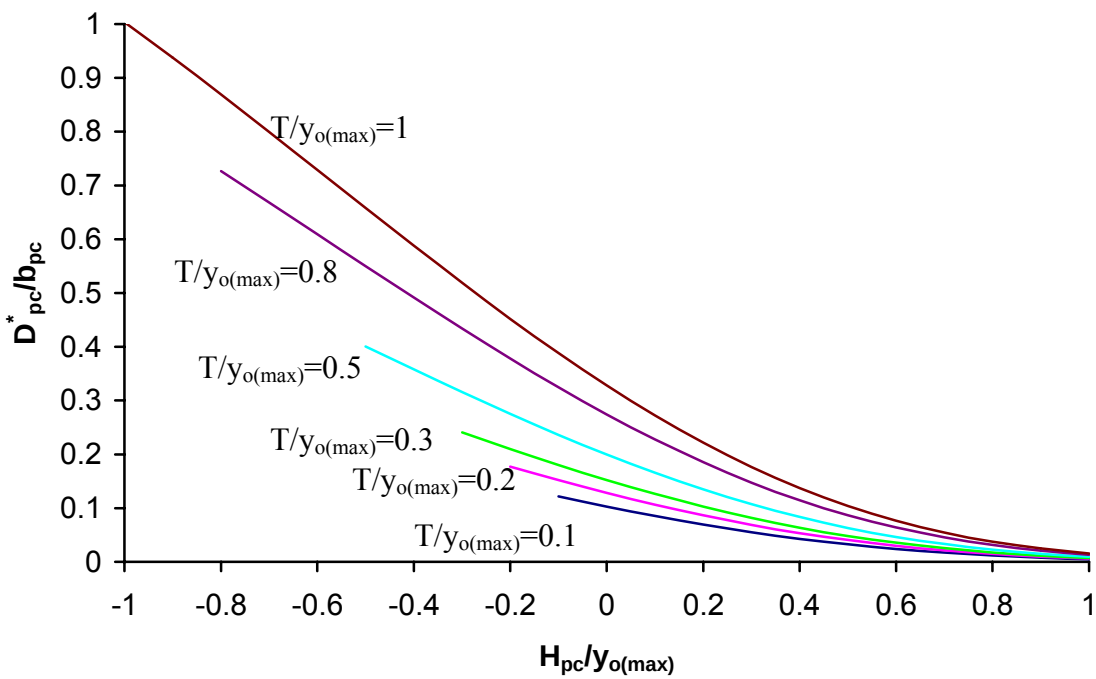

Figure 4-9 Graph of normalized pile cap effective diameter.

4.2.1.3. Effective Diameter of the Pile Group

The scour potential of the pile group (and thus the magnitude of D^*_{pg}) increases with increasing exposure of the group to the flow. The pile group's greatest exposure to the flow occurs after the bed is scoured by the column and pile cap. For this reason the bed is lowered by the scour depth produced by the column and pile cap prior to

computing D^*_{pg}. To compute the scour depth produced by the column and pile cap an effective diameter for the combination is obtained by summing their individual effective diameters:

$$D^*_{(col+pc)} = D^*_{col} + D^*_{pc} \qquad 4.14$$

The scour depth produced by the combination, $y_{s(col+pc)}$, can be computed using Equations 3.4-3.15. This depth is then added to both H_{pg} and y_o as shown in Equation 4.15 and 4.16.

$$\overline{H}_{pg} = H_{pg} + y_{s(col+pc)} \qquad 4.15$$

$$\overline{y}_0 = y_o + y_{s(col+pc)} \qquad 4.16$$

The pile group differs from the column and pile cap in that it is composed of several piles and the arrangement of these piles can have a different shape from that of the individual piles. For example, there can be a rectangular array of circular piles. As the spacing between the piles becomes small the group takes on the shape of the array rather than that of the individual piles. Likewise, as the spacing becomes large it is the shape of the individual pile that is important. The shape factor for the pile group, K_s, takes this into consideration. The procedure for computing the effective diameter for the pile group, D^*_{pg}, is described in Steps A through I below.

A. Calculate the scour produced by the combination of the column and pile cap effective diameter, $y_{s(col+pc)}$, using Equation 4.14 to compute $D^*_{(col+pc)}$ and using Equations 3.4-3.15 to compute the scour depth.

B. Calculate the $\overline{H}_{pg}$ and $\overline{y}_0$ using Equation 4.15 and 4.16.

C. Calculate the shape factor for the pile group using Equations 4.17 and 4.18.

$$K_s = \frac{K_{s\,(pile)} - K_{s(pile\ group)}}{9}\left(\frac{s}{b}\right) + K_{s(pile)} - \frac{10}{9}\left(K_{s\,(pile)} - K_{s(pile\ group)}\right) \qquad 4.17$$

where,

$$K_{s(\text{pile or pile group})} = \begin{cases} 1 & \text{for circular piles or pile group arrays} \\ 0.86 + 0.97\left|\alpha\frac{\pi}{180^{o}} - \frac{\pi}{4}\right|^{4} & \text{for square piles or rectangular pile group arrays} \end{cases} \qquad 4.18$$

D. Calculate the projected width of the pile group, W_p, as illustrated in Figure 4-10.

The projected width of the pile group is the sum of the projections of the non-overlapping widths of the individual piles in the first 2 rows and the first column on a plane normal to the flow direction.

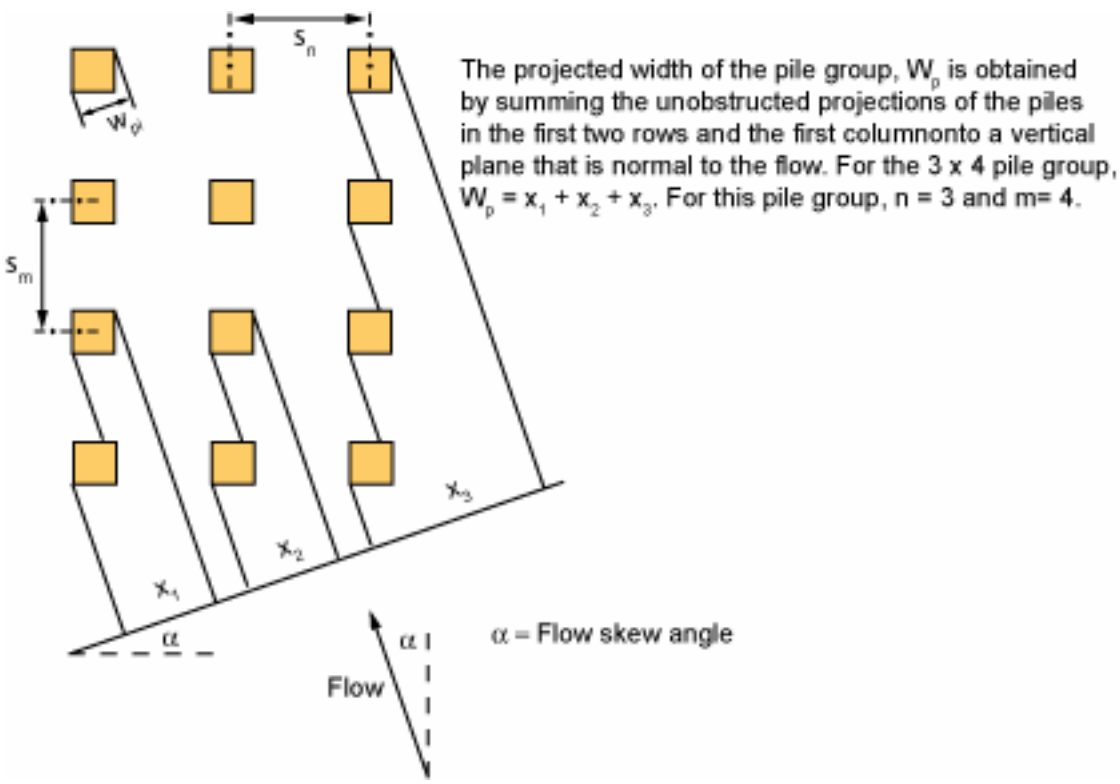

Figure 4-10 Diagram illustrating the projected width of a pile group, W_p.

E. Calculate the pile spacing coefficient, K_{sp}, using Equation 4.19. When the spacing between piles varies ($s_n \neq s_m$), use the smallest centerline spacing for s in Equation 4.19.

$$K_{sp} = 1 - \frac{4}{3}\left(1 - \frac{w_{pi}}{W_p}\right)\left(1 - \frac{1}{\left(\frac{s}{w_{pi}}\right)^{0.6}}\right) \qquad 4.19$$

F. Compute K_m for the pile group using Equation 4.20. K_m accounts for the number of piles inline with the flow for small skew angles. If the skew angle is greater then 5 degrees Km =1.

$$K_m = \begin{cases} 0.045(m) + 0.96 & |\alpha| < 5^o, \text{and } m \le 5 \\ 1.19 & |\alpha| < 5^o, \text{and } m > 5 \\ 1 & |\alpha| > 5^o \end{cases} \qquad 4.20$$

G. Compute $\overline{y}_{0(max)}$ using Equation 4.21.

$$\overline{y}_{0(max)} = \begin{cases} \overline{y}_0 & \text{for } \overline{y}_0 \le 2K_s\ W_p\ K_{sp}\ K_m \\ 2K_s\ W_p\ K_{sp}\ K_m & \text{for } \overline{y}_0 > 2K_s\ W_p\ K_{sp}\ K_m \end{cases} \qquad 4.21$$

H. Compute K_h using Equation 4.22. Note that the maximum value of $H_{pg}/y_{0(max)}$ is 1. If the calculated ratio is greater than 1, then set it equal to 1 in Equation 4.22.

$$K_h = \begin{cases} 1.5\,tanh\left(0.8\sqrt{\frac{\overline{H}_{pg}}{\overline{y}_{0(max)}}}\right) & \text{for } 0 \le \frac{\overline{H}_{pg}}{\overline{y}_{0(max)}} \le 1 \\ 0 & \text{for } \frac{\overline{H}_{pg}}{\overline{y}_{0(max)}} < 0 \\ 1 & \text{for } \frac{\overline{H}_{pg}}{\overline{y}_{0(max)}} > 1 \end{cases} \qquad 4.22$$

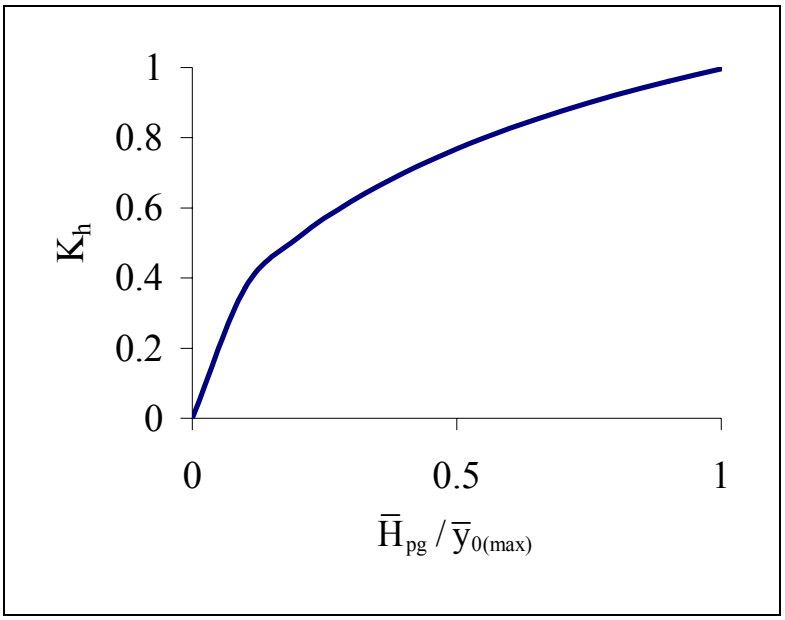

Figure 4-11 Graph of K_h versus $H_{pg}/y_{0(max)}$.

I. Compute D^*_{pg} using Equation 4.23.

$$D^*_{pg} = K_{sp} K_h K_m K_s W_p \qquad 4.23$$

4.2.1.4. Equilibrium Local Scour Depth at a Case 1 Complex Pier

Once the effective diameters for the complex pier components have been computed the overall effective diameter, D^*, can be computed using Equation 4.24.

$$D^* \equiv D^*_{col} + D^*_{pc} + D^*_{pg} \qquad 4.24$$

The equilibrium local scour depth prediction for the complex pier is then computed by substituting D^* from Equation 4.24 and the flow and sediment parameters of interest into Equations 3.4 – 3.6.

4.2.1.5. Case 1 Example Problem

This section presents an example calculation for a typical complex pier as illustrated in Figure 4-12. The flow and sediment variables used for the calculations are listed in Table 4-1.

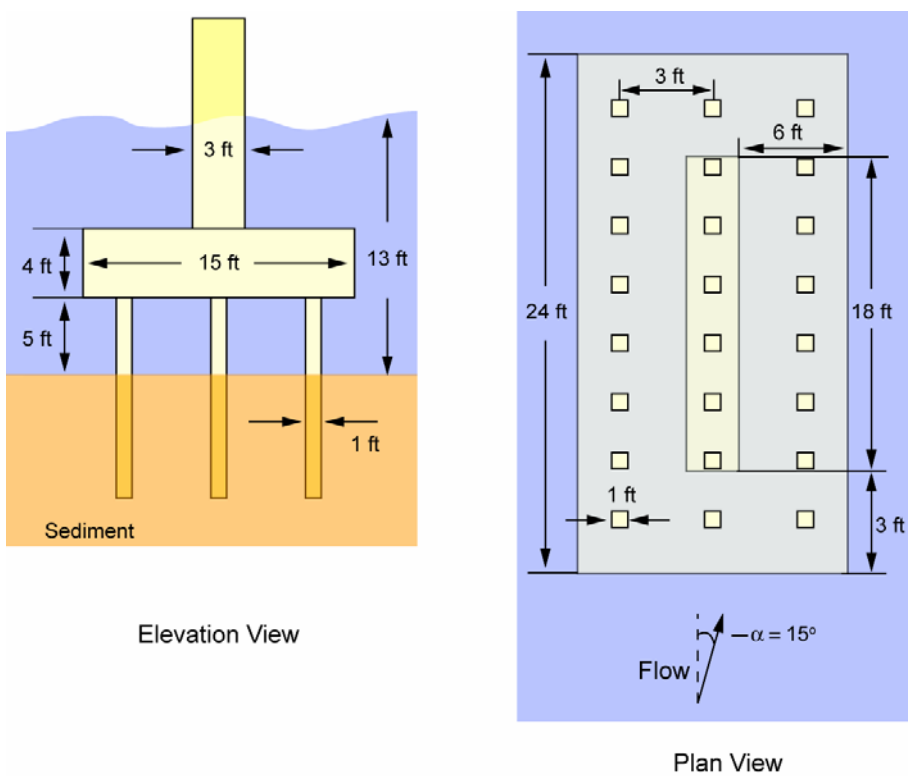

Figure 4-12 Elevation and plan view of the complex pier used in the Case 1 example scour calculation.

Table 4-1 Flow and sediment inputs for the example calculation.

Skew Angle Degrees	Velocity (ft/s)	Critical Velocity (ft/s)	Live Bed Peak Velocity (ft/s)	Water Depth (ft)	Temp (F^o)	Salinity (ppt)	D_{50} (mm)
15	11.0	1.16	16.36	13	65	35	0.20

A. Calculate $y_{o(max)}$ for the column.

$$y_{0(max)} = \begin{cases} 5\,b_{col} & \text{for } y_o \geq 5\,b_{col} \\ y_o & \text{for } y_o < 5\,b_{col} \end{cases}$$

$$5\,b_{col} = 5(3\text{ ft}) = 15\text{ ft} \quad \text{and } y_o = 13\text{ ft}$$

$$\text{Since } y_o < 5\,b_{col}, \quad y_{0(max)} = y_o = 13\text{ ft}$$

B. Compare the column's base height, H_{col}, to $y_{0(max)}$. If $H_{col} < y_{0(max)}$ continue on to step C.

$$H_{col} = 9\text{ft}, \; y_{o(max)} = 13\text{ft}$$

$$\text{Since } H_{col} < y_{o(max)} \text{ so continue on to step C}$$

C. Compute the shape factor for the square column, K_s.

$$K_s = 0.86 + 0.97\left|15^o \frac{\pi}{180^o} - \frac{\pi}{4}\right|^4 = 0.93$$

D. Compute the column skew coefficient, K_α.

$$K_\alpha = \frac{3\text{ ft}\,cos(15^o) + 18\text{ ft}\,sin(15^o)}{3\text{ft}} = 2.52$$

E. Calculate the pile cap extension coefficient, K_f.

$$f = \frac{3f_1 + f_2}{4} \quad \text{for } \alpha \leq 45^0$$

$$f = \frac{3(3\text{ ft}) + (6\text{ ft})}{4} = 3.75\text{ ft}$$

$$K_f = -0.12\left(\frac{3.38\text{ ft}}{3\text{ ft}}\right)^2 + 0.03\left(\frac{3.38\text{ ft}}{3\text{ ft}}\right) + 1 = 0.85$$

F. Compute the column effective diameter, D^*_{col}.

$$D^*_{col} = K_s K_\alpha K_f b_{col}\left[0.1162\left(\frac{H_{col}}{y_{0(max)}}\right)^2 - 0.3617\left(\frac{H_{col}}{y_{0(max)}}\right) + 0.2476\right]$$

$$D^*_{col} = (0.93)(2.52)(0.85)(3\text{ ft})\left[0.1162\left(\frac{9\text{ ft}}{13\text{ ft}}\right)^2 - 0.3617\left(\frac{9\text{ ft}}{13\text{ ft}}\right) + 0.2476\right] = 0.32\text{ ft}$$

Next, the pile cap effective diameter is calculated below following Steps A-E in Section 4.2.1.2.

A. Compute the shape factor for the square pile cap, K_s.

$$K_s = 0.86 + 0.97\left|15^\circ\frac{\pi}{180^\circ} - \frac{\pi}{4}\right|^4 = 0.93$$

B. Compute the column skew coefficient, K_α.

$$K_\alpha = \frac{15\text{ ft}\cos(15^\circ) + 24\text{ ft}\sin(15^\circ)}{15\text{ ft}} = 1.38$$

C. Compute $y_{o(max)}$ for the pile cap..

$$y_{0(max)} = \begin{cases} 1.64\left(T\left(K_s b_{pc}\right)^{\frac{5}{2}}\right)^{\frac{2}{7}} & y_o \geq 1.64\left(T\left(K_s b_{pc}\right)^{\frac{5}{2}}\right)^{\frac{2}{7}} \\ y_o & y_o < 1.64\left(T\left(K_s b_{pc}\right)^{\frac{5}{2}}\right)^{\frac{2}{7}} \end{cases}$$

$y_o = 13\text{ ft},$

$$1.64\left(4\text{ ft}\left(0.93*15\text{ ft}\right)^{\frac{5}{2}}\right)^{\frac{2}{7}} = 16.01\text{ ft}$$

Therefore,

$y_{0(max)} = y_o = 13\text{ ft}$

D. Determine if $H_{pc} < y_{o(max)}$.

Since $H_{pc} < y_{o(max)}$, continue to Step E.

E. Compute the pile cap effective diameter, D^*_{pc}.

$$D^*_{pc} = K_s\, K_\alpha\, b_{pc}\, exp\left[-1.04 - 1.77\, exp\left(\frac{H_{pc}}{y_{0(max)}}\right) + 1.695\left(\frac{T}{y_{0(max)}}\right)^{\frac{1}{2}}\right]$$

$$D^*_{pc} = \left(0.93\right)\left(1.38\right)\left(15\text{ ft}\right) exp\left[-1.04 - 1.77\, exp\left(\frac{5\text{ ft}}{13\text{ ft}}\right) + 1.695\left(\frac{4\text{ ft}}{13\text{ ft}}\right)^{\frac{1}{2}}\right]$$

$D^*_{pc} = 1.29\text{ ft}$

Finally, the effective diameter for the pile group, D^*_{pg}, is calculated below following Steps A-I in Section 4.2.1.3.

A. Calculate the scour created by the combination of the column and pile cap. This is accomplished by first adding the two effective diameters and then calculating the scour with the computed effective diameter.

$$D^*_{(col+pc)} = D^*_{col} + D^*_{pc} = 0.33\text{ ft} + 1.29\text{ ft} = 1.62\text{ ft}$$

$$\frac{y_s}{D^*_{(col+pc)}} = \tanh\left[\left(\frac{y_o}{D^*_{(col+pc)}}\right)^{0.4}\right] \times \left[\begin{array}{l} 2.2\left(\dfrac{V/V_c - 1}{V_{lp}/V_c - 1}\right) + \\ 2.5\left\{\dfrac{D^*_{(col+pc)}/D_{50}}{0.4\left(D^*_{(col+pc)}/D_{50}\right)^{1.2} + 10.6\left(D^*_{(col+pc)}/D_{50}\right)^{-0.13}}\right\} \\ \left(\dfrac{V_{lp}/V_c - V/V_c}{V_{lp}/V_c - 1}\right) \end{array}\right]$$

$$\frac{y_s}{1.62\text{ ft}} = tanh\left[\left(\frac{13\text{ ft}}{1.62\text{ ft}}\right)^{0.4}\right] \times \left[\begin{array}{l} 2.2\left(\dfrac{11\frac{ft}{s}/1.16\frac{ft}{s} - 1}{16.36\frac{ft}{s}/1.16\frac{ft}{s} - 1}\right) + \\ 2.5\left\{\dfrac{1.62\text{ ft}/6.56\text{ x }10^{-4}\text{ ft}}{0.4\left(1.62\text{ ft}/6.56\text{ x }10^{-4}\text{ ft}\right)^{1.2} + 10.6\left(1.62\text{ ft}/6.56\text{ x }10^{-4}\text{ ft}\right)^{-0.13}}\right\} \\ \left(\dfrac{16.36\frac{ft}{s}/1.16\frac{ft}{s} - 11\frac{ft}{s}/1.16\frac{ft}{s}}{16.36\frac{ft}{s}/1.16\frac{ft}{s} - 1}\right) \end{array}\right]$$

$y_{s(col+pc)} = 2.98$ ft

B. Calculate the $\overline{H}_{pg}$ and $\overline{y}_0$ using Equation 4.15 and 4.16.

$$\overline{H}_{pg} = H_{pg} + y_{s(col+pc)} = 5\text{ ft} + 2.98\text{ ft} = 7.98\text{ ft}$$
$$\overline{y}_0 = y_o + y_{s(col+pc)} = 13\text{ ft} + 2.98\text{ ft} = 15.98\text{ ft}$$

C. Compute the shape factor for the pile group, K_s. K_s accounts for the shape of the pile group and the shape of the individual piles.

$$K_s = \frac{K_{s(pile)} - K_{s(pile\ group)}}{9}\left(\frac{s}{b}\right) + K_{s(pile)} - \frac{10}{9}\left(K_{s(pile)} - K_{s(pile\ group)}\right),$$

$$K_{s(\text{pile or pile group})} = \begin{cases} 1 & \text{for circular piles or pile group arrays} \\ 0.86+0.97\left|\alpha\dfrac{\pi}{180^0}-\dfrac{\pi}{4}\right|^4 & \text{for square piles or pile group arrays} \end{cases}$$

Since both the individual piles and pile group are both square, the shape factor will be the same for both.

$$K_{s(\text{pile})} = 0.86+0.97\left|15^o\frac{\pi}{180^o}-\frac{\pi}{4}\right|^4 = 0.93$$

$$K_{s(\text{pilegroup})} = 0.86+0.97\left|15^o\frac{\pi}{180^o}-\frac{\pi}{4}\right|^4 = 0.93$$

$$K_s = \frac{0.93-0.93}{9}\left(\frac{6\text{ ft}}{2\text{ ft}}\right)+0.93-\frac{10}{9}(0.93-0.93) = 0.93$$

D. Calculate the projected width of the pile group.

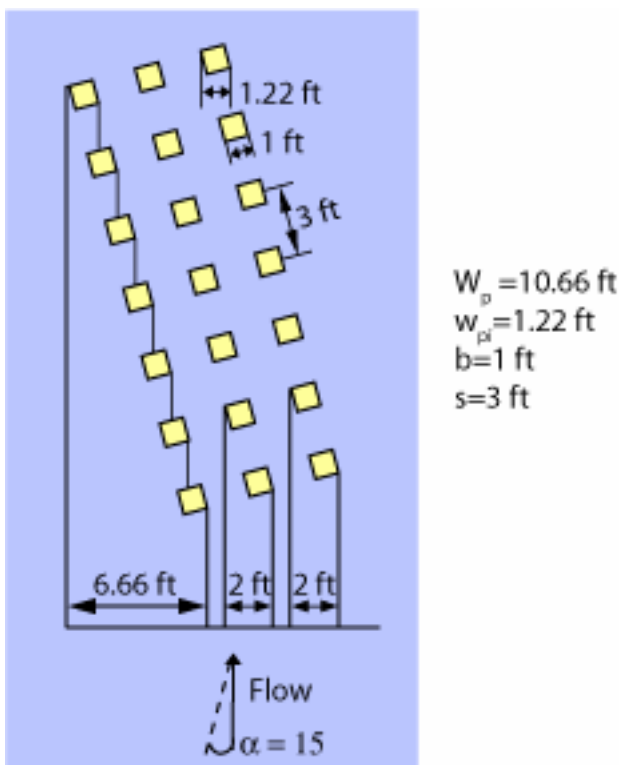

Figure 4-13 The Projected Width of the Pile Group

E. Calculate the pile spacing coefficient, K_{sp}.

$$K_{sp} = 1 - \frac{4}{3}\left(1 - \frac{w_{pi}}{W_p}\right)\left(1 - \frac{1}{\left(\frac{s}{w_{pi}}\right)^{0.6}}\right) = 1 - \frac{4}{3}\left(1 - \frac{1.22\text{ ft}}{10.66\text{ ft}}\right)\left(1 - \frac{1}{\left(\frac{3\text{ ft}}{1.22\text{ ft}}\right)^{0.6}}\right) = 0.51$$

F. Calculate K_m coefficient that accounts for the number of piles in line with the flow.

$$K_m = \begin{cases} 0.045(m) + 0.96 & |\alpha| < 5^0, \text{and } m \le 5 \\ 1.19 & |\alpha| < 5^0, \text{and } m > 5 \\ 1 & |\alpha| > 5^0 \end{cases}$$

$\alpha = 15^0$, therefore $K_m = 1$

G. Compute $\overline{y}_{0(max)}$ for the pile group.

$$\overline{y}_{0(max)} = \begin{cases} \overline{y}_0 & \text{for } \overline{y}_0 \le 2K_s\ W_p\ K_{sp}\ K_m \\ 2K_s\ W_p\ K_{sp}\ K_m & \text{for } \overline{y}_0 > 2K_s\ W_p\ K_{sp}\ K_m \end{cases}$$

$2K_s\ W_p\ K_{sp}\ K_m = 2(0.93)(10.66\text{ ft})(0.51)(1) = 10.11\text{ ft}$

$\overline{y}_0 = 15.98\text{ ft}$,

therefore,

$\overline{y}_{0(max)} = 10.11\text{ft}$

H. Compute the submerged pile group coefficient, K_h.

$$K_h = 1.5\ tanh\left(0.8\sqrt{\frac{8\text{ ft}}{10.11\text{ ft}}}\right) = 0.92$$

I. Compute the pile group effective diameter, D^*_{pg}.

$$D^*_{pg} = K_{sp}K_hK_mK_sW_p = (0.51)(0.92)(1)(0.93)(10.66\text{ ft}) = 4.65\text{ ft}$$

The effective diameter of the complex pier is the sum of each component effective diameter.

$$D^* \equiv D^*_{col} + D^*_{pc} + D^*_{pg}$$
$$D^* = 0.32\,\text{ft} + 1.29\,\text{ft} + 4.65\text{ft} = 6.26\,\text{ft}$$

The total scour for the complex pier is computed using the flow conditions listed in Table 4-1 and an effective diameter of 6.26 ft in Equations 3.4 through 3.6.

$$\frac{y_s}{6.26\text{ ft}} = tanh\left[\left(\frac{13\text{ ft}}{6.26\text{ ft}}\right)^{0.4}\right] \times \left[\begin{array}{l} 2.2\left(\dfrac{11\frac{\text{ft}}{\text{s}}/1.16\frac{\text{ft}}{\text{s}}-1}{16.36\frac{\text{ft}}{\text{s}}/1.16\frac{\text{ft}}{\text{s}}-1}\right)+ \\ 2.5\left\{\dfrac{6.26\text{ ft}/6.56\text{ x }10^{-4}\text{ ft}}{0.4\left(6.26\text{ ft}/6.56\text{ x }10^{-4}\text{ ft}\right)^{1.2}+10.6\left(6.26\text{ ft}/6.56\text{ x }10^{-4}\text{ ft}\right)^{-0.13}}\right\} \\ \left(\dfrac{16.36\frac{\text{ft}}{\text{s}}/1.16\frac{\text{ft}}{\text{s}}-11\frac{\text{ft}}{\text{s}}/1.16\frac{\text{ft}}{\text{s}}}{16.36\frac{\text{ft}}{\text{s}}/1.16\frac{\text{ft}}{\text{s}}-1}\right) \end{array}\right]$$

The resulting local scour depth for the complex pier is **9.69 ft**.

4.2.2. Complex Pier Local Scour Depth Prediction - Case 2 Piers (Partially Buried Pile Cap)

The methodology for computing local scour depth at a complex pier with a partially buried pile cap, as shown in Figure 4-5, is described in this section. Because the shape of the structure exposed to the flow changes as the local scour progresses, an iterative scheme must be used to determine the effective diameter of the structure. For this case the effective diameter will also depend on the flow and sediment parameters.

4.2.2.1. Effective Diameter of the Column

The procedure for calculating the effective diameter of the column is described in this section. Since the bottom of the column is above the bed for Case 2 piers the procedure for computing D^*_{col} is the same as for Case 1 piers. However, for completeness, the procedure is repeated below.

A. Calculate $y_{0(max)}$ for the column. Equilibrium scour depth for a given structure depends on the water depth up to a certain depth. This limiting depth, denoted by $y_{0(max)}$ depends on the structure size and its location relative to the bed and can be estimated using Equation 4.25.

$$y_{0(max)} = \begin{cases} 5\,b_{col} & \text{for } y_o \geq 5\,b_{col} \\ y_o & \text{for } y_o < 5\,b_{col} \end{cases} \qquad 4.25$$

B. Compare the column's base height, H_{col}, to $y_{0(max)}$. If H_{col} is greater than $y_{0(max)}$, set $D^*_{col} = 0$ and proceed to the computation of the pile cap effective diameter, D^*_{pc}. The column will not influence the overall structure's effective diameter unless the base of the column lies below $y_{0(max)}$. That is:

$$\text{If} \begin{cases} H_{col} > y_{0(max)}, \ D^*_{col} = y_{s(col)} = 0, \text{ proceed to Section 4.2.2.2.} \\ H_{col} \leq y_{0(max)}, \ \text{proceed to Step C.} \end{cases} \qquad 4.26$$

C. Compute the column's shape factor, K_s, with Equation 4.27

$$K_s = \begin{cases} 1 & \text{for circular columns} \\ 0.86 + 0.97\left|\alpha \dfrac{\pi}{180^o} - \dfrac{\pi}{4}\right|^4 & \text{for rectangular columns} \end{cases} \qquad 4.27$$

where α is the flow skew angle between the axis of the column and the flow direction. Equation 4.27 is valid for $0^o \leq \alpha \leq 90^o$.

D. Compute the column's skew factor, K_α, with Equation 4.28.

$$K_\alpha = \frac{b_{col}\cos(\alpha) + l_{col}\sin(\alpha)}{b_{col}} \qquad 4.28$$

E. Compute the weighted average value of the pile cap extension (or overhang), f, using f_1 and f_2 as inputs into Equation 4.29 (see Figure 4-6). The non-dimensional ratio of f/b_{col} is then used in Equation 4.30 to calculate the pile cap

extension factor, K_f. K_f attenuates the column's effective diameter as the ratio of f/b_{col} increases. The column's contribution to the scour hole is reduced to zero for values of $f/b_{col} > 3$.

$$f = \begin{cases} \dfrac{3f_1 + f_2}{4} & \text{for } \alpha \le 45^o \\ \dfrac{3f_2 + f_1}{4} & \text{for } \alpha > 45^o \end{cases} \qquad 4.29$$

$$K_f = \begin{cases} -0.12\left(\dfrac{f}{b_{col}}\right)^2 + 0.03\left(\dfrac{f}{b_{col}}\right) + 1 & \text{for } 0 \le \dfrac{f}{b_{col}} \le 3 \\ 0 & \text{for } \dfrac{f}{b_{col}} > 3 \end{cases} \qquad 4.30$$

F. Once the coefficients K_s, K_α and K_f are known D^*_{col} can be computed using Equation 4.31.

$$D^*_{col} = \begin{cases} K_s\, K_\alpha\, K_f\, b_{col}\left[0.1162\left(\dfrac{H_{col}}{y_{0(max)}}\right)^2 - 0.3617\left(\dfrac{H_{col}}{y_{0(max)}}\right) + 0.2476\right] & \text{for } 0 \le \dfrac{H_{col}}{y_{0(max)}} \le 1 \\ 0 & \text{for } \dfrac{H_{col}}{y_{0(max)}} > 1 \end{cases} \qquad 4.31$$

4.2.2.2. Effective Diameter of the Pile Cap

The procedure for calculating the effective diameter for a pile cap, D^*_{pc}, is presented below in steps A through L. This procedure is applied to pile caps that are partially buried relative to the pre-locally scoured bed ($-T < H_{pc} < 0$). The procedure for computing D^*_{pc} for Case 2 piers is different from that used for Case 1 piers. For Case 2 piers iterative calculations can be necessary since the shape and size of the structure exposed to the flow can change as the local scour progresses. The pile cap thickness, denoted by T', is considered to be the distance from the top of the pile cap to the bottom of the scour hole during each iteration until either the scour depth reaches an equilibrium value or the bottom of the pile cap is uncovered. Likewise the height of the pile cap,

denoted by H'_{pc}, is considered to be the distance from the pre-locally scoured bed to the bottom of the scour hole until an equilibrium scour is reached or the pile cap is uncovered. Figure 4-14 is a definition sketch for T' and H'_{pc}. Another unique feature of D^*_{pc} for this case is that its magnitude depends on all of the structure, sediment and flow parameters that affect the scour depth. Therefore, the effective diameter obtained in the following analysis is, in general, only valid for the flow and sediment conditions used in the analysis.

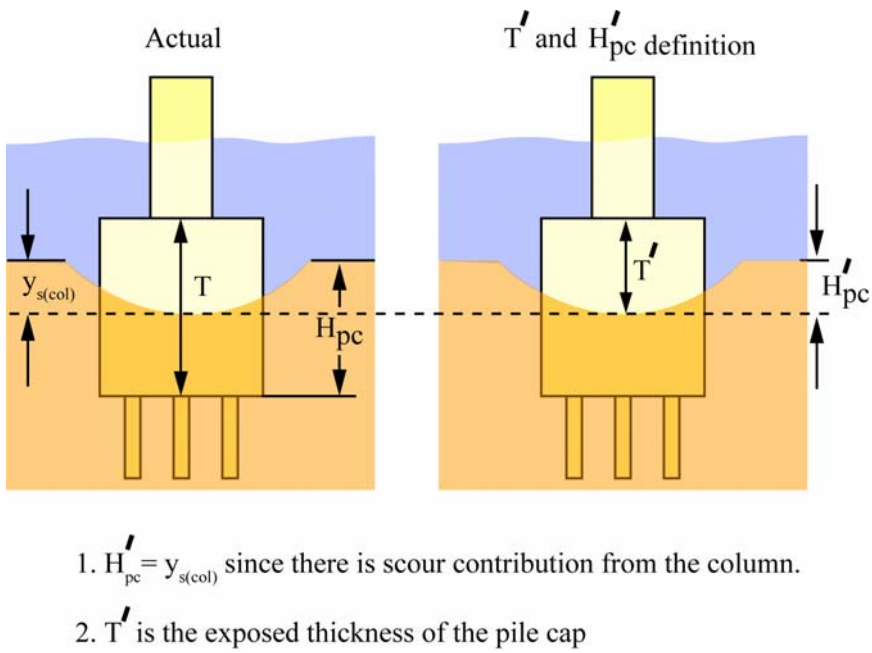

Figure 4-14 Definition sketch for T' and H'_{pc}.

The procedure for computing D^*_{pc} is presented in Steps A–N below.

A. Compute the scour depth produced by the column, $y_{s(col)}$, using Equations 3.4 - 3.15 with D^* replaced by D^*_{col} from Equation 4.31. Note that the water depth, y_0, in Equations 3.4 - 3.15 is the actual water depth just upstream of the structure.

B. Calculate the pile cap's shape factor, K_s using Equation 4.32.

$$K_s = \begin{cases} 1 & \text{for circular pile caps} \\ 0.86 + 0.97\left|\alpha \dfrac{\pi}{180^o} - \dfrac{\pi}{4}\right|^4 & \text{for rectangular pile caps} \end{cases} \qquad 4.32$$

C. Calculate the pile cap's skew angle coefficient, K_α, using Equation 4.33.

$$K_\alpha = \frac{b_{pc}\, cos(\alpha) + l_{pc}\, sin(\alpha)}{b_{pc}} \qquad 4.33$$

where α is the flow's skew angle (angle between the column axis and the flow direction).

D. Check to see if the scour depth due to the column, $y_{s(col)}$, uncovers the bottom of the pile cap.

$$\text{If} \begin{cases} y_{s(col)} \geq |H_{pc}|, & \text{pile cap bottom uncovered, proceed to Step E} \\ y_{s(col)} < |H_{pc}|, & \text{proceed to Step F} \end{cases} \qquad 4.34$$

E. Compute $y_{0(max)}$ and D^*_{pc} using Equations 4.35 and 4.36.

$$y_{0(max)} = \begin{cases} 1.64\left(T\left(K_s b_{pc}\right)^{\frac{5}{2}}\right)^{\frac{2}{7}} & y_o \geq 1.64\left(T\left(K_s b_{pc}\right)^{\frac{5}{2}}\right)^{\frac{2}{7}} \\ y_o & y_o < 1.64\left(T\left(K_s b_{pc}\right)^{\frac{5}{2}}\right)^{\frac{2}{7}} \end{cases} \text{ and} \qquad 4.35$$

$$D^*_{pc} = K_s\, K_\alpha\, b_{pc}\, exp\left[-1.04 - 1.77\, exp\left(\frac{H_{pc}}{y_{0(max)}}\right) + 1.695\left(\frac{T}{y_{0(max)}}\right)^{\frac{1}{2}}\right]. \qquad 4.36$$

Note that $-1 \leq H_{pc} / y_{o(max)} \leq 1$ and $0 \leq T / y_{o(max)} \leq 1$.

Proceed to Section 4.2.2.3

F. Compute T' and H'_{pc} using Equations 4.37 and 4.38 (see definition sketch in Figure 4-14).

$$H'_{pc} = -y_{s(col)} \tag{4.37}$$

$$T' = T + H_{pc} - H'_{pc} \tag{4.38}$$

Note that T and T' are always positive. H_{pc} and H'_{pc} are always negative for partially buried pile caps.

G. Calculate $y_{0(max)(i)}$ for the pile cap using Equation 4.39. The subscript "i" refers to the number of iterations (e.g. i = 1 for the first iteration, 2 for the second, etc.).

$$y_{0(max)(i)} = \begin{cases} 1.64\left(T'\left(K_s b_{pc}\right)^{\frac{5}{2}}\right)^{\frac{2}{7}} & y_o \geq 1.64\left(T'\left(K_s b_{pc}\right)^{\frac{5}{2}}\right)^{\frac{2}{7}} \\ y_o & y_o < 1.64\left(T'\left(K_s b_{pc}\right)^{\frac{5}{2}}\right)^{\frac{2}{7}} \end{cases} \tag{4.39}$$

H. Compute the pile cap's effective diameter using Equation 4.40. Note that $-1 \leq H'_{pc} / y_{o(max)(i)} \leq 1$ and $0 \leq T' / y_{o(max)(i)} \leq 1$ in equation 4.40.

$$D^*_{pc(i)} = K_s\, K_\alpha\, b_{pc}\, exp\left[-1.04 - 1.77\, exp\left(\frac{H'_{pc}}{y_{0(max)(i)}}\right) + 1.695\left(\frac{T'}{y_{0(max)(i)}}\right)^{\frac{1}{2}}\right] \tag{4.40}$$

I. Compute the effective diameter of the column and the portion of the pile cap above the bed.

$$D^*_{(col+pc)(i)} = D^*_{col} + D^*_{pc(i)} \tag{4.41}$$

J. Compute the scour depth due to the column and the portion of the pile cap above the bed, $Y_{s(col+pc)(i)}$, using Equations 3.4 - 3.15 with D^* replaced by $D^*_{(col+pc)(i)}$ from

Equation 4.41. Note that Y_s (instead of y_s) is used for scour depth in the iterative calculations.

K. Compute H'_{pc} and T' using Equations 4.42 and 4.43.

$$H'_{pc} = \begin{cases} H_{pc} & Y_{s(col+pc)(i)} \geq \left|H_{pc}\right| \\ -Y_{s(col+pc)(i)} & Y_{s(col+pc)(i)} < \left|H_{pc}\right| \end{cases} \qquad 4.42$$

$$T' = \begin{cases} T & Y_{s(col+pc)(i)} \geq \left|H_{pc}\right| \\ T + H_{pc} - H'_{pc} & Y_{s(col+pc)(i)} < \left|H_{pc}\right| \end{cases} \qquad 4.43$$

L. Check for convergence using Equation 4.44.

If $i = 1$, proceed to Step G above using the values for T' and H'_{pc} computed in Step K above.

If $i > 1$

1) Compute $\Delta \equiv \left| \dfrac{Y_{s(col+pc)(i)} - Y_{s(col+pc)(i-1)}}{Y_{s(col+pc)(i-1)}} \right|$ 4.44

2) If $\begin{cases} \Delta \leq 0.05 \text{ proceed to Step M below} \\ \Delta > 0.05 \text{ proceed to Step G above} \end{cases}$

M. Pile Cap Summary

$$\begin{aligned} D^*_{pc} &= D^*_{pc(i)} \\ D^*_{(col+pc)} &= D^*_{(col+pc)(i)} \\ y_{s(col+pc)} &= Y_{s(col+pc)(i)} \end{aligned} \qquad 4.45$$

N. Determine if pile group is exposed.

$$\text{If } \begin{cases} y_{s(col+pc)} \leq \left|H_{pg}\right|, D^*_{pg} = 0, \text{ proceed to 4.2.2.4} \\ y_{s(col+pc)} > \left|H_{pg}\right|, \text{ pile group exposed, proceed to 4.2.2.3} \end{cases} \qquad 4.46$$

4.2.2.3. Effective Diameter of the Pile Group

For the case of a partially or fully buried pile cap the pile group is initially buried. If the scour produced by the pile cap and column is sufficient to uncover the top of the piles then the pile group will contribute to the total effective diameter of the pier. Since the only information available for local scour at pile groups is for situations where the piles protrude above the pre-locally scoured bed (i.e. there is no data for scour produced by piles exposed to the flow in a scour hole) the reference or datum from which the height of the pile group is measured must be changed as shown in Figure 4-16. The datum is no longer the pre-locally scoured bed, but rather the bottom of the scour hole produced by the column and pile cap. Likewise, the water depth is increased by the scour depth produced by the column and pile cap for purposes of computing effective diameter of the pile group, D^*_{pg}. The pile group also differs from the column and the pile cap in that it is composed of several piles and the arrangement of these piles can have a different shape from that of the individual piles. For example, there can be a rectangular array of circular piles. As the piles become closer together the group takes on the shape of the array rather than that of the individual piles. Likewise, as the spacing becomes large, it is the shape of the individual pile that is important. The shape factor, K_s, takes this into consideration. The procedure for computing the effective diameter for the pile group, D^*_{pg}, is described in Steps A through H below.

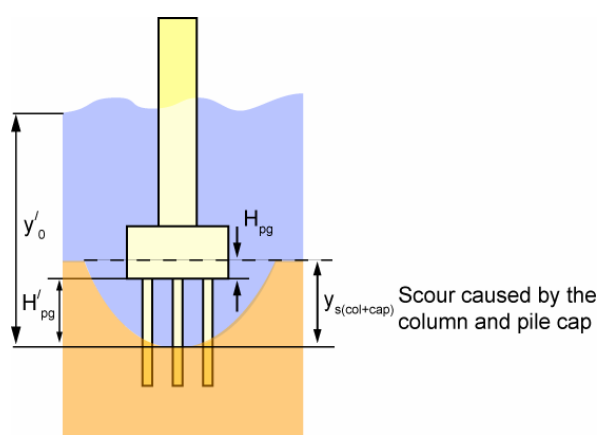

Figure 4-15 Definition sketch showing datum for pile group effective diameter, D^*_{pg}, computations.

A. Compute $\overline{H}_{pg}$ and $\overline{y}_o$ based on the datum being at the bottom of the scour hole (produced by the column and pile cap) instead of the pre-locally scoured bed.

$$\overline{H}_{pg} = H_{pg} + y_{s(col+pc)} \quad \text{and}$$
$$\overline{y}_0 = y_0 + y_{s(col+pc)} \qquad 4.47$$

Note that H_{pg} is negative and $\overline{H}_{pg}$ is positive.

B. Compute the shape factor for the pile group using Equations 4.48 and 4.49.

$$K_s = \frac{K_{s\,(pile)} - K_{s(pile\ group)}}{9}\left(\frac{s}{b}\right) + K_{s(pile)} - \frac{10}{9}\left(K_{s\,(pile)} - K_{s(pile\ group)}\right) \qquad 4.48$$

where,

$$K_{s(pile\ or\ pile\ group)} = \begin{cases} 1 & \text{for circular piles or pile group arrays} \\ 0.86 + 0.97\left|\alpha\dfrac{\pi}{180^o} - \dfrac{\pi}{4}\right|^4 & \text{for square piles or rectangular pile group arrays} \end{cases} \qquad 4.49$$

C. Compute the projected width of the pile group, W_p, as illustrated in Figure 4-10. The projected width of the pile group is the sum of the non-overlapping widths of the individual piles in the first 2 rows and first column on a plane normal to the flow direction.

D. Compute the pile spacing coefficient, K_{sp}, using Equation 4.50. Note that when the center line spacing is not uniform ($s_n \neq s_m$), use the smallest value for the centerline spacing, s, in Equation 4.50.

$$K_{sp} = 1 - \frac{4}{3}\left(1 - \frac{w_{pi}}{W_p}\right)\left(1 - \frac{1}{\left(\dfrac{s}{w_{pi}}\right)^{0.6}}\right), \qquad 4.50$$

where w_{pi} is the projected width of an individual pile.

E. Compute K_m using Equation 4.51 which accounts for the number of piles in line with the flow for skew angles less than 5°.

$$K_m = \begin{cases} 0.045(m) + 0.96 & \text{for } |\alpha| < 5^o, \text{and } m \le 5 \\ 1.19 & \text{for } |\alpha| < 5^o, \text{and } m > 5 \\ 1 & \text{for } |\alpha| \ge 5^o \end{cases} \qquad 4.51$$

F. Compute $\overline{y}_{0(max)}$ for the pile group using Equation 4.52.

$$\overline{y}_{0(max)} = \begin{cases} \overline{y}_0 & \text{for } \overline{y}_0 \le 2K_s\ W_p\ K_{sp}\ K_m \\ 2K_s\ W_p\ K_{sp}\ K_m & \text{for } \overline{y}_0 > 2K_s\ W_p\ K_{sp}\ K_m \end{cases} \qquad 4.52$$

G. Compute the pile group height coefficient, K_h using Equation 4.53. Note that if the calculated value of $\overline{H}_{pg} / \overline{y}_{0(max)}$ is greater than 1 in Equation 4.53, set it equal to 1.

$$K_h = \begin{cases} 1.5\, tanh\left(0.8\sqrt{\dfrac{\overline{H}_{pg}}{\overline{y}_{0(max)}}}\right) & \text{for } 0 \le \dfrac{\overline{H}_{pg}}{\overline{y}_{0(max)}} \le 1 \\ 0 & \text{for } \dfrac{\overline{H}_{pg}}{\overline{y}_{0(max)}} < 0 \\ 1 & \text{for } \dfrac{\overline{H}_{pg}}{\overline{y}_{0(max)}} > 1 \end{cases} \qquad 4.53$$

H. Compute the effective diameter of the pile group using Equation 4.54.

$$D^*_{pg} = K_{sp} K_h K_m K_s W_p \qquad 4.54$$

4.2.2.4. Complex Pier Effective Diameter

The effective diameter of the complete complex pier is the sum of the effective diameters of its components. As stated above for situations where the pile cap is partially or fully buried (Cases 2 and 3) the effective diameter is only valid for the flow and sediment conditions used in its computation.

$$D^* = D^*_{col} + D^*_{pc} + D^*_{pg} \qquad 4.55$$

4.2.2.5. Equilibrium Local Scour Depth at a Case 2 Complex Pier

Once the effective diameter of the complex pier has been obtained, the equilibrium local scour depth (for the conditions under which the effective diameter was determined) can be computed using Equations 3.4 - 3.15.

4.2.2.6. Case 2 Example Problem

This section details an example calculation for a typical complex pier as illustrated in Figure 4-16. The flow and sediment variables used for the calculations are listed in Table 4-2.

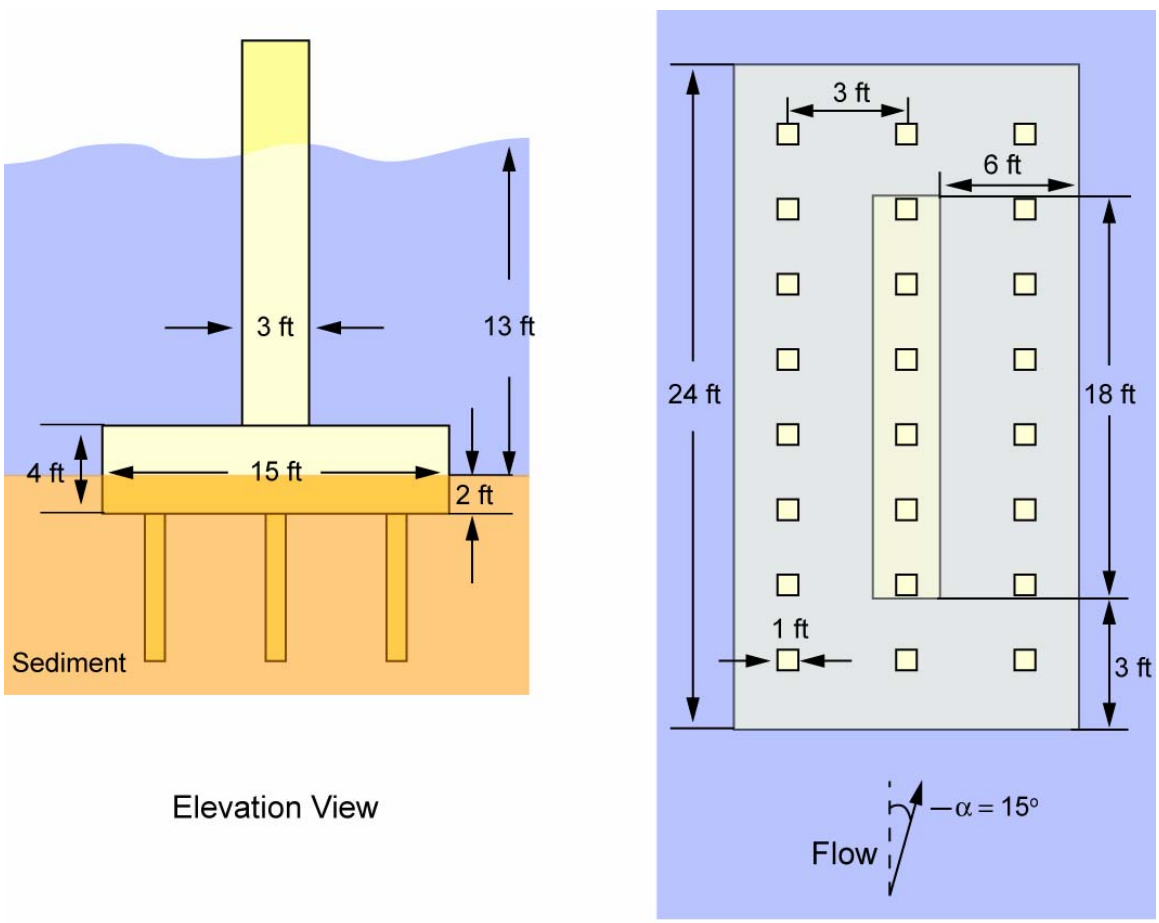

Figure 4-16 Elevation and plan view of the complex pier used in the Case 2 example scour calculation

Table 4-2 Flow and sediment inputs for the example calculation.

Skew Angle Degrees	Velocity (ft/s)	Critical Velocity (ft/s)	Live Bed Peak Velocity (ft/s)	Water Depth (ft)	Temp (F^o)	Salinity (ppt)	D_{50} (mm)
15	6.0	1.60	16.36	13	65	35	0.80

Calculate the effective diameter of the column following Steps A – F in Section 4.4.2.1.

A. Calculate $y_{o(max)}$ for the column.

$$y_{0(max)} = \begin{cases} 5\,b_{col} & \text{for } y_o \geq 5\,b_{col} \\ y_o & \text{for } y_o < 5\,b_{col} \end{cases}$$

$$5\,b_{col} = 5(3\text{ ft}) = 15\text{ ft} \quad \text{and } y_o = 13\text{ ft}$$

$$\text{Since } y_o < 5\,b_{col}, \quad y_{0(max)} = y_o = 13\text{ ft}$$

B. Compare the column's base height, H_{col}, to $y_{0(max)}$. If $H_{col} < y_{0(max)}$ continue on to Step C.

$$H_{col} = 9\text{ft}, \; y_{o(max)} = 13\text{ft}$$

$$\text{Since } H_{col} < y_{o(max)} \text{ so continue on to Step C}$$

C. Compute the shape factor for the square column, K_s.

$$K_s = 0.86 + 0.97\left|15^o \frac{\pi}{180^o} - \frac{\pi}{4}\right|^4 = 0.93$$

D. Compute the column's skew coefficient, K_α.

$$K_\alpha = \frac{3\text{ ft}\,cos(15^o) + 18\text{ ft}\,sin(15^o)}{3\text{ft}} = 2.52$$

E. Calculate the pile cap's extension coefficient, K_f.

$$f = \frac{3f_1 + f_2}{4} \quad \text{for } \alpha \le 45^0$$

$$f = \frac{3(3\text{ ft}) + (6\text{ ft})}{4} = 3.75\text{ ft}$$

$$K_f = -0.12\left(\frac{3.38\text{ ft}}{3\text{ ft}}\right)^2 + 0.03\left(\frac{3.38\text{ ft}}{3\text{ ft}}\right) + 1 = 0.85$$

F. Compute the column's effective diameter.

$$D^*_{col} = K_s K_\alpha K_f b_{col}\left[0.1162\left(\frac{H_{col}}{y_{0(max)}}\right)^2 - 0.3617\left(\frac{H_{col}}{y_{0(max)}}\right) + 0.2476\right]$$

$$D^*_{col} = (0.93)(2.52)(0.85)(3\text{ ft})\left[0.1162\left(\frac{2\text{ ft}}{13\text{ ft}}\right)^2 - 0.3617\left(\frac{2\text{ ft}}{13\text{ ft}}\right) + 0.2476\right]$$

$D^*_{col} = 1.16$ ft.

Next, the pile cap's effective diameter is calculated below following Steps A-E in Section 4.2.2.2.

A. Compute the scour caused by the column, $y_{s(col)}$.

$$\frac{y_s}{D^*_{(col)}} = \tanh\left[\left(\frac{y_o}{D^*_{(col)}}\right)^{0.4}\right] \times \left[\begin{array}{l} 2.2\left(\dfrac{V/V_c - 1}{V_{lp}/V_c - 1}\right) + \\ 2.5\left\{\dfrac{D^*_{(col)}/D_{50}}{0.4\left(D^*_{(col)}/D_{50}\right)^{1.2} + 10.6\left(D^*_{(col)}/D_{50}\right)^{-0.13}}\right\} \\ \left(\dfrac{V_{lp}/V_c - V/V_c}{V_{lp}/V_c - 1}\right) \end{array}\right]$$

$$\frac{y_{s(col)}}{1.16\,\text{ft}} = \tanh\left[\left(\frac{13\,\text{ft}}{1.16\,\text{ft}}\right)^{0.4}\right] \times \left[\begin{array}{l} 2.2\left(\dfrac{6.0\frac{\text{ft}}{\text{s}}/1.6\frac{\text{ft}}{\text{s}}-1}{16.36\frac{\text{ft}}{\text{s}}/1.6\frac{\text{ft}}{\text{s}}-1}\right)+ \\ 2.5\left\{\dfrac{1.16\,\text{ft}/\left(2.63\text{ x }10^{-3}\,\text{ft}\right)}{0.4\left(1.16\,\text{ft}/\left(2.63\text{ x }10^{-3}\,\text{ft}\right)\right)^{1.2}+10.6\left(1.16\,\text{ft}/\left(2.63\text{ x }10^{-3}\,\text{ft}\right)\right)^{-0.13}}\right\} \\ \left(\dfrac{16.36\frac{\text{ft}}{\text{s}}/1.6\frac{\text{ft}}{\text{s}}-6.0\frac{\text{ft}}{\text{s}}/1.6\frac{\text{ft}}{\text{s}}}{16.36\frac{\text{ft}}{\text{s}}/1.6\frac{\text{ft}}{\text{s}}-1}\right) \end{array}\right]$$

$y_{s(col)} = 2.23$ ft

B. Compute the shape factor for the square pile cap, K_s.

$$K_s = 0.86+0.97\left|15^{\circ}\frac{\pi}{180^{\circ}}-\frac{\pi}{4}\right|^4 = 0.93$$

C. Compute the column's skew coefficient, K_α.

$$K_\alpha = \frac{15\text{ ft}\,cos\left(15^{\circ}\right)+24\text{ ft}\,sin\left(15^{\circ}\right)}{15\,\text{ft}} = 1.38$$

D. Determine if the column scour uncovers the bottom of the pile cap.

The column scour computed in step A, 2.23 ft, is enough to uncover the bottom of the pile cap. Continue on to step E.

E. Compute $y_{o(max)}$ and the pile cap effective diameter.

$$y_{0(max)} = \begin{cases} 1.64\left(T\left(K_s b_{pc}\right)^{\frac{5}{2}}\right)^{\frac{2}{7}} & y_o \geq 1.64\left(T\left(K_s b_{pc}\right)^{\frac{5}{2}}\right)^{\frac{2}{7}} \\ y_o & y_o < 1.64\left(T\left(K_s b_{pc}\right)^{\frac{5}{2}}\right)^{\frac{2}{7}} \end{cases}$$

$$y_o = 13\text{ ft},$$

$$1.64\left(4\text{ ft}\left(0.93*15\text{ ft}\right)^{\frac{5}{2}}\right)^{\frac{2}{7}} = 16.01\text{ ft}$$

Therefore, $y_{o(max)} = y_o = 13\text{ ft}$

$$D^*_{pc} = K_s\, K_\alpha\, b_{pc}\, exp\left[-1.04 - 1.77\, exp\left(\frac{H'_{pc}}{y_{0(max)}}\right) + 1.695\left(\frac{T'}{y_{0(max)}}\right)^{\frac{1}{2}}\right]$$

$$D^*_{pc} = (0.93)(1.38)(15\text{ ft})\, exp\left[-1.04 - 1.77\, exp\left(\frac{-2\text{ ft}}{13\text{ ft}}\right) + 1.695\left(\frac{4\text{ ft}}{13\text{ ft}}\right)^{\frac{1}{2}}\right]$$

$D^*_{pc} = 3.81$ ft

Continue on to calculate the pile group's effective diameter, D^*_{pg}.

Finally, compute the pile group's effective diameter following Steps A-I from Section 4.2.2.3.

A. Calculate the scour created by the combination of the column and pile cap. This is accomplished by first adding the two effective diameters and then calculating the scour with the computed effective diameter.

$$D^*_{(col+pc)} = D^*_{col} + D^*_{pc} = 1.16\text{ ft} + 3.81\text{ ft} = 4.97\text{ ft}$$

$$\frac{y_{s(col+pc)}}{D^*_{(col+pc)}} = \tanh\left[\left(\frac{y_o}{D^*_{(col+pc)}}\right)^{0.4}\right] \times \left[\begin{array}{l} 2.2\left(\dfrac{V/V_c - 1}{V_{lp}/V_c - 1}\right) + \\ 2.5\left\{\dfrac{D^*_{(col+pc)}/D_{50}}{0.4\left(D^*_{(col+pc)}/D_{50}\right)^{1.2} + 10.6\left(D^*_{(col+pc)}/D_{50}\right)^{-0.13}}\right\} \\ \left(\dfrac{V_{lp}/V_c - V/V_c}{V_{lp}/V_c - 1}\right) \end{array}\right]$$

$$\frac{y_{s(col+pc)}}{4.97\text{ ft}} = tanh\left[\left(\frac{13\text{ ft}}{4.97\text{ ft}}\right)^{0.4}\right] \times \left[\begin{array}{l} 2.2\left(\dfrac{6.0\frac{ft}{s}/1.6\frac{ft}{s}-1}{16.36\frac{ft}{s}/1.6\frac{ft}{s}-1}\right)+ \\ 2.5\left\{\dfrac{4.97\text{ ft}/2.63\text{ x }10^{-3}\text{ ft}}{0.4\left(4.97\text{ ft}/2.63\text{ x }10^{-3}\text{ ft}\right)^{1.2}+10.6\left(4.97\text{ ft}/2.63\text{ x }10^{-3}\text{ ft}\right)^{-0.13}}\right\} \\ \left(\dfrac{16.36\frac{ft}{s}/1.6\frac{ft}{s}-6.0\frac{ft}{s}/1.6\frac{ft}{s}}{16.36\frac{ft}{s}/1.6\frac{ft}{s}-1}\right) \end{array}\right]$$

$y_{s(col+pc)} = 7.26$ ft

B. Calculate the $\overline{H}_{pg}$ and $\overline{y}_o$ using Equation 4.15 and 4.16.

$$\overline{H}_{pg} = H_{pg} + y_{s(col+pc)} = -2\text{ ft} + 7.26\text{ ft} = 5.26\text{ ft}$$
$$\overline{y}_o = y_o + y_{s(col+pc)} = 13\text{ ft} + 7.26\text{ ft} = 20.26\text{ ft}$$

C. Compute the shape factor for the pile group, K_s. K_s accounts for the shape of the pile group and the shape of the individual piles.

$$K_s = \frac{K_{s(pile)} - K_{s(pile\ group)}}{9}\left(\frac{s}{b}\right) + K_{s(pile)} - \frac{10}{9}\left(K_{s(pile)} - K_{s(pile\ group)}\right),$$

$$K_{s(pile\ or\ pile\ group)} = \left\{\begin{array}{ll} 1 & \text{for circular piles or pile group arrays} \\ 0.86+0.97\left|\alpha\dfrac{\pi}{180^0}-\dfrac{\pi}{4}\right|^4 & \text{for square piles or pile group arrays} \end{array}\right\}$$

Since both the individual piles and pile group are both square, the shape factor will be the same for both.

$$K_{s(pile)} = 0.86+0.97\left|15^{o}\frac{\pi}{180^{o}}-\frac{\pi}{4}\right|^{4} = 0.93$$

$$K_{s(pilegroup)} = 0.86+0.97\left|15^{o}\frac{\pi}{180^{o}}-\frac{\pi}{4}\right|^{4} = 0.93$$

$$K_{s} = \frac{0.93-0.93}{9}\left(\frac{6\text{ ft}}{2\text{ ft}}\right)+0.93-\frac{10}{9}\left(0.93-0.93\right) = 0.93$$

D. Calculate the projected width of the pile group.

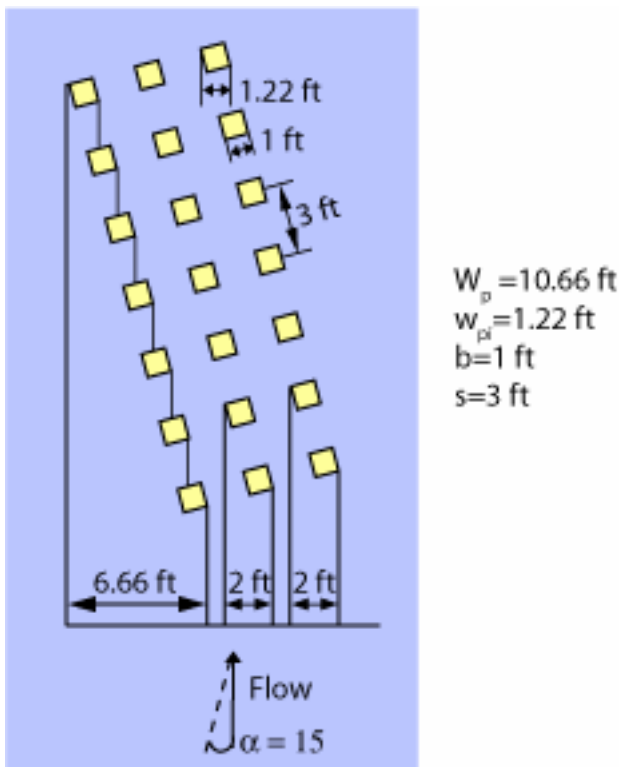

Figure 4-17 The Projected Width of the Pile Group

E. Calculate the pile spacing coefficient, K_{sp}.

$$K_{sp} = 1-\frac{4}{3}\left(1-\frac{w_{pi}}{W_{p}}\right)\left(1-\frac{1}{\left(\frac{s}{w_{pi}}\right)^{0.6}}\right) = 1-\frac{4}{3}\left(1-\frac{1.22\text{ ft}}{10.66\text{ ft}}\right)\left(1-\frac{1}{\left(\frac{3\text{ ft}}{1.22\text{ ft}}\right)^{0.6}}\right) = 0.51$$

F. Calculate K_m coefficient that accounts for the number of piles in line with the flow.

$$K_m = \begin{cases} 0.045(m) + 0.96 & \text{for } |\alpha| < 5^0, \text{and } m \le 5 \\ 1.19 & \text{for } |\alpha| < 5^0, \text{and } m > 5 \\ 1 & \text{for } |\alpha| \ge 5^0 \end{cases}$$

$$\alpha = 15^0, \text{ therefore } K_m = 1$$

G. Compute $\overline{y}_{0(max)}$ for the pile group.

$$\overline{y}_{0(max)} = \begin{cases} \overline{y}_0 & \text{for } \overline{y}_0 \le 2K_s\ W_p\ K_{sp}\ K_m \\ 2K_s\ W_p\ K_{sp}\ K_m & \text{for } \overline{y}_0 > 2K_s\ W_p\ K_{sp}\ K_m \end{cases}$$

$$2K_s\ W_p\ K_{sp}\ K_m = 2(0.93)(10.66\text{ ft})(0.51)(1) = 10.11\text{ ft}$$

$$\overline{y}_0 = 20.26\text{ ft},$$

$$\text{therefore, } \overline{y}_{0(max)} = 10.11\text{ ft}$$

H. Compute the submerged pile group's coefficient, K_h.

$$K_h = 1.5\ tanh\left(0.8\sqrt{\frac{5.29\text{ ft}}{10.11\text{ ft}}}\right) = 0.78$$

I. Compute the pile group's effective diameter, D^*_{pg}.

$$D^*_{pg} = K_{sp}K_hK_mK_sW_p = (0.51)(0.78)(1)(0.93)(10.66\text{ ft}) = 3.94\text{ ft}$$

The effective diameter of the complex pier is the sum of each component's effective diameter.

$$D^* \equiv D^*_{col} + D^*_{pc} + D^*_{pg}$$

$$D^* = 1.16\text{ft} + 3.81\text{ft} + 3.94\text{ft} = 8.91\text{ft}$$

$$\frac{y_s}{D^*_{(col+pc+pg)}} = \tanh\left[\left(\frac{y_o}{D^*_{(col+pc+pg)}}\right)^{0.4}\right] \times \left[\begin{array}{l} 2.2\left(\dfrac{V/V_c - 1}{V_{lp}/V_c - 1}\right) + \\ 2.5\left\{\dfrac{D^*_{(col+pc+pg)}/D_{50}}{0.4\left(D^*_{(col+pc+pg)}/D_{50}\right)^{1.2} + 10.6\left(D^*_{(col+pc+pg)}/D_{50}\right)^{-0.13}}\right\} \\ \left(\dfrac{V_{lp}/V_c - V/V_c}{V_{lp}/V_c - 1}\right) \end{array}\right]$$

$$\frac{y_s}{8.91\,\text{ft}} = tanh\left[\left(\frac{13\,\text{ft}}{8.91\,\text{ft}}\right)^{0.4}\right] \times \left[\begin{array}{l} 2.2\left(\dfrac{6.0\frac{\text{ft}}{\text{s}}/1.6\frac{\text{ft}}{\text{s}} - 1}{16.36\frac{\text{ft}}{\text{s}}/1.6\frac{\text{ft}}{\text{s}} - 1}\right) + \\ 2.5\left\{\dfrac{8.91\,\text{ft}/2.63\text{ x }10^{-3}\text{ ft}}{0.4\left(8.91\,\text{ft}/2.63\text{ x }10^{-3}\text{ ft}\right)^{1.2} + 10.6\left(8.91\,\text{ft}/2.63\text{ x }10^{-3}\text{ ft}\right)^{-0.13}}\right\} \\ \left(\dfrac{16.36\frac{\text{ft}}{\text{s}}/1.6\frac{\text{ft}}{\text{s}} - 6.0\frac{\text{ft}}{\text{s}}/1.6\frac{\text{ft}}{\text{s}}}{16.36\frac{\text{ft}}{\text{s}}/1.6\frac{\text{ft}}{\text{s}} - 1}\right) \end{array}\right]$$

$y_s = 11.12$ ft

The total scour for the complex pier is computed using the flow conditions listed in Table 4-2 and an effective diameter of 8.91 ft in equation 3.4 to 3.15.

The resulting local scour depth for the complex pier is **11.12 ft**.

4.2.3. Complex Pier Local Scour Depth Prediction - Case 3 Piers (Fully Buried Pile Cap)

The methodology for computing local scour depth for a complex pier with a fully buried pile cap, as shown in Figure 4-5, is described in this section. As in the partially buried pile cap case (Case 2) the shape of the structure exposed to the flow can change as the local scour progresses so an iterative scheme must be used to determine the effective diameter of the structure.

The effective diameter of each pier component is computed for the sediment and flow conditions of interest. The sum of the effective diameters of its components is the effective diameter of the complete structure.

4.2.3.1. Effective Diameter of the Column

The procedure for computing the effective diameter for the column is presented in Steps A-J below.

A. Calculate the column's shape factor, K_s, using Equation 4.56

$$K_s = \begin{cases} 1 & \text{for circular columns} \\ 0.86 + 0.97\left|\alpha\dfrac{\pi}{180^o} - \dfrac{\pi}{4}\right|^4 & \text{for rectangular columns} \end{cases} \qquad 4.56$$

where α is the flow's skew angle between the column and the flow direction. Equation 4.56 is valid for $0^o \le \alpha \le 90^o$.

B. Calculate the column's skew angle coefficient, K_α, using Equation 4.57.

$$K_\alpha = \frac{b_{col}\, cos(\alpha) + l_{col}\, sin(\alpha)}{b_{col}} \qquad 4.57$$

C. Compute the effective diameter of the column using Equation 4.58. This value corresponds to an infinitely deep column.

$$D^*_{col(max)} = K_s\, K_\alpha\, b_{col} \qquad 4.58$$

D. Compute the maximum scour depth for the column, $y_{s(col)(max)}$ for the sediment and flow conditions of interest and the effective diameter, $D^*_{col(max)}$, using Equations 3.4-3.15.

E. Compare the scour depth computed in step D with the distance from the pre-locally scoured bed to the bottom of the column, $|H_{col}|$. If the scour due to the column (computed in Step D) does not uncover the base of the column, then the effective diameter of the complex pier is equal to $D^*_{col(max)}$ for the conditions examined. If the scour depth exceeds $|H_{col}|$, the analysis continues with Step F. That is:

$$\text{If} \begin{cases} y_{s(col)(max)} \le |H_{col}| & D^* = D^*_{col(max)}\text{, proceed to 4.2.3.4} \\ y_{s(col)(max)} > |H_{col}| & \text{the pile cap is exposed, proceed to Step F} \end{cases} \qquad 4.59$$

F. In general, the effect of the pile cap being wider and longer than the column is to reduce the effective diameter of the column. This reduction is accounted for with the pile cap extension coefficient, K_f. Note, however, that the reduction in the column's effective diameter, D^*_{col}, cannot go beyond that required to take the scour depth (due to the column) down to the bottom of the column (top of the pile cap). This minimum value of D^*_{col} is denoted by $D^*_{col(min)}$. Compute $D^*_{col(min)}$ by setting $y_s = |H_{col}|$ in Equations 3.4 – 3.15 and solving for D^*.

G. Compute the pile cap extension coefficient, K_f using Equation 4.61 with the weighted average of the front and side extensions given in Equation 4.60 (see the definition sketch for f_1 and f_2 in Figure 4-6).

$$f = \begin{cases} \dfrac{2f_1 + f_2}{3} & \text{for } \alpha \le 45^0 \\ \dfrac{2f_2 + f_1}{3} & \text{for } \alpha > 45^0 \end{cases} \qquad 4.60$$

$$K_f = \begin{cases} -0.12\left(\dfrac{f}{b_{col}}\right)^2 + 0.03\left(\dfrac{f}{b_{col}}\right) + 1 & \text{for } 0 < \left(\dfrac{f}{b_{col}}\right) < 3 \\ 0 & \text{for } \left(\dfrac{f}{b_{col}}\right) \ge 3 \end{cases} \qquad 4.61$$

H. Compute the attenuated effective diameter of the column, $D^*_{col(f)}$, using Equation 4.62

$$D^*_{col(f)} = K_f D^*_{col(max)} \left[-.75\left(\frac{H_{col}}{y_{s(col)(max)}}\right) + 0.25 \right], \qquad 4.62$$

where $y_{s(col)(max)}$ is the scour depth evaluated in Step D above.

I. The effective diameter of the column, D^*_{col}, is computed using Equation 4.63.

$$D^*_{col} = \begin{cases} D^*_{col(f)} & \text{if } D^*_{col(f)} \ge D^*_{col(min)} \\ D^*_{col(min)} & \text{if } D^*_{col(f)} < D^*_{col(min)} \end{cases} \qquad 4.63$$

4.2.3.2. Effective Diameter of the Pile Cap

The procedure for calculating the effective diameter for a pile cap, D^*_{pc}, is presented below in Steps A-L. This procedure is applied to pile caps that are fully buried relative to the pre-locally scoured bed. The procedure for computing D^*_{pc} for Case 3 piers is similar to that used for Case 2 piers. As with Case 2 piers, iterative calculations are necessary since the shape and size of the structure changes as the local scour progresses. In the iterative calculations the pile cap thickness, T', is considered to be the distance from the top of the pile cap to the bottom of the scour hole. The iterations continue until either an

equilibrium scour depth is reached or the bottom of the pile cap is uncovered. Likewise, the height of the pile cap, H'_{pc}, is considered to be the distance from the pre-locally scoured bed to the bottom of the scour hole.

The procedure for computing D^*_{pc} is presented in Steps A–O below.

A. Compute the scour depth produced by the column, $y_{s(col)}$, using Equations 3.4 - 3.15 with D^* replaced by D^*_{col} in Equation 4.63. Note that the water depth, y_0, in Equations 3.4 - 3.15 is the actual water depth just upstream of the structure.

B. When the pile cap is completely buried there is an additional coefficient required in the computation of the effective diameter for the pile cap. Laboratory data indicates that the position of the pile cap in the scour hole affects the magnitude of its effective diameter. The coefficient that accounts for this dependence, K_{bpc}, is given in Equations 4.64. This coefficient is a function of f from Equation 4.60 and the scour depth computed in Step A above.

$$K_{bpc} = \begin{cases} (A)(B) & \text{for } 0 \le \dfrac{-H_{col}}{y_{s(col)}} \le 1, \text{ and } 0 \le \dfrac{f}{b_{col}} \le 3 \\ 0 & \text{else} \end{cases},$$

$$A = -1.166\left(\frac{-H_{col}}{y_{s(col)}}\right)^2 + .166\left(\frac{-H_{col}}{y_{s(col)}}\right) + 1, \text{ and} \qquad 4.64$$

$$B = -0.333\left(\frac{f}{b_{col}}\right) + 1.$$

Coefficients A and B are plotted in Figure 4-18 and Figure 4-19, respectively and the buried pile cap coefficient is plotted in Figure 4-20

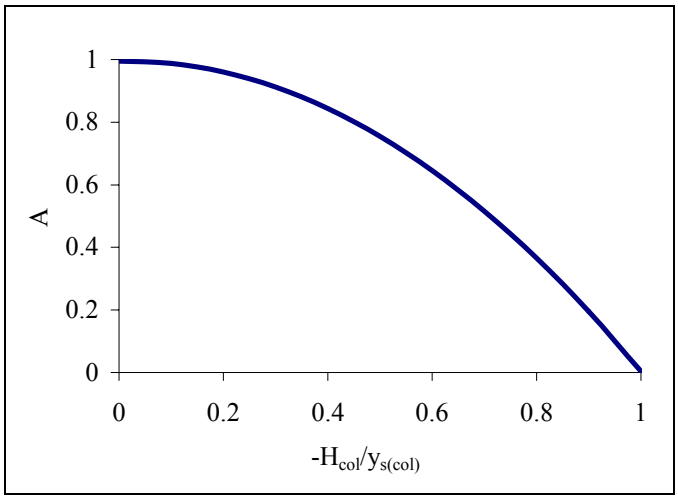

Figure 4-18 Graph of the A coefficient in Equation 4.64

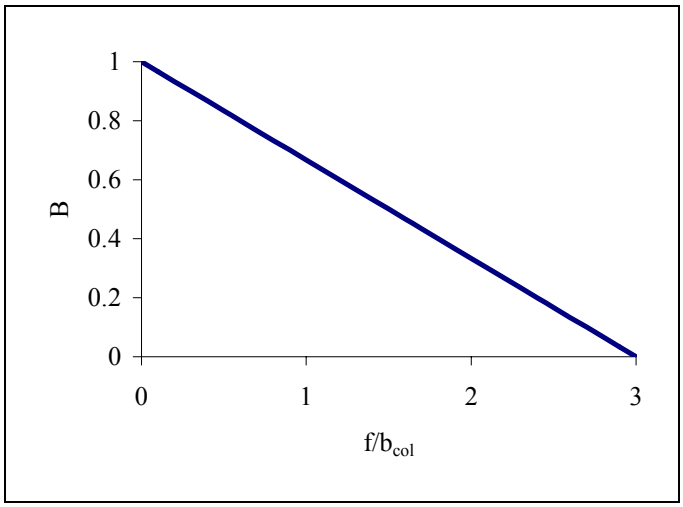

Figure 4-19 Graph of the B coefficient in Equation 4.64

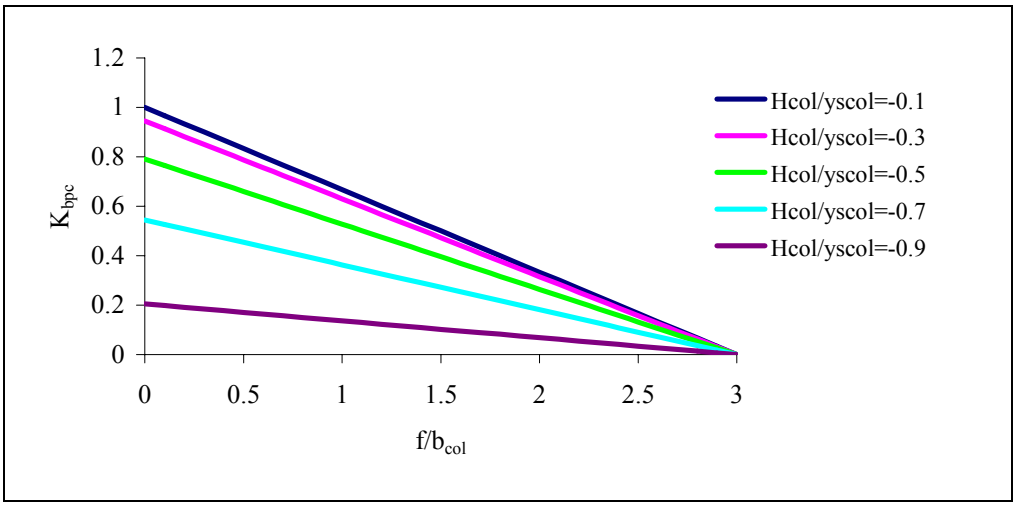

Figure 4-20 Graph of the buried pile cap's coefficient, $K_{bpc.}$

C. Compute the pile cap's shape factor, K_s using Equation 4.65.

$$K_s = \begin{cases} 1 & \text{for circular pile caps} \\ 0.86 + 0.97\left|\alpha \dfrac{\pi}{180^o} - \dfrac{\pi}{4}\right|^4 & \text{for rectangular pile caps} \end{cases} \qquad 4.65$$

where α is the flow skew angle between the column and the flow direction. Equation 4.65 is valid for $0^o \le \alpha \le 90^o$.

D. Compute the pile cap's skew angle coefficient, K_α, using Equation 4.66.

$$K_\alpha = \frac{b_{pc}\, cos(\alpha) + l_{pc}\, sin(\alpha)}{b_{pc}} \qquad 4.66$$

E. Check to see if the scour depth due to the column, $y_{s(col)}$, uncovers the bottom of the pile cap

$$\text{If} \begin{cases} y_{s(col)} \ge |H_{pc}|, & \text{pile cap bottom uncovered, proceed to Step F} \\ y_{s(col)} < |H_{pc}|, & \text{proceed to Step G} \end{cases} \qquad 4.67$$

F. Compute $y_{0(max)}$ and D^*_{pc} using Equations

$$y_{0(max)} = \begin{cases} 1.64\left(T\left(K_s b_{pc}\right)^{\frac{5}{2}}\right)^{\frac{2}{7}} & y_o \ge 1.64\left(T\left(K_s b_{pc}\right)^{\frac{5}{2}}\right)^{\frac{2}{7}} \\ y_o & y_o < 1.64\left(T\left(K_s b_{pc}\right)^{\frac{5}{2}}\right)^{\frac{2}{7}} \end{cases} \text{ and} \qquad 4.68$$

$$D^*_{pc} = K_s\, K_\alpha K_{bpc}\, b_{pc}\, exp\left[-1.04 - 1.77\, exp\left(\frac{H_{pc}}{y_{0(max)}}\right) + 1.695\left(\frac{T}{y_{0(max)}}\right)^{\frac{1}{2}}\right]. \qquad 4.69$$

Note that $-1 \le H_{pc} / y_{o(max)} \le 1$ and $0 \le T / y_{o(max)} \le 1$.

Proceed to Section 4.2.3.3.

G. Compute T' and H'_{pc} using Equations 4.70 and 4.71 (see definition sketch in Figure 4-14).

$$T' = \left(T + H_{pc}\right) + y_{s(col)} \text{ and} \qquad 4.70$$

$$H'_{pc} = -y_{s(col)} \qquad 4.71$$

T and T' are always positive. H_{pc} and H'_{pc} are always negative for partially and fully buried pile caps.

H. Calculate $y_{0(max)(i)}$ for the pile cap using Equation 4.72. The subscript "i" refers to the number of the iteration (e.g. i = 1 for the first iteration, 2 for the second, etc.).

$$y_{0(max)(i)} = \begin{cases} 1.64\left(T'\left(K_s b_{pc}\right)^{\frac{5}{2}}\right)^{\frac{2}{7}} & y_o \geq 1.64\left(T'\left(K_s b_{pc}\right)^{\frac{5}{2}}\right)^{\frac{2}{7}} \\ y_o & y_o < 1.64\left(T'\left(K_s b_{pc}\right)^{\frac{5}{2}}\right)^{\frac{2}{7}} \end{cases}. \qquad 4.72$$

I. Compute the effective diameter of the pile cap with Equation 4.73. Note that $-1 \leq H'_{pc} / y_{o(max)(i)} \leq 1$ and $0 \leq T' / y_{o(max)(i)} \leq 1$ in equation. 4.73.

$$D^*_{pc(i)} = K_s\, K_\alpha\, K_{bpc}\, b_{pc}\, exp\left[-1.04 - 1.77\, exp\left(\frac{H'_{pc}}{y_{0(max)(i)}}\right) + 1.695\left(\frac{T'}{y_{0(max)(i)}}\right)^{\frac{1}{2}}\right] \qquad 4.73$$

J. Compute the effective diameter for the column and the portion of the pile cap above the bed.

$$D^*_{(col+pc)(i)} = D^*_{col} + D^*_{pc(i)} \qquad 4.74$$

K. Compute the scour depth due to the column and the portion of the pile cap above the bed, $Y_{s(col+pc)(i)}$ using Equations 3.4 - 3.15 with D^* replaced by $D^*_{(col+pc)(i)}$ from

Equation 4.74. Note that the water depth, y_0, in Equations 3.4 – 3.15 is the actual water depth just upstream of the structure.

L. Compute H'_{pc} and T' using Equations 4.75 and 4.76.

$$H'_{pc} = \begin{cases} H_{pc} & Y_{s(col+pc)(i)} \geq \left|H_{pc}\right| \\ -Y_{s(col+pc)(i)} & Y_{s(col+pc)(i)} < \left|H_{pc}\right| \end{cases} \qquad 4.75$$

$$T' = \begin{cases} T & Y_{s(col+pc)(i)} \geq \left|H_{pc}\right| \\ T + H_{pc} - H'_{pc} & Y_{s(col+pc)(i)} < \left|H_{pc}\right| \end{cases} \qquad 4.76$$

M. Check for convergence using Equations 4.77.

If $i = 1$, proceed to Step H above

If $i > 1$

1) Compute $\Delta \equiv \left|\dfrac{Y_{s(col+pc)(i)} - Y_{s(col+pc)(i-1)}}{Y_{s(col+pc)(i-1)}}\right|$

2) If $\begin{cases} \Delta \leq 0.05,\ D^*_{pc} = D^*_{pc(i)},\ \text{proceed to Step N below} \\ \Delta > 0.05 \text{ proceed to Step H above} \end{cases}$

4.77

N. Pile cap summary.

$$D^*_{pc} = D^*_{pc(i)}$$
$$D^*_{(col+pc)} = D^*_{(col+pc)(i)}$$
$$y_{s(col+pc)} = Y_{s(col+pc)(i)}$$

O. Determine if pile group is exposed.

$$\text{If } \begin{cases} Y_{s(col+pc)(i)} \leq \left|H_{pg}\right|,\ D^*_{pg} = 0,\ \text{proceed to Section 4.2.3.4} \\ Y_{s(col+pc)(i)} > \left|H_{pg}\right|,\ \text{bottom of pile cap uncovered, proceed to Section 4.2.3.3} \end{cases} \qquad 4.78$$

4.2.3.3. Effective Diameter of the Pile Group

If the scour depth produced by the pile cap and column is sufficient to uncover the top of the piles, the pile group will contribute to the total effective diameter of the pier. Since the only information available for local scour at pile groups is for situations where the piles protrude above the pre-locally scoured bed (i.e. there is no data for scour produced by piles exposed to the flow in a scour hole) the reference or datum from which the height of the pile group is measured must be changed as shown in Figure 4-15. The datum is no longer the pre-locally scoured bed but rather the bottom of the scour hole produced by the column and pile cap. Likewise, the water depth is increased by this scour depth for purposes of computing the effective diameter of the pile group, D^*_{pg}. The pile group also differs from the column and the pile cap in that it is composed of several piles and the arrangement of these piles can have a different shape from that of the individual piles. For example, there could be a rectangular array of circular piles. If the piles are located close together the structure takes on the approximate shape of the array rather than that of the individual piles. Likewise, as the spacing between the piles becomes large it is the shape of the individual pile that is important. The shape factor, K_s, in this analysis takes this into consideration. Laboratory data also suggests that the scour potential of the pile group (and therefore the effective diameter of the pile group) decreases as the location of the top of the piles reside deeper in the scour hole produced by the column and pile cap. To account for this a buried pile group coefficient, K_{bpg}, has been introduced based on laboratory data. The procedure for computing the effective diameter for the pile group, D^*_{pg}, is described in Steps A through I below.

A. Compute $\overline{H}_{pg}$ and $\overline{y}_0$ based on a datum located at the bottom of the scour hole (instead of the pre-locally scoured bed).

$$\overline{H}_{pg} = H_{pg} + y_{s(col+pc)} \quad \text{and}$$
$$\overline{y}_0 = y_o + y_{s(col+pc)} \qquad 4.79$$

Note that with this datum H_{pg} is negative and $\overline{H}_{pg}$ is positive.

B. Compute the shape factor for the pile group using Equations 4.80 and 4.81.

$$K_s = \frac{K_{s\,(pile)} - K_{s(pile\ group)}}{9}\left(\frac{s}{b}\right) + K_{s(pile)} - \frac{10}{9}\left(K_{s\,(pile)} - K_{s(pile\ group)}\right) \qquad 4.80$$

where,

$$K_{s(pile\ or\ pile\ group)} = \begin{cases} 1 & \text{for circular piles or pile group arrays} \\ 0.86 + 0.97\left|\alpha\frac{\pi}{180^o} - \frac{\pi}{4}\right|^4 & \text{for square piles or rectangular pile group arrays} \end{cases} \qquad 4.81$$

C. Calculate the projected width of the pile group, W_p, as illustrated in Figure 4-10. The projected width of the pile group is the sum of the non-overlapping widths of the individual piles in the first 2 rows and first column on a plane normal to the flow direction.

D. Calculate pile spacing coefficient, K_{sp}, using Equation 4.82. Note that when the center line spacing is not uniform ($s_n \neq s_m$), use the smallest value for the centerline spacing, s, in Equation 4.50.

$$K_{sp} = 1 - \frac{4}{3}\left(1 - \frac{w_{pi}}{W_p}\right)\left(1 - \frac{1}{\left(\frac{s}{w_{pi}}\right)^{0.6}}\right), \qquad 4.82$$

where w_{pi} is the projected width of an individual pile.

E. Calculate K_m using Equation 4.83 which accounts for the number of piles in line with the flow.

$$K_m = \begin{cases} 0.045(m) + 0.96 & \text{for } |\alpha| < 5^o, \text{and } m \leq 5 \\ 1.19 & \text{for } |\alpha| < 5^o, \text{and } m > 5 \\ 1 & \text{for } |\alpha| \geq 5^o \end{cases} \qquad 4.83$$

F. Compute $\overline{y}_{0(max)}$ using Equation 4.84.

$$\overline{y}_{0(max)} = \begin{cases} \overline{y}_0 & \text{for } \overline{y}_0 \le 2\,K_s\ W_p\ K_{sp}\ K_m \\ 2\,K_s\ W_p\ K_{sp}\ K_m & \text{for } \overline{y}_0 > 2\,K_s\ W_p\ K_{sp}\ K_m \end{cases} \qquad 4.84$$

G. Compute the pile group height coefficient, K_h using Equation 4.85. Note that if the calculated value of $\overline{H}_{pg} / \overline{y}_{0(max)}$ is greater than 1 in Equation 4.85, set it equal to 1.

$$K_h = \begin{cases} 1.5\,tanh\left(0.8\sqrt{\dfrac{\overline{H}_{pg}}{\overline{y}_{0(max)}}}\right) & \text{for } 0 \le \dfrac{\overline{H}_{pg}}{\overline{y}_{0(max)}} \le 1 \\ 0 & \text{for } \dfrac{\overline{H}_{pg}}{\overline{y}_{0(max)}} < 0 \\ 1 & \text{for } \dfrac{\overline{H}_{pg}}{\overline{y}_{0(max)}} > 1 \end{cases} \qquad 4.85$$

H. Compute the buried pile group attenuation coefficient, K_{bpg}, using Equation 4.86

$$K_{bpg} = \frac{\overline{H}_{pg}}{y_{s(col+pc)}} \qquad 4.86$$

I. Compute the effective diameter of the pile group using Equation 4.87.

$$D^*_{pg} = K_s\,K_{sp}\,K_m\,K_h\,K_{bpg}\,W_p \qquad 4.87$$

4.2.3.4. Complex Pier Effective Diameter

The effective diameter of the complete complex pier is the sum of the effective diameters of its components. As stated above for situations where the pile cap is partially or fully buried (Cases 2 and 3) the effective diameter is only valid for the flow and sediment conditions for which it is computed.

$$D^* \equiv D^*_{col} + D^*_{pc} + D^*_{pg} \qquad 4.88$$

4.2.3.5. Equilibrium Local Scour Depth at a Case 3 Complex Pier

Once the effective diameter of the complex pier has been obtained, the equilibrium local scour depth (for the conditions under which the effective diameter was determined) can be computed using Equations 3.4 - 3.15.

4.2.3.6. Case 3 Example Problem

An example calculation for the complex pier as illustrated in Figure 4-21 is presented in this section. The flow and sediment variables used for the calculations are listed below in Table 4-3.

Table 4-3 Flow and sediment inputs for the example calculation.

Skew Angle Degrees	Velocity (ft/s)	Critical Velocity (ft/s)	Live Bed Peak Velocity (ft/s)	Water Depth (ft)	Temp (F^o)	Salinity (ppt)	D_{50} (mm)
15	6.0	1.60	16.36	13	65	35	0.80

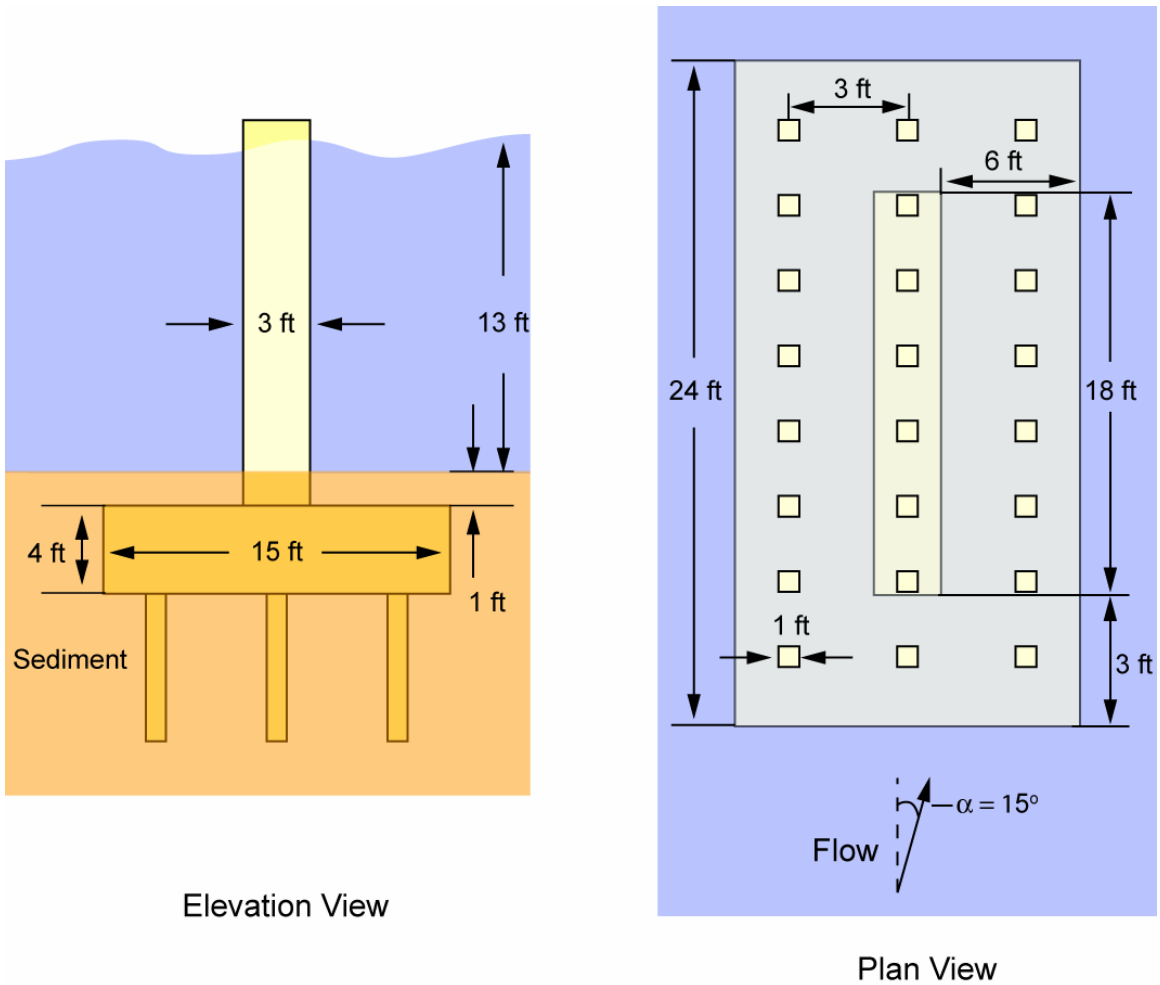

Figure 4-21 Elevation and plan view of the complex pier used in the Case 3 example scour calculation

The column's effective diameter, D^*_{col}, is calculated below following Steps A-I of section 4.2.3.1.

A. Compute the shape factor for the square column, K_s.

$$K_s = 0.86 + 0.97\left|15^\circ \frac{\pi}{180^\circ} - \frac{\pi}{4}\right|^4 = 0.93$$

B. Compute the column skew coefficient, K_α.

$$K_\alpha = \frac{3\text{ ft}\cos\left(15^\circ\right) + 18\text{ ft}\sin\left(15^\circ\right)}{3\text{ft}} = 2.52$$

C. Compute the maximum column effective diameter, $D^*_{col(max)}$, using Equation 4.58.

$$D^*_{col(max)} = K_s\, K_\alpha\, b_{col} = 0.93 \text{ x } 2.52 \text{ x } 3.0\,\text{ft} = 7.03\,\text{ft}$$

D. Compute the maximum scour depth for the column, $y_{s(col)(max)}$.

$$\frac{y_{s(col)(max)}}{D^*_{(col)(max)}} = \tanh\left[\left(\frac{y_o}{D^*_{(col)(max)}}\right)^{0.4}\right] \times \left[\begin{array}{l} 2.2\left(\dfrac{V/V_c - 1}{V_{lp}/V_c - 1}\right) + \\ 2.5\left\{\dfrac{D^*_{(col)(max)}/D_{50}}{0.4\left(D^*_{(col)(max)}/D_{50}\right)^{1.2} + 10.6\left(D^*_{(col)(max)}/D_{50}\right)^{-0.13}}\right\} \\ \left(\dfrac{V_{lp}/V_c - V/V_c}{V_{lp}/V_c - 1}\right) \end{array}\right]$$

$$\frac{y_{s(col)(max)}}{7.03\,\text{ft}} = \tanh\left[\left(\frac{13\,\text{ft}}{7.03\,\text{ft}}\right)^{0.4}\right] \times \left[\begin{array}{l} 2.2\left(\dfrac{6.0\frac{\text{ft}}{\text{s}}/1.6\frac{\text{ft}}{\text{s}} - 1}{16.36\frac{\text{ft}}{\text{s}}/1.6\frac{\text{ft}}{\text{s}} - 1}\right) + \\ 2.5\left\{\dfrac{7.03\,\text{ft}/\left(2.63 \text{ x } 10^{-3}\,\text{ft}\right)}{0.4\left(7.03\,\text{ft}/\left(2.63 \text{ x } 10^{-3}\,\text{ft}\right)\right)^{1.2} + 10.6\left(7.03\,\text{ft}/\left(2.63 \text{ x } 10^{-3}\,\text{ft}\right)\right)^{-0.13}}\right\} \\ \left(\dfrac{16.36\frac{\text{ft}}{\text{s}}/1.6\frac{\text{ft}}{\text{s}} - 6.0\frac{\text{ft}}{\text{s}}/1.6\frac{\text{ft}}{\text{s}}}{16.36\frac{\text{ft}}{\text{s}}/1.6\frac{\text{ft}}{\text{s}} - 1}\right) \end{array}\right]$$

$y_{s(col)(max)} = 9.48$ ft

E. Compare the scour depth computed in Step D with the distance from the pre-locally scoured bed to the bottom of the column, $\left|H_{col}\right|$.

$y_{s(col)(max)} > |H_{col}|$, so continue to Step F.

F. Compute $D^*_{col(min)}$ by setting $y_s = |H_{col}|$ in Equations 3.4 – 3.15 and solving for D^*.

Note: The process of computing D*min is iterative. Only the last iteration is shown in this step. Once the predicted scour was within 1% of |Hcol|, the iterations were stopped.

$D^*_{min} = 0.46$ ft

$$y_s = (0.46\,\text{ft})\tanh\left[\left(\frac{13\,\text{ft}}{0.46\,\text{ft}}\right)^{0.4}\right]\times\left[\begin{array}{l} 2.2\left(\dfrac{6.0\frac{\text{ft}}{\text{s}}/1.6\frac{\text{ft}}{\text{s}}-1}{16.36\frac{\text{ft}}{\text{s}}/1.6\frac{\text{ft}}{\text{s}}-1}\right)+ \\ 2.5\left\{\dfrac{0.46\,\text{ft}/\left(2.63\text{ x }10^{-3}\,\text{ft}\right)}{0.4\left(0.46\,\text{ft}/\left(2.63\text{ x }10^{-3}\,\text{ft}\right)\right)^{1.2}+10.6\left(0.46\,\text{ft}/\left(2.63\text{ x }10^{-3}\,\text{ft}\right)\right)^{-0.13}}\right\} \\ \left(\dfrac{16.36\frac{\text{ft}}{\text{s}}/1.6\frac{\text{ft}}{\text{s}}-6.0\frac{\text{ft}}{\text{s}}/1.6\frac{\text{ft}}{\text{s}}}{16.36\frac{\text{ft}}{\text{s}}/1.6\frac{\text{ft}}{\text{s}}-1}\right) \end{array}\right]$$

$y_s = 1.0$ ft, therefore $D^*_{min} = 0.46$ ft.

G. Calculate the pile cap's extension coefficient, K_f.

$$f = \frac{3f_1+f_2}{4} \quad \text{for } \alpha \le 45^0$$

$$f = \frac{3(3\,\text{ft})+(6\,\text{ft})}{4} = 3.75\,\text{ft}$$

$$K_f = -0.12\left(\frac{3.38\,\text{ft}}{3\,\text{ft}}\right)^2 + 0.03\left(\frac{3.38\,\text{ft}}{3\,ft}\right) + 1 = 0.85$$

H. Compute the attenuated effective diameter of the column, $D^*_{col(f)}$, using Equation 4.62.

$$D^*_{col(f)} = K_f D^*_{col(max)} \left[-.75 \left(\frac{H_{col}}{y_{s(col)(max)}} \right) + 0.25 \right]$$

$$D^*_{col(f)} = (0.85)(7.03\,\text{ft}) \left[-.75 \left(\frac{-1\,\text{ft}}{9.48\,\text{ft}} \right) + 0.25 \right]$$

$D^*_{col(f)} = 1.97$ ft

I. The effective diameter of the column, D^*_{col}, is computed using Equation 4.63.

$$D^*_{col} = D^*_{col(f)} = 1.97\,\text{ft}$$

Next, the pile cap's effective diameter is calculated below following Steps A-O in Section 4.2.2.2.

A. Compute the scour caused by the column, $y_{s(col)}$.

$$\frac{y_{s(col)}}{1.96\,\text{ft}} = \tanh\left[\left(\frac{13\,\text{ft}}{1.96\,\text{ft}} \right)^{0.4} \right] \times \left[\begin{array}{l} 2.2 \left(\dfrac{6.0\frac{\text{ft}}{\text{s}} / 1.6\frac{\text{ft}}{\text{s}} - 1}{16.36\frac{\text{ft}}{\text{s}} / 1.6\frac{\text{ft}}{\text{s}} - 1} \right) + \\ 2.5 \left\{ \dfrac{1.96\,\text{ft} / \left(2.63 \text{ x } 10^{-3}\,\text{ft}\right)}{0.4\left(1.96\,\text{ft} / \left(2.63 \text{ x } 10^{-3}\,\text{ft}\right)\right)^{1.2} + 10.6\left(1.96\,\text{ft} / \left(2.63 \text{ x } 10^{-3}\,\text{ft}\right)\right)^{-0.13}} \right\} \\ \left(\dfrac{16.36\frac{\text{ft}}{\text{s}} / 1.6\frac{\text{ft}}{\text{s}} - 6.0\frac{\text{ft}}{\text{s}} / 1.6\frac{\text{ft}}{\text{s}}}{16.36\frac{\text{ft}}{\text{s}} / 1.6\frac{\text{ft}}{\text{s}} - 1} \right) \end{array} \right]$$

$y_{s(col)} = 3.48$ ft

B. Compute the buried pile cap coefficient, K_{bpc} using Equations 4.64.

$$\frac{-H_{col}}{y_{s(col)}} = 0.29, \text{ and } \frac{f}{b_{col}} = 1.25$$

$$A = -1.166(0.29)^2 + 0.166(0.29) + 1 = 0.95$$

$$B = -0.333\ (1.25) + 1 = 0.58$$

$$K_{bpc} = 0.55$$

C. Compute the shape factor for the square pile cap, K_s.

$$K_s = 0.86 + 0.97\left|15^o \frac{\pi}{180^o} - \frac{\pi}{4}\right|^4 = 0.93$$

D. Compute the column skew coefficient, K_α.

$$K_\alpha = \frac{15\text{ ft}\, cos(15^o) + 24\text{ ft}\, sin(15^o)}{15\text{ ft}} = 1.38$$

E. Determine if the column scour uncovers the bottom of the pile cap.

The column scour computed in Step A, 3.58 ft, is not enough to uncover the bottom of the pile cap. Continue on to Step G.

F. Skip this step.

G. Compute T' and H'_{pc} using Equations 4.70 and 4.71 (see definition sketch in Figure 4-14).

$$T' = (T + H_{pc}) + y_{s(col)} = 4\text{ ft} + -1\text{ ft} + 3.48\text{ ft} = 2.48\text{ ft}$$

$$H'_{pc} = -y_{s(col)} = -3.48\text{ ft}$$

H. Compute $y_{o(max)(1)}$ and the pile cap effective diameter, $D^*_{pc(1)}$.

$$y_o = 13\text{ ft},$$

$$1.64\left(2.47\text{ ft}\left(0.93*15\text{ ft}\right)^{\frac{5}{2}}\right)^{\frac{2}{7}} = 13.95\text{ ft}$$

Therefore, $y_{o(max)(1)} = y_o = 13\text{ ft}$

I. Calculate $D^*_{pc(1)}$.

$$D^*_{pc(1)} = \left(0.55\right)\left(0.93\right)\left(1.38\right)\left(15\text{ ft}\right)exp\left[-1.04 - 1.77\,exp\left(\frac{-3.47\text{ ft}}{13\text{ ft}}\right) + 1.695\left(\frac{2.47\text{ ft}}{13\text{ ft}}\right)^{\frac{1}{2}}\right]$$

$D^*_{pc(1)} = 2.03$ ft

J. Calculate $D^*_{(col+pc)(1)}$.

$$D^*_{(col+pc)(1)} = 1.97\text{ ft} + 2.03\text{ ft} = 4.0\text{ ft}$$

K. Calculate $Y_{s(col+pc)(1)}$.

$$Y_{s(col+pc)(1)} = \left(4.0\text{ ft}\right)\tanh\left[\left(\frac{13\text{ ft}}{4.0\text{ ft}}\right)^{0.4}\right]\times\left[\begin{array}{l} 2.2\left(\dfrac{6.0\frac{\text{ft}}{\text{s}}/1.6\frac{\text{ft}}{\text{s}}-1}{16.36\frac{\text{ft}}{\text{s}}/1.6\frac{\text{ft}}{\text{s}}-1}\right)+ \\ 2.5\left\{\dfrac{4.0\text{ ft}/\left(2.63\text{ x }10^{-3}\text{ ft}\right)}{0.4\left(4.0\text{ ft}/\left(2.63\text{ x }10^{-3}\text{ ft}\right)\right)^{1.2}+10.6\left(4.0\text{ ft}/\left(2.63\text{ x }10^{-3}\text{ ft}\right)\right)^{-0.13}}\right\} \\ \left(\dfrac{16.36\frac{\text{ft}}{\text{s}}/1.6\frac{\text{ft}}{\text{s}}-6.0\frac{\text{ft}}{\text{s}}/1.6\frac{\text{ft}}{\text{s}}}{16.36\frac{\text{ft}}{\text{s}}/1.6\frac{\text{ft}}{\text{s}}-1}\right) \end{array}\right]$$

$Y_{s(col+pc)(1)} = 6.15$ ft

L. Compute H'_{pc} and T' using Equations 4.75 and 4.76.

$$H'_{pc} = H_{pc} = -5\text{ ft since } Y_{s(col+pc)(1)} \geq \left|H_{pc}\right|$$

$$T' = T = 4 \text{ ft since } Y_{s(col+pc)(1)} \geq |H_{pc}|$$

M. Check for convergence using Equations 4.77.

Since i =1, go to Step H.

H. Compute $y_{o(max)(2)}$ and the pile cap's effective diameter, $D^*_{pc(2)}$.

$$y_o = 13 \text{ ft},$$

$$1.64\left(5\text{ft}\left(0.93*15\text{ft}\right)^{\frac{5}{2}}\right)^{\frac{2}{7}} = 16.01\text{ft}$$

Therefore, $y_{o(max)(2)} = y_o = 13.0$ ft

I. Calculate $D^*_{pc(2)}$.

$$D^*_{pc(2)} = (0.55)(0.93)(1.38)(15\text{ ft})\,exp\left[-1.04 - 1.77\,exp\left(\frac{-5.0\text{ ft}}{13\text{ ft}}\right) + 1.695\left(\frac{4.0\text{ ft}}{13\text{ ft}}\right)^{\frac{1}{2}}\right]$$

$D^*_{pc(2)} = 2.87$ ft

J. Calculate $D^*_{(col+pc)(2)}$.

$$D^*_{(col+pc)(2)} = 1.97 \text{ ft} + 2.87 \text{ ft} = 4.84 \text{ ft}$$

K. Calculate $Y_{s(col+pc)(2)}$.

$$Y_{s(col+pc)(2)} = (4.84\,\text{ft})\ \tanh\left[\left(\frac{13\,\text{ft}}{4.84\,\text{ft}}\right)^{0.4}\right] \times \left[\begin{array}{l} 2.2\left(\dfrac{6.0\frac{\text{ft}}{\text{s}}/1.6\frac{\text{ft}}{\text{s}}-1}{16.36\frac{\text{ft}}{\text{s}}/1.6\frac{\text{ft}}{\text{s}}-1}\right)+ \\ 2.5\left\{\dfrac{4.84\,\text{ft}/\left(2.63\text{ x }10^{-3}\text{ ft}\right)}{0.4\left(4.84\,\text{ft}/\left(2.63\text{ x }10^{-3}\text{ ft}\right)\right)^{1.2}+10.6\left(4.84\,\text{ft}/\left(2.63\text{ x }10^{-3}\text{ ft}\right)\right)^{-0.13}}\right\} \\ \left(\dfrac{16.36\frac{\text{ft}}{\text{s}}/1.6\frac{\text{ft}}{\text{s}}-6.0\frac{\text{ft}}{\text{s}}/1.6\frac{\text{ft}}{\text{s}}}{16.36\frac{\text{ft}}{\text{s}}/1.6\frac{\text{ft}}{\text{s}}-1}\right) \end{array}\right]$$

$Y_{s(col+pc)(2)}$=7.12 ft

L. Compute H'_{pc} and T' using Equations 4.75 and 4.76.

$$H'_{pc} = H_{pc} = \text{-5 ft since } Y_{s(col+pc)(2)} \geq \left|H_{pc}\right|$$

$$T' = T = 4\text{ ft since } Y_{s(col+pc)(2)} \geq \left|H_{pc}\right|$$

M. Check for convergence using Equations 4.77.

$$1)\ \Delta \equiv \left|\frac{Y_{s(col+pc)(2)} - Y_{s(col+pc)(1)}}{Y_{s(col+pc)(1)}}\right| = \left|\frac{7.12\text{ ft} - 6.15\text{ ft}}{6.15\text{ ft}}\right| = 0.16$$

2) Since $\Delta > 0.05$ proceed to Step H above

H. Compute $y_{o(max)(3)}$ and the pile cap's effective diameter, $D^*_{pc(3)}$.

$$y_o = 13\text{ ft},$$

$$1.64\left(5\,\text{ft}\left(0.93*15\,\text{ft}\right)^{\frac{5}{2}}\right)^{\frac{2}{7}} = 16.01\,\text{ft}$$

Therefore, $y_{o(max)(3)} = y_o = 13.0$ ft

I. Calculate $D^*_{pc(3)}$.

$$D^*_{pc(3)} = (0.55)(0.93)(1.38)(15\text{ ft})\,exp\left[-1.04 - 1.77\,exp\left(\frac{-5.0\text{ ft}}{13\text{ ft}}\right) + 1.695\left(\frac{4.0\text{ ft}}{13\text{ ft}}\right)^{\frac{1}{2}}\right]$$

$D^*_{pc(3)} = 2.87$ ft

J. Calculate $D^*_{(col+pc)(3)}$.

$$D^*_{(col+pc)(2)} = 1.97\text{ ft} + 2.87\text{ ft} = 4.84\text{ ft}$$

K. Calculate $Y_{s(col+pc)(3)}$.

$$Y_{s(col+pc)(3)} = (4.84\text{ ft})\tanh\left[\left(\frac{13\text{ ft}}{4.84\text{ ft}}\right)^{0.4}\right]\times\left[\begin{array}{l} 2.2\left(\dfrac{6.0\frac{\text{ft}}{\text{s}}/1.6\frac{\text{ft}}{\text{s}}-1}{16.36\frac{\text{ft}}{\text{s}}/1.6\frac{\text{ft}}{\text{s}}-1}\right)+ \\ 2.5\left\{\dfrac{4.84\text{ ft}/\left(2.63\text{ x }10^{-3}\text{ ft}\right)}{0.4\left(4.84\text{ ft}/\left(2.63\text{ x }10^{-3}\text{ ft}\right)\right)^{1.2}+10.6\left(4.84\text{ ft}/\left(2.63\text{ x }10^{-3}\text{ ft}\right)\right)^{-0.13}}\right\} \\ \left(\dfrac{16.36\frac{\text{ft}}{\text{s}}/1.6\frac{\text{ft}}{\text{s}}-6.0\frac{\text{ft}}{\text{s}}/1.6\frac{\text{ft}}{\text{s}}}{16.36\frac{\text{ft}}{\text{s}}/1.6\frac{\text{ft}}{\text{s}}-1}\right) \end{array}\right]$$

$Y_{s(col+pc)(3)} = 7.12$ ft

L. Compute H'_{pc} and T' using Equations 4.75 and 4.76.

$$H'_{pc} = H_{pc} = -5\text{ ft since } Y_{s(col+pc)(3)} \geq |H_{pc}|$$

$$T' = T = 4\text{ ft since } Y_{s(col+pc)(3)} \geq |H_{pc}|$$

M. Check for convergence using Equations 4.77.

1) $\Delta \equiv \left| \frac{Y_{s(col+pc)(3)} - Y_{s(col+pc)(2)}}{Y_{s(col+pc)(2)}} \right| = \left| \frac{7.12 \text{ ft} - 7.12 \text{ ft}}{7.12 \text{ ft}} \right| = 0.0$

2) Since $\Delta < 0.05$ proceed to Step N

N. Pile cap summary.

$$D^*_{pc} = D^*_{pc(3)} = 2.87 \text{ ft}$$
$$D^*_{(col+pc)} = D^*_{(col+pc)(3)} = 4.83 \text{ ft}$$
$$y_{s(col+pc)} = Y_{s(col+pc)(3)} = 7.13 \text{ ft}$$

O. Determine if pile group is exposed.

Since the $y_{s(col+pc)}$ exposes the pile group, continue on to compute the pile group effective diameter.

Finally, compute the pile group's effective diameter following Steps A-I from Section 4.2.3.3.

A. Calculate the $\overline{H}_{pg}$ and $\overline{y}_o$ using Equation 4.15 and 4.16.

$$\overline{H}_{pg} = H_{pg} + y_{s(col+pc)} = -5 \text{ ft} + 7.12 \text{ ft} = 2.12 \text{ ft}$$
$$\overline{y}_o = y_o + y_{s(col+pc)} = 13 \text{ ft} + 7.12 \text{ ft} = 20.12 \text{ ft}$$

B. Compute the shape factor for the pile group, K_s.

$$K_s = \frac{K_{s(pile)} - K_{s(pile\ group)}}{9}\left(\frac{s}{b}\right) + K_{s(pile)} - \frac{10}{9}\left(K_{s(pile)} - K_{s(pile\ group)}\right),$$

$$K_{s(pile\ or\ pile\ group)} = \begin{cases} 1 & \text{for circular piles or pile group arrays} \\ 0.86 + 0.97\left|\alpha \frac{\pi}{180^0} - \frac{\pi}{4}\right|^4 & \text{for square piles or pile group arrays} \end{cases}$$

Since both the individual piles and pile group are both square, the shape factor will be the same for both.

$$K_{s(pile)} = 0.86+0.97\left|15^{o}\frac{\pi}{180^{o}}-\frac{\pi}{4}\right|^{4} = 0.93$$

$$K_{s(pilegroup)} = 0.86+0.97\left|15^{o}\frac{\pi}{180^{o}}-\frac{\pi}{4}\right|^{4} = 0.93$$

$$K_{s} = \frac{0.93-0.93}{9}\left(\frac{6\text{ ft}}{2\text{ ft}}\right)+0.93-\frac{10}{9}(0.93-0.93) = 0.93$$

C. Calculate the projected width of the pile group.

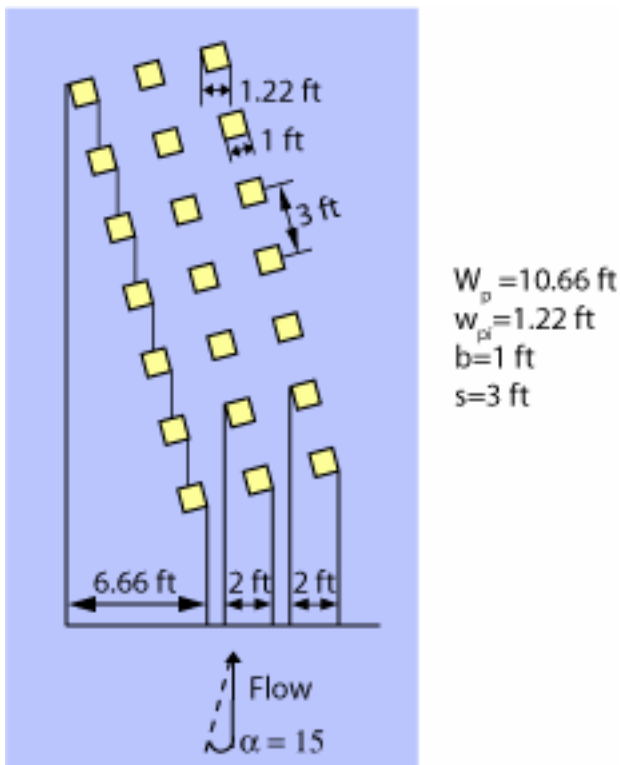

Figure 4-22 The Projected Width of the Pile Group

D. Calculate the pile spacing coefficient, K_{sp}.

$$K_{sp} = 1-\frac{4}{3}\left(1-\frac{w_{pi}}{W_{p}}\right)\left(1-\frac{1}{\left(\frac{s}{w_{pi}}\right)^{0.6}}\right) = 1-\frac{4}{3}\left(1-\frac{1.22\text{ ft}}{10.66\text{ ft}}\right)\left(1-\frac{1}{\left(\frac{3\text{ ft}}{1.22\text{ ft}}\right)^{0.6}}\right) = 0.51$$

E. Calculate K_m coefficient that accounts for the number of piles in line with the flow.

$$K_m = \begin{cases} 0.045(m) + 0.96 & |\alpha| < 5^0, \text{and } m \le 5 \\ 1.19 & |\alpha| < 5^0, \text{and } m > 5 \\ 1 & |\alpha| \ge 5^0 \end{cases}$$

$$\alpha = 15^0, \text{ therefore } K_m = 1$$

F. Compute $\overline{y}_{0(max)}$ for the pile group.

$$\overline{y}_{0(max)} = \begin{cases} \overline{y}_0 & \text{for } \overline{y}_0 \le 2K_s\ W_p\ K_{sp}\ K_m \\ 2K_s\ W_p\ K_{sp}\ K_m & \text{for } \overline{y}_0 > 2K_s\ W_p\ K_{sp}\ K_m \end{cases}$$

$$2K_s\ W_p\ K_{sp}\ K_m = 2(0.93)(10.66\text{ ft})(0.51)(1) = 10.11\text{ ft}$$

$$\overline{y}_0 = 20.12\text{ ft},$$

$$\text{therefore, } \overline{y}_{0(max)} = 10.11\text{ft}$$

G. Compute the submerged pile group coefficient, K_h.

$$K_h = 1.5\ tanh\left(0.8\sqrt{\frac{2.12\text{ ft}}{10.11\text{ ft}}}\right) = 0.53$$

H. Compute the buried pile group attenuation coefficient, K_{bpg}, using Equation 4.86.

$$K_{bpg} = \frac{\overline{H}_{pg}}{y_{s(col+pc)}} = \frac{2.12\text{ ft}}{7.12\text{ ft}} = 0.30$$

I. Compute the pile group effective diameter, D^*_{pg}.

$$D^*_{pg} = K_s\ K_{sp}\ K_m\ K_h\ K_{bpg}\ W_p = (0.93)(0.51)(1)(0.53)(0.30)(10.66\text{ ft}) = 0.80\text{ ft}$$

The effective diameter of the complex pier is the sum of each component's effective diameter.

$$D^* \equiv D^*_{col} + D^*_{pc} + D^*_{pg}$$

$$D^* = 1.97\,\text{ft} + 2.87\,\text{ft} + 0.80\,\text{ft} = 5.64\,\text{ft}$$

$$\frac{y_s}{D^*_{(col+pc+pg)}} = \tanh\left[\left(\frac{y_o}{D^*_{(col+pc+pg)}}\right)^{0.4}\right] \times \left[\begin{array}{l} 2.2\left(\dfrac{V/V_c - 1}{V_{lp}/V_c - 1}\right) + \\ 2.5\left\{\dfrac{D^*_{(col+pc+pg)}/D_{50}}{0.4\left(D^*_{(col+pc+pg)}/D_{50}\right)^{1.2} + 10.6\left(D^*_{(col+pc+pg)}/D_{50}\right)^{-0.13}}\right\} \\ \left(\dfrac{V_{lp}/V_c - V/V_c}{V_{lp}/V_c - 1}\right) \end{array}\right]$$

$$y_s = \left(5.64\text{ ft}\right) tanh\left[\left(\frac{13\text{ ft}}{5.64\text{ ft}}\right)^{0.4}\right] \times \left[\begin{array}{l} 2.2\left(\dfrac{6.0\frac{ft}{s}/1.6\frac{ft}{s} - 1}{16.36\frac{ft}{s}/1.6\frac{ft}{s} - 1}\right) + \\ 2.5\left\{\dfrac{5.64\text{ ft}/2.63\text{ x }10^{-3}\text{ ft}}{0.4\left(5.64\text{ ft}/2.63\text{ x }10^{-3}\text{ ft}\right)^{1.2} + 10.6\left(5.64\text{ ft}/2.63\text{ x }10^{-3}\text{ ft}\right)^{-0.13}}\right\} \\ \left(\dfrac{16.36\frac{ft}{s}/1.6\frac{ft}{s} - 6.0\frac{ft}{s}/1.6\frac{ft}{s}}{16.36\frac{ft}{s}/1.6\frac{ft}{s} - 1}\right) \end{array}\right]$$

y_s = <u>7.99 ft</u>

The total scour for the complex pier is computed using the flow conditions listed in Table 4-3 and an effective diameter of 4.94 ft in Equations 3.4 to 3.15.

The resulting local scour depth for the complex pier is **7.99 ft**.

4.3. Predicted versus Measured Laboratory Data

The methodology for computing local scour at complex piers was developed using laboratory data. Data from scour tests performed by Sterling Jones at the Turner Fairbanks Laboratory located in Virginia, Steven Coleman at the University of Auckland in New Zealand, and by D. Max Sheppard at the University of Florida, the University of Auckland and at the USGS-CAFRC laboratory in Turners Falls, Massachusetts were used in the formulation. The revised procedure was the result of additional laboratory data becoming available for both partially buried and completely buried pile caps. In order to validate the revised procedure, it was used to predict the scour experiments from the different researchers. A brief summary of the more recent experiments performed by Sterling Jones, Stephen Coleman and Max Sheppard along with their data is presented in the following section.

4.3.1. Laboratory Experiments

4.3.1.1. Jones' Experiments

The structures used in Jones' tests are composed of two components, a column (stem) and a Pile cap (footer). Figure 4-23 illustrates the three piers used in the experiments, all having a 0.15 m square column, and 0.03 ft thick square pile caps with varying widths. Figure 4-24 presents the four different positions the piers were tested in and Table 4-4 and Table 4-5 list the conditions during the experiments and the measured scour depths. Figure 4-25 shows the measured scour depth, the predicted scour depth using the revised methodology presented in this chapter, and the predicted scour depth using the current HEC-18 procedure.

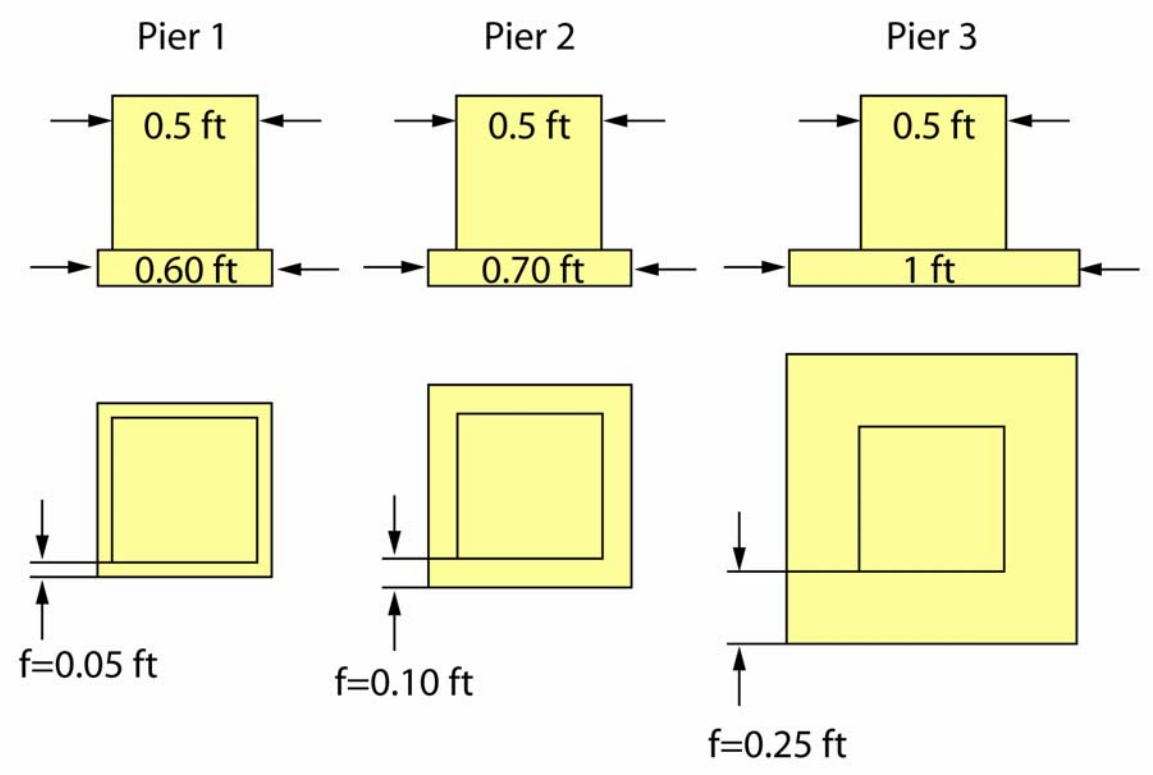

Figure 4-23 Structures used in Sterling Jones' experiments.

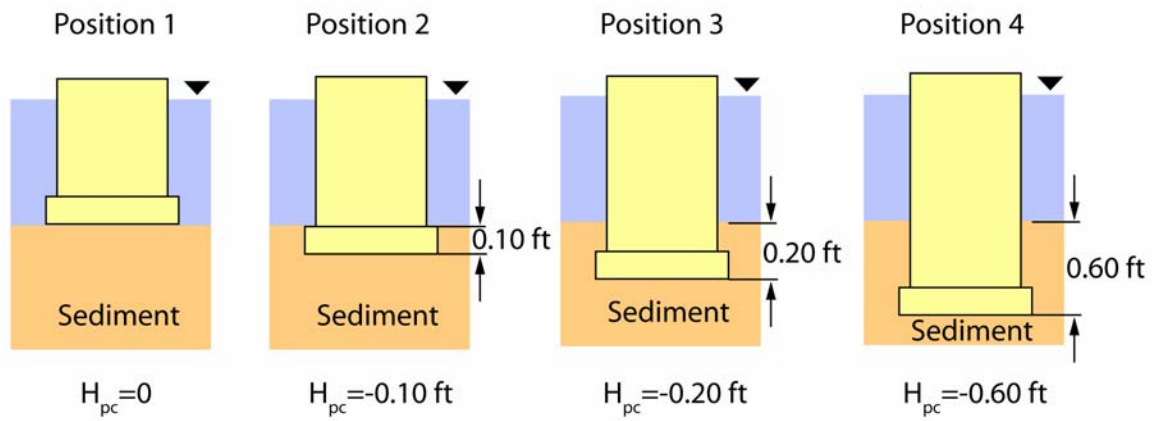

Figure 4-24 Position of the structures in Sterling Jones' experiments.

Table 4-4 Flow conditions for Jones' experiments.

Experiment	D_{50} (mm)	Skew	Velocity (ft/s)	Critical Velocity (ft/s)	Water Depth (ft)	y_s (ft)
1	1.0	0.0	1.55	1.31	1.0	1.00
2	1.0	0.0	1.55	1.31	1.0	0.57
3	1.0	0.0	1.55	1.31	1.0	0.50
4	1.0	0.0	1.55	1.31	1.0	0.40
5	1.0	0.0	1.55	1.31	1.0	1.11
6	1.0	0.0	1.55	1.31	1.0	0.71
7	1.0	0.0	1.55	1.31	1.0	0.56
8	1.0	0.0	1.55	1.31	1.0	0.47
9	1.0	0.0	1.55	1.31	1.0	0.79
10	1.0	0.0	1.55	1.31	1.0	0.82
11	1.0	0.0	1.55	1.31	1.0	0.59
12	1.0	0.0	1.55	1.31	1.0	0.52

Table 4-5 Pier information for Jones' experiments.

Experiment	b_{col} (ft)	l_{col} (ft)	f_1 (ft)	f_2 (ft)	H_{col} (ft)	b_{pc} (ft)	l_{pc} (ft)	T (ft)	H_{pc} (ft)
1	0.5	0.5	0.1	0.1	-0.5	0.6	0.6	0.1	-0.6
2	0.5	0.5	0.1	0.1	-0.1	0.6	0.6	0.1	-0.2
3	0.5	0.5	0.1	0.1	0.0	0.6	0.6	0.1	-0.1
4	0.5	0.5	0.1	0.1	0.1	0.6	0.6	0.1	0.0
5	0.5	0.5	0.2	0.2	-0.5	0.7	0.7	0.1	-0.6
6	0.5	0.5	0.2	0.2	-0.1	0.7	0.7	0.1	-0.2
7	0.5	0.5	0.2	0.2	0.0	0.7	0.7	0.1	-0.1
8	0.5	0.5	0.2	0.2	0.1	0.7	0.7	0.1	0.0
9	0.5	0.5	0.5	0.5	-0.5	1.0	1.0	0.1	-0.6
10	0.5	0.5	0.5	0.5	-0.1	1.0	1.0	0.1	-0.2
11	0.5	0.5	0.5	0.5	0.0	1.0	1.0	0.1	-0.1
12	0.5	0.5	0.5	0.5	0.1	1.0	1.0	0.1	0.0

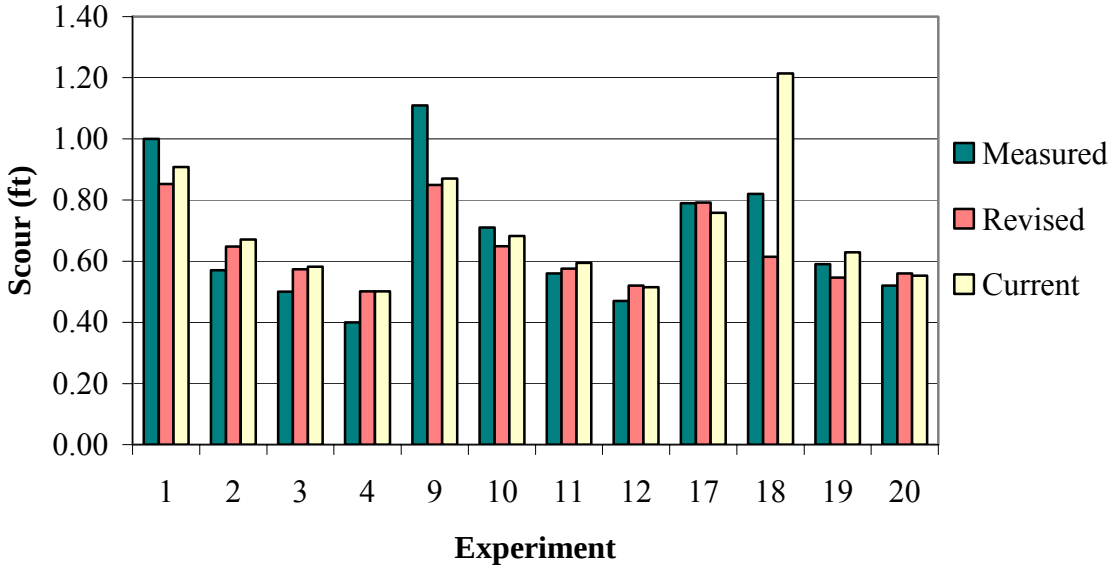

Figure 4-25 Scour predictions of Jones' laboratory complex pier local scour experiments using the current scour prediction procedures (HEC-18) and using the revised procedures (UF).

4.3.1.2. Coleman's Experiments

Steven Coleman's experiments were conducted with three different complex piers as shown in Figure 4-26 through Figure 4-28. All three piers are composed of three components (column, pile cap, and pile group). Coleman varied the position of the pile cap by starting with the pile cap out of the water. The pile cap was lowered down in the water column after each successive test until the bottom of the pile cap was not uncovered by the column scour. He repeated this procedure for each of the piers tested. Table 4-6 and Table 4-7 list the conditions and extrapolated equilibrium scour depth for each of the reported experiments. The scour predictions for non buried pile caps (Case 1) are illustrated in Figure 4-29 versus extrapolated equilibrium scour depths. Figure 4-30 presents the predictions for the complex structures having a buried or partially buried pile cap (Case 2 and Case3) versus extrapolated equilibrium scour depths.

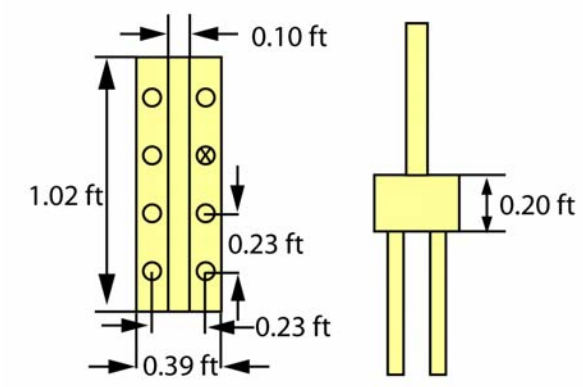

Figure 4-26 Plan and elevation view of model complex pier 1 (Type A, All dimensions are in feet).

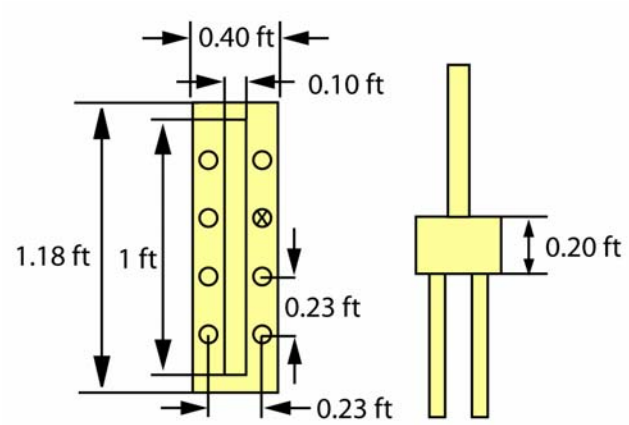

Figure 4-27 Plan and elevation view of model complex pier 2 (Type B, All dimensions are in feet).

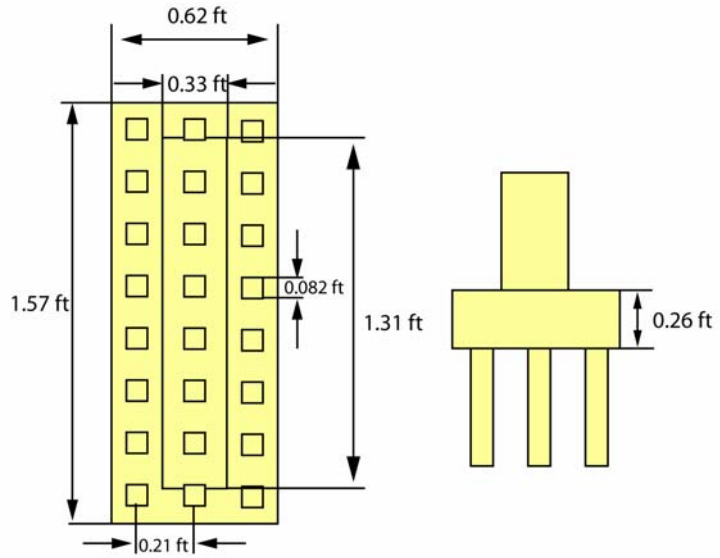

Figure 4-28 Plan and elevation view of model complex pier 3 (Type C, All dimensions are in feet).

Table 4-6 Flow conditions during the laboratory scour experiments.

Experiment	D_{50} (mm)	Skew	Velocity (ft/s)	Critical Velocity (ft/s)	Water Depth (ft)
1	0.84	0	1.08	1.41	1.97
2	0.84	0	1.08	1.41	1.97
3	0.84	0	1.08	1.41	1.97
4	0.84	0	1.08	1.41	1.97
5	0.84	0	1.08	1.41	1.97
6	0.84	0	1.08	1.41	1.97
7	0.84	0	1.08	1.41	1.97
8	0.84	0	1.08	1.41	1.97
9	0.84	0	1.25	1.41	1.97
10	0.84	0	1.25	1.41	1.97
11	0.84	0	1.25	1.41	1.97
12	0.84	0	1.25	1.41	1.97
13	0.84	0	1.25	1.41	1.97
14	0.84	0	1.25	1.41	1.97
15	0.84	0	1.25	1.41	1.97
16	0.84	0	1.25	1.41	1.97
17	0.84	0	1.25	1.41	1.97
18	0.84	0	1.25	1.41	1.97
19	0.84	0	1.25	1.41	1.97
20	0.84	0	1.25	1.41	1.97
21	0.84	0	1.25	1.41	1.97
22	0.84	0	1.25	1.41	1.97
23	0.84	0	1.25	1.41	1.97
24	0.84	0	1.25	1.41	1.97
25	0.84	0	1.12	1.31	1.08
26	0.84	0	1.12	1.31	1.08
27	0.84	0	1.12	1.31	1.08
28	0.84	0	1.12	1.31	1.08
29	0.84	0	1.12	1.31	1.08
30	0.84	0	1.12	1.31	1.08

Table 4-7 Scale model geometrical information for the laboratory scour experiments.

Experiment	Type	b_{col} (ft)	l_{col} (ft)	f_1 (ft)	f_2 (ft)	H_{col} (ft)	b_{pc} (ft)	l_{pc} (ft)	T (ft)	H_{pc} (ft)	n	m	s (ft)
1	A	0.098	1.024	0.00	0.148	2.165	0.394	1.024	0.197	1.969	2	4	0.236
2	A	0.098	1.024	0.00	0.148	1.083	0.394	1.024	0.197	0.886	2	4	0.236
3	A	0.098	1.024	0.00	0.148	0.394	0.394	1.024	0.197	0.197	2	4	0.236
4	A	0.098	1.024	0.00	0.148	0.197	0.394	1.024	0.197	0.000	2	4	0.236
5	A	0.098	1.024	0.00	0.148	0.148	0.394	1.024	0.197	-0.049	2	4	0.236
6	A	0.098	1.024	0.00	0.148	0.000	0.394	1.024	0.197	-0.197	2	4	0.236
7	A	0.098	1.024	0.00	0.148	-0.098	0.394	1.024	0.197	-0.295	2	4	0.236
8	A	0.098	1.024	0.00	0.148	-0.253	0.394	1.024	0.197	-0.449	2	4	0.236
9	B	0.098	1.024	0.164	0.148	1.969	0.394	1.188	0.197	1.772	2	4	0.236
10	B	0.098	1.024	0.164	0.148	1.640	0.394	1.188	0.197	1.444	2	4	0.236
11	B	0.098	1.024	0.164	0.148	1.640	0.394	1.188	0.197	1.444	2	4	0.236
12	B	0.098	1.024	0.164	0.148	1.312	0.394	1.188	0.197	1.115	2	4	0.236
13	B	0.098	1.024	0.164	0.148	0.984	0.394	1.188	0.197	0.787	2	4	0.236
14	B	0.098	1.024	0.164	0.148	0.656	0.394	1.188	0.197	0.459	2	4	0.236
15	B	0.098	1.024	0.164	0.148	0.328	0.394	1.188	0.197	0.131	2	4	0.236
16	B	0.098	1.024	0.164	0.148	0.197	0.394	1.188	0.197	0.000	2	4	0.236
17	B	0.098	1.024	0.164	0.148	0.180	0.394	1.188	0.197	-0.016	2	4	0.236
18	B	0.098	1.024	0.164	0.148	0.098	0.394	1.188	0.197	-0.098	2	4	0.236
19	B	0.098	1.024	0.164	0.148	0.000	0.394	1.188	0.197	-0.197	2	4	0.236
20	C	0.098	1.024	0.164	0.148	1.345	0.394	1.188	0.197	1.083	2	4	0.236
21	C	0.328	1.312	0.164	0.148	0.755	0.394	1.188	0.197	0.492	2	4	0.236
22	C	0.328	1.312	0.164	0.148	0.509	0.394	1.188	0.197	0.246	2	4	0.236
23	C	0.328	1.312	0.164	0.148	0.344	0.394	1.188	0.197	0.082	2	4	0.236
24	C	0.328	1.312	0.164	0.148	0.262	0.394	1.188	0.197	0.000	2	4	0.236
25	C	0.328	1.312	0.131	0.148	0.131	0.623	1.575	0.262	-0.131	3	8	0.213
26	C	0.328	1.312	0.131	0.148	0.000	0.623	1.575	0.262	-0.262	3	8	0.213
27	C	0.328	1.312	0.131	0.148	-0.131	0.623	1.575	0.262	-0.394	3	8	0.213
28	C	0.098	1.024	0.131	0.148	-0.262	0.623	1.575	0.262	-0.525	3	8	0.213
29	C	0.098	1.024	0.148	0.131	-0.492	0.623	1.575	0.262	-0.755	3	8	0.213
30	C	0.098	1.024	0.148	0.131	-0.689	0.623	1.575	0.262	-0.951	3	8	0.213

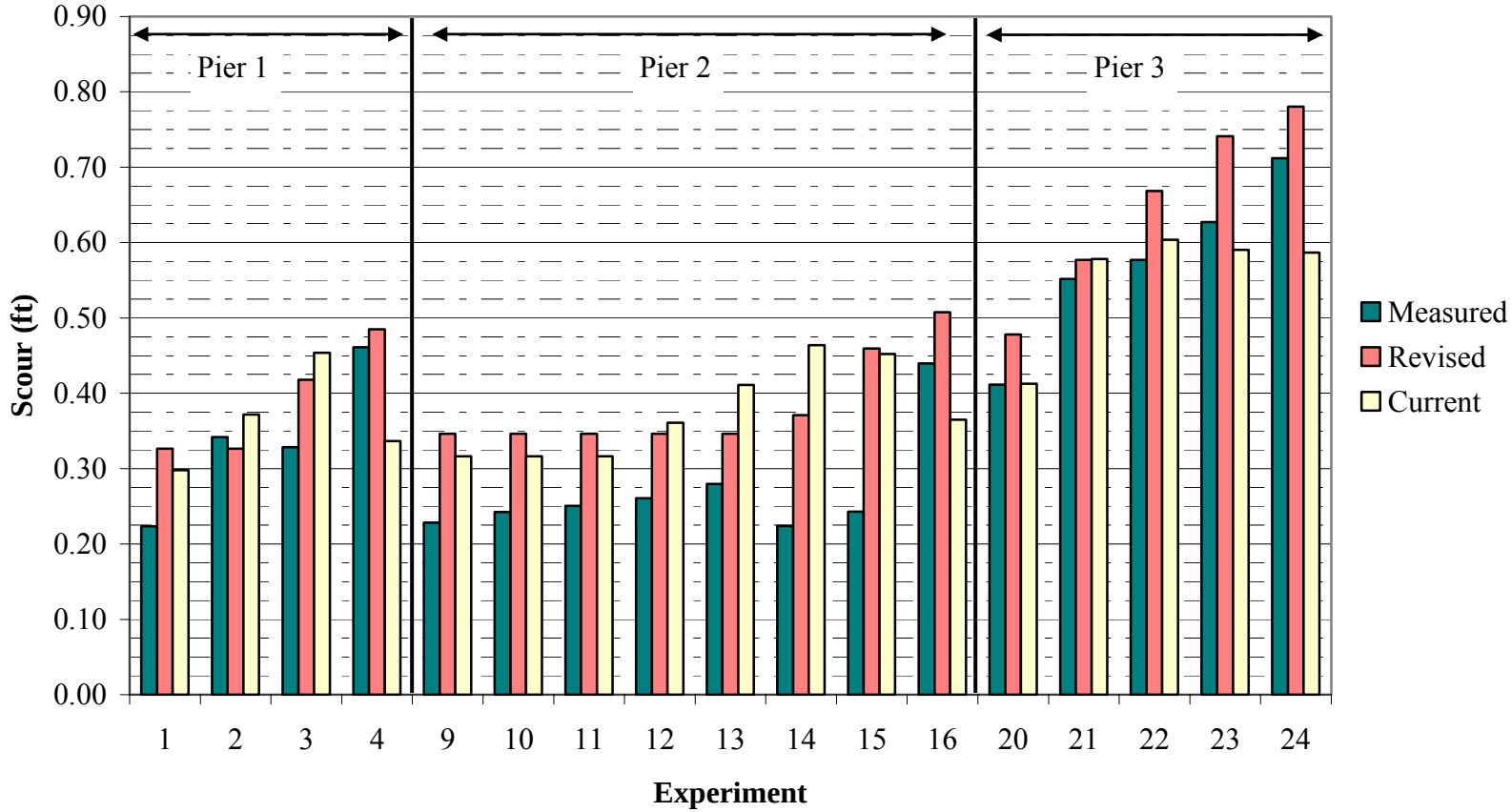

Figure 4-29 Scour predictions of laboratory complex pier local scour experiments (non-buried complex piers) using the current scour prediction procedures (HEC-18) and using the revised procedures (UF).

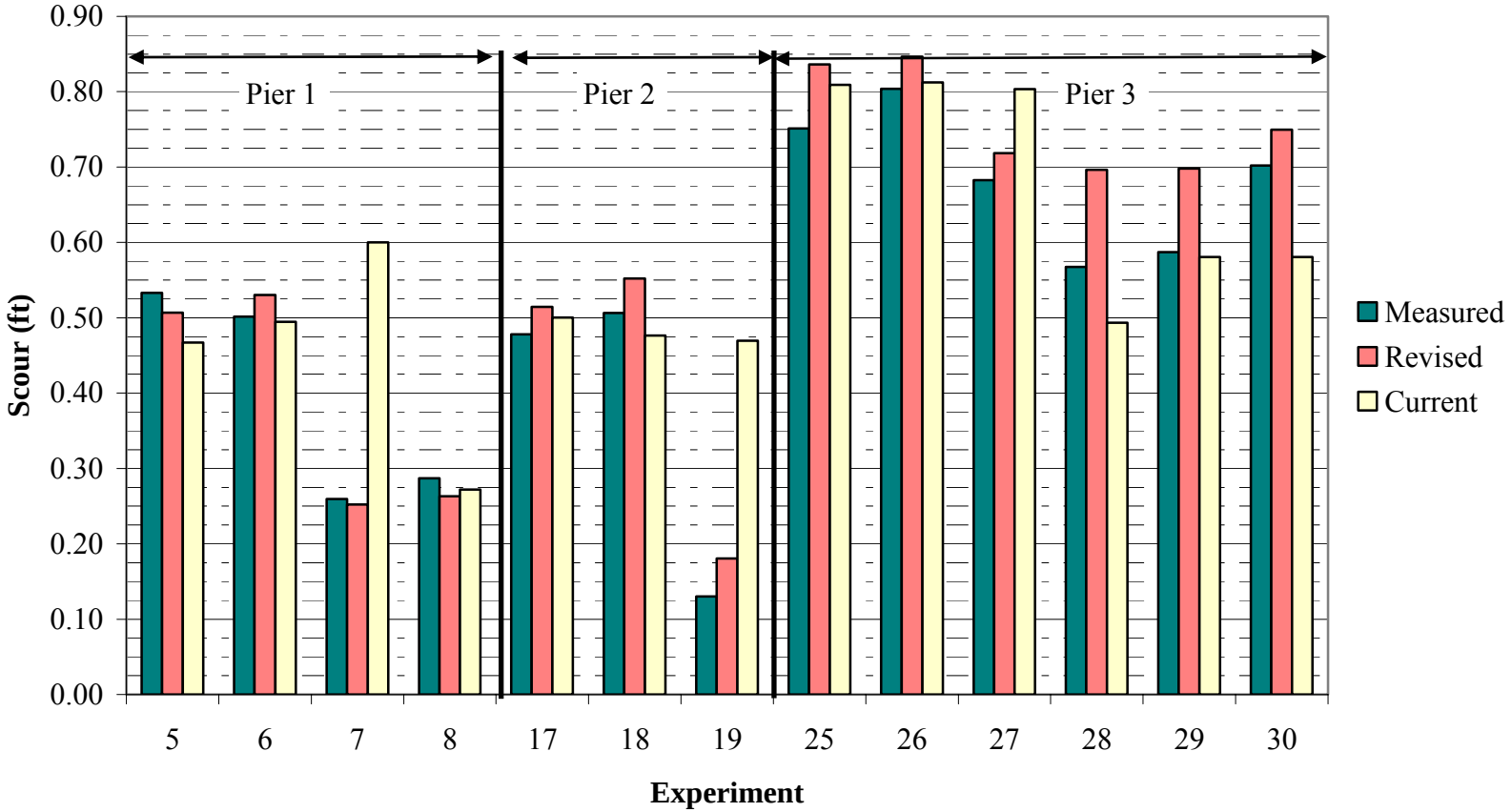

Figure 4-30 Scour predictions of laboratory buried or partially buried complex pier local scour experiments using the current scour prediction procedures (HEC-18) and using the revised procedures (UF).

4.3.1.3. Sheppard's Experiments

Sheppard's experiments were performed at the University of Auckland with the pier shown in Figure 4 28. The vertical position of the pier was varied as illustrated in Figure 4 31. The scour experiments were all performed in live bed flow conditions. Table 4-8 and Table 4-9 lists the conditions present during the experiments and the equilibrium scour depth for each test. The equilibrium scour depth listed for each experiment was established by fitting the time rate data for each test with a curve fit, and extrapolating the curve fit out to infinity. The reported equilibrium scour depths were all greater than the measured values. An average bed elevation was determined for each test because live bed flow generates sand waves that propagate downstream into and out of the developing scour hole.

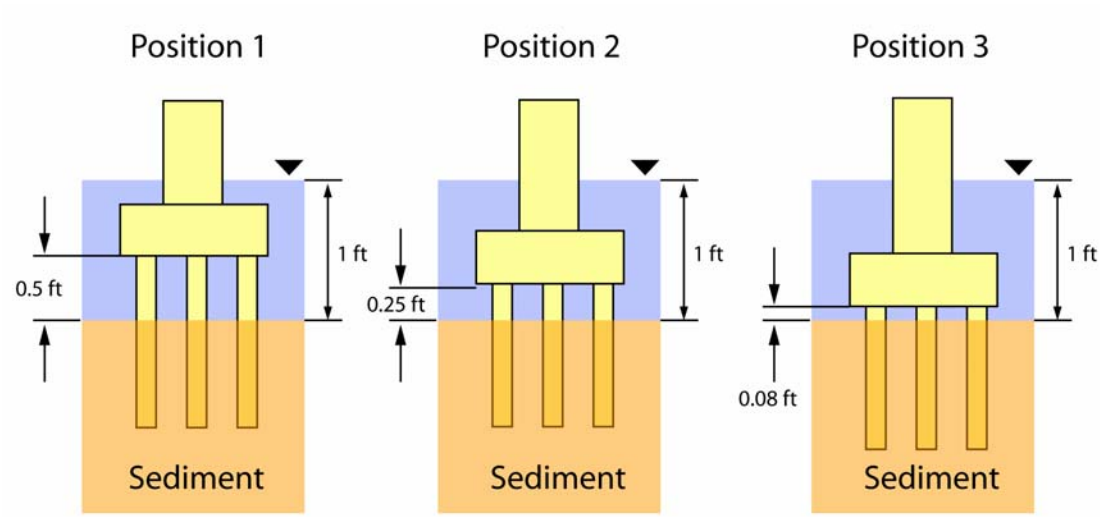

Figure 4-31 Position of the piers in Sheppard's experiments.

Table 4-8 Flow conditions for Sheppard's experiments.

Experiment	Position	D_{50} (mm)	Skew Angle	Velocity (ft/s)	Critical Velocity (ft/s)	Water Depth (ft)	y_s (ft)
1	2	0.84	0	2.69	1.31	1.07	0.44
2	3	0.84	0	2.69	1.31	1.07	0.59
3	2	0.84	0	4.04	1.31	1.07	0.47
4	3	0.84	0	4.04	1.31	1.07	0.62
5	1	0.84	0	2.69	1.31	1.10	0.52
6	1	0.84	0	3.97	1.31	1.08	0.39
7	1	0.84	0	2.00	1.31	1.09	0.43

Table 4-9 Pier information for Sheppard's experiments.

Experiment	b_{col} (ft)	l_{col} (ft)	f_1 (ft)	f_2 (ft)	H_{col} (ft)	b_{pc} (ft)	l_{pc} (ft)	T (ft)	H_{pc} (ft)	n	m	s (ft)
1	0.33	1.31	0.13	0.15	0.51	0.62	1.57	0.26	0.25	3	8	0.21
2	0.33	1.31	0.13	0.15	0.34	0.62	1.57	0.26	0.08	3	8	0.21
3	0.33	1.31	0.13	0.15	0.51	0.62	1.57	0.26	0.25	3	8	0.21
4	0.33	1.31	0.13	0.15	0.34	0.62	1.57	0.26	0.08	3	8	0.21
5	0.33	1.31	0.13	0.15	0.75	0.62	1.57	0.26	0.49	3	8	0.21
6	0.33	1.31	0.13	0.15	0.75	0.62	1.57	0.26	0.49	3	8	0.21
7	0.33	1.31	0.13	0.15	0.75	0.62	1.57	0.26	0.49	3	8	0.21

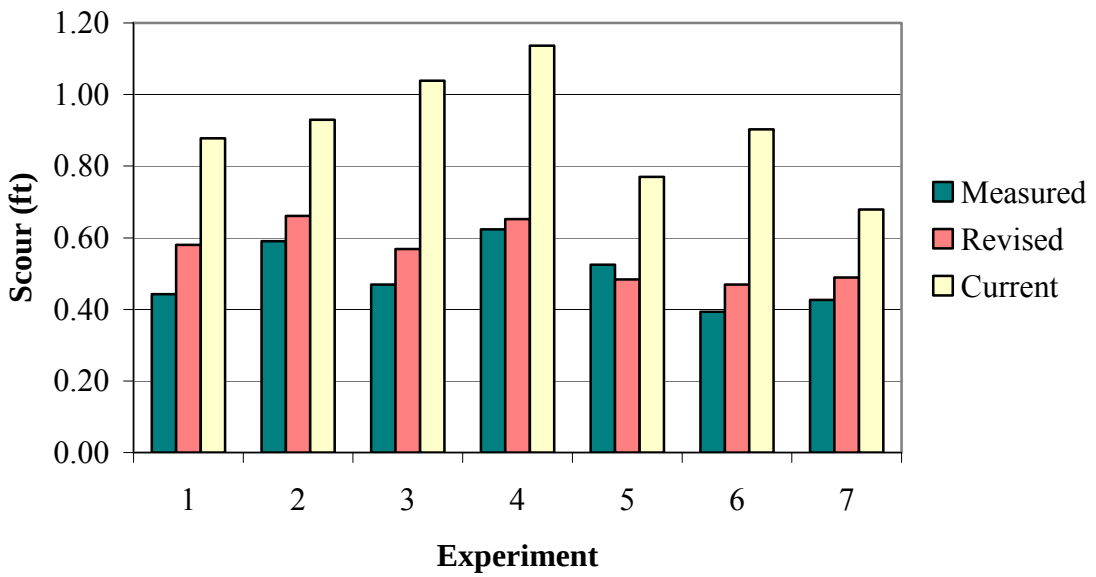

Figure 4-32 Scour predictions of Sheppards' laboratory complex pier local scour experiments using the current scour prediction procedures (HEC-18) and using the revised procedures (UF).

CHAPTER 5 CONSERVATISM IN APPROACH TO SCOUR ESTIMATION

The scour prediction equations discussed in Chapter 3 are designed to be conservative; i.e., they are designed to predict scour depths that are greater than would be experienced for the given structure, sediment and flow conditions. The implied conservatism is a result of performing scour experiments in laboratory conditions that are rarely found, if ever, at bridge sites. Factors in the laboratory not commonly found in the field that can influence local scour depths include a very narrow sediment size distribution and minimal fine sediments in the water column, both of which produce larger scour depths than would occur under normal field conditions. In addition for many, if not most, field situations the duration of the design flow event is not sufficient for the scour depth to reach an equilibrium value. The following sections discuss the sediment size distribution, suspended fine sediments (washload) in the water column, local scour time dependency, and additional geometric effects not included in the complex pier analysis that add a level of conservatism to the scour estimation.

5.1. Sediment Size Distribution

Laboratory experiments show [see e.g. Ettema (1976)] that the greatest local scour depths occur for uniform diameter sediments. For this reason most researchers conduct their experiments with near uniform sediments [i.e. sediments with as low a value of sigma ($\sigma = \sqrt{D_{84} / D_{16}}$) as possible]. The empirical scour prediction equations in Chapter 3 are based on data from laboratory experiments with near uniform diameter sediments. Prototype sediments will always have a distribution of sediment sizes and thus will experience smaller scour depths than predicted by these equations. The reason for the reduced scour in sediments with a distribution in sediment sizes is due to "armoring" of the scour hole by the larger particles left behind as the smaller particles are removed. In effect, the median grain size increases as the scour progresses, resulting in a lower value of V / V_c. It should be pointed out that the level of conservatism decreases as the value of V / V_c increases. That is, the larger the design flow velocity the less sensitive the equilibrium scour depth is to changes in grain size distribution. Figure 5-1 illustrates the

work of Ettema (1976) in quantifying the effects of σ on equilibrium scour depths. K_σ is a multiplier that decreases the equilibrium scour depth with increasing values of σ.

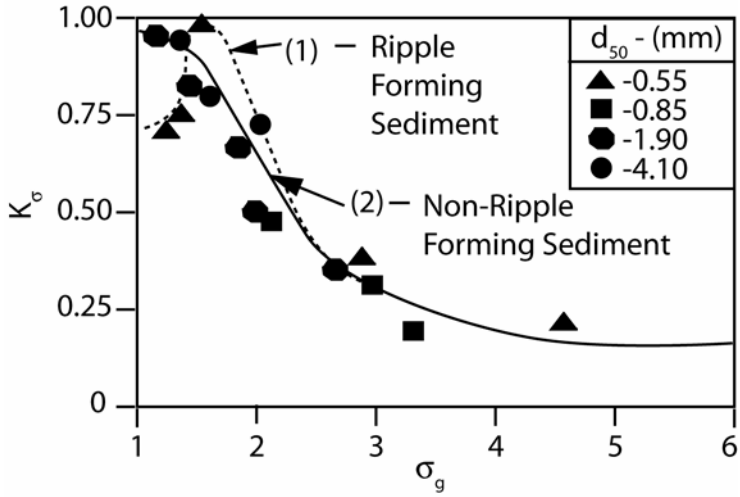

Figure 5-1 Effects of sediment size distribution, σ, on equilibrium scour depths.

5.2. Fine Sediment Suspensions

Researchers have known for some time that the presence of suspended fine sediment reduces the drag force exerted on the bed by the flowing water. Observations indicate that the shear stress reduction increases with increasing concentration and decreases with increasing velocity. Sheppard (2002) observed the impact of suspended fine sediment on local scour in his local scour experiments. Equilibrium scour depths were reduced by 90% or more when suspended fine sediments entered the tests. Further studies by Sheppard (2003) and Sheppard (2004) determined that even small concentrations of suspended fine sediment cause reductions in bed shear stress and local scour depth. The effects of the suspended fine sediment do, however, decrease as the flow velocities become large. Since for most streams, the amount of suspended sediment increases dramatically during design storm events, the scour depth prediction methods and equations presented in Chapters 3 and 4 will produce conservative results.

5.3. Time Dependency of Local Scour

When a structure located in an erodible bed is subjected to a steady current, the rate of local scour is large at first but then decreases as the scour hole deepens. The time

required to reach an equilibrium scour depth for a given structure, sediment and flow situation is not well understood. However, it is known to depend on a number of the structure, sediment and flow parameters as well as the equilibrium scour depth. For many coastal locations where the design storm event results from a hurricane storm surge generated (or hurricane wind generated) currents, the duration of the event may not be sufficient to achieve equilibrium scour conditions. This is particularly true if the sediment includes cohesive materials. Thus, employing equations that predict equilibrium scour depths will produce conservative values if the time to reach equilibrium scour depths is not taken into consideration.

5.4. Geometric Considerations

For bridges over navigable waterways conveying large ships (e.g. ICWW, Tampa Bay), the piers on either side of the main navigation channel are always protected from ship impact by fender systems. Physical model studies conducted at the University of Florida and at the FHWA Turner Fairbanks Hydraulics Research Center in McLean, Virginia show that fender systems tend to reduce the local scour depth at the pier protected by the fender system. For flows aligned with the channel, the reduction can be significant. Unless a physical model study of the combined pier and fender system is conducted, this reduction is not normally accounted for in the local scour prediction process thus the actual scour depths experienced by the pier will be less than the predicted values.

BIBLIOGRAPHY

Ahmad, M. (1953) "Experiments on Design and Behavior of Spur Dikes." *Proceedings of International Hydraulics Convention*, St. Anthony Falls Hydraulic Laboratory, Minneapolis, MN, 145-159.

Ahmad, M. (1962) "Discussion of 'Scour at Bridge Crossings' by E.M. Laursen." *Trans. of ASCE*, 127, pt. I(3294), 198-206.

Allen, J.R.L. (1976) "Computational Models for Dune Time Lag: General Ideas, Difficulties and Early Results," Sedimentary Geology, Vol. 16, p 255-279

Baker, R.E. (1986) "Local Scour at Bridge Piers in Non-uniform Sediment." Report No. 402, Department of Civil Engineering, University of Auckland, Auckland, New Zealand.

Basak V. (1975) "Scour at Square Piers." Devlet su isteri genel mudulugu, Report No. 583, Ankara, Turkey.

Blench, T. (1962) "Discussion of 'Scour at bridge crossings' by E.M. Laursen." *Trans. of ASCE*, 127, pt. I(3294), 180-183.

Bonasoundas M. (1973) "Non-stationary Hydromorphological Phenomena and Modelling of Scour Process." *Proc. 16th IAHR Congress*, Vol. 2, Sao Paulo, Brazil, 9-16.

Breusers, H.N.C., Nicollet, G. and Shen, H.W. (1977) "Local Scour Around Cylindrical piers." *Journal of Hydraulic Research*, 15(3), 211-252.

Chabert, J., and Engeldinger, P. (1956) "Etude des affouillements autour des piles des ponts." Laboratoire National d'Hydraulique, Chatou, France.

Chiew, Y.M. (1984) "Local scour at bridge piers." Master's Thesis, Auckland University, Auckland, New Zealand.

Ettema, R., (1980), "Scour at Bridge Piers," Ph.D. Thesis, Department of Civil Engineering, Auckland University, February 1980.

Chitale, S.V. (1962) "Discussion of 'Scour at bridge crossings' by E.M. Laursen." *Trans. of ASCE*, 127, pt. I(3294), 191-196.

Cunha, L.V. (1970) "Discussion of 'Local scour at bridge crossings' by Shen H.W., Schneider V.R. and Karaki S.S." *Trans. of ASCE*, 96(HY8), 191-196.

Dean, R. G., Dalrymple, R.A. (2002) "Coastal Processes with Engineering Applications", Cambridge University Press, ISBN 0521495350.

Ettema, R. (1976) “Influence of material gradation on local scour.” Master’s Thesis, Auckland University, Auckland, New Zealand.

Ettema, R. (1980) “Scour at bridge piers.” PhD Thesis, Auckland University, Auckland, New Zealand.

Fredsoe, J. (1980) “The formation of Dunes” Int. Symp. On River Sedimentation, Beijing, China.

Froehlich, D.C. (1988) “Analysis of on-site measurements of scour at piers.” *Proc. of the 1988 National Conference on Hydraulic Engineering*, ASCE, New York, 534-539.

Gao Dong Guang, Posada, G., and Nordin C.F. (1992) “Pier scour equations used in the People’s Republic of China.” Draft, Department of Civil Engineering, Colorado State University, Fort Collins, CO.

Garde, R.J, Ranga Raju, K.G., and Kothyari, U.C. (1993) *Effect on unsteadiness and stratification on local scour*. International Science Publisher, New York.

Graf, W.H. (1995) “Local scour around piers.” Annu. Rep., Laboratoire de Recherches Hydrauliques, Ecole Polytechnique Federale de Lausanne, Lausanne, Switzerland.

Gust, Giselher, (1976). "Observations on turbulent-drag reduction in a dilute suspension of clay in sea-water." Fluid Mechanics: 75 (1); p. 29-47.

Hancu, S. (1971) “Sur le calcul des affouillements locaux dams la zone des piles de ponts.” *Proc. 14th IAHR Congress*, Vol. 3, Paris, France, 299-313.

Hanna, C.R. (1978) “Scour at pile groups.” Master of Engineering Thesis, University of Cantebury, Christchurch, New Zealand.

http://vortex.spd.louisville.edu/BridgeScour/whatis.htm (1998) “What is Bridge Scour?” Department of Civil Engineering, University of Louisville.

Inglis, S.C. (1949) “The behavior and control of rivers and canals.” Central Water Power Irrigation and Navigation Report, Publication 13, part II, Poona Research Station, Poona, India.

Jain, S.C., and Fischer, E.E. (1979) “Scour around circular bridge piers at high Froude numbers.” Rep. No. FHWA-RD-79-104, FHWA, Washington DC.

Jette, C.D., and Hanes, D.M. (1997) “High resolution sea-bed imaging: an acoustic multiple transducer array.” *Measurement Science and Technology*, 8, 787-792.

Jones, J. Sterling and D. Max Sheppard. (2000) “Scour at Wide Piers,” Proceedings for the 2000 Joint Conference on Water Resources Engineering and Water Resources Planning and Management Conference, Minneapolis, MN, July 30-August 2, 2000.

Krishnamurthy, M. (1970) "Discussion of 'Local scour at bridge crossings' by Shen H.W., Schneider V.R. and Karaki S.S." *Trans. of ASCE*, 96(HY7), 1637-1638.

Larras, J. (1963) "Profondeurs Maximales d'Erosion des Fonds Mobiles autour des Piles en Riviere." Annales des Ponts et Chausses, Vol. 133, No. 4, 424-441.

Laursen E.M. (1962) "Scour at bridge crossings." *Trans. of ASCE*, 84(HY1), 166-209.

Laursen, E.M. (1958) "Scour at Bridge Crossings." Iowa Highway Research Bd., Bulletin No. 8.

Laursen E.M., and Toch A. (1956) "Scour around bridge piers and abutments." Bulletin No. 4, Iowa Highway Research Board, Ames, IA.

Melville, B.W., and Chiew, Y.M. (1999) "Time scale for local scour at bridge piers." *Journal of Hydraulic Engineering*, 125(1), 59-65.

Melville, B.W. (1997) "Pier and abutment scour-an integrated approach." *Journal of Hydraulic Engineering*, 123(2), 125-136.

Melville, B.W., and Sutherland, A.J. (1988) "Design method for local scour at bridge piers." *Journal of Hydraulic Engineering*, 114(10), 1210-1226.

Melville, B.W. (1984) "Live Bed Scour at Bridge Piers." J. Hydraulic Engineering, Vol. 110, No. 9, pp 1234-1247.

Melville, B.W. (1975) "Local scour at bridge sites." Report no. 117, University of Auckland, School of Engineering, Auckland, New Zealand.

Neill, C.R. (1964) "River bed scour, a review for bridge engineers." Contract No. 281, Res. Council of Alberta, Calgary, Alberta, Canada.

Neill, C.R. (1973) *Guide to Bridge Hydraulics*. Roads and Transportation Association of Canada, University of Toronto Press, Canada.

Nicollet, G., and Ramette, M. (1971) "Affouillement au voisinage de pont cylindriques circularies" *Proc. of the 14th IAHR Congress*, Vol. 3, Paris, France, 315-322.

Pilarczyk, K.W. (1995) "Design tools related to revetments including riprap." *River, coastal and shoreline protection: Erosion control using riprap and armour stone*, John Wiley & Sons, New York, 17-38.

Ranga Raju, K.G. and Soni, J.P. (1976) "Geometry of Ripples and Dunes in Alluvial Channels," *Journal of Hydraulic Research*, Vol. 14, No. 3, The Netherlands

Raudkivi, A.J., and Ettema, R. (1977) "Effect of sediment gradation on clear water scour." *Journal of Hydraulic Engineering*, 103(10), 1209-1212.

Rouse, H. (1946) *Elementary Fluid Mechanics*. John Wiley & Sons, New York.

Shen, H.W. (1971) “Scour near piers.” *River Mechanics*, Vol. II, Chapter 23, Colorado State University, Fort Collins, CO.

Shen, H.W., Schneider, V.R. and Karaki, S.S. (1969) “Local Scour around Bridge Piers.” Proc. ASCE, J. Hydraulics Div., Vol. 95, No. HY6.

Shen, H.W., Schneider, V.R. and Karaki, S.S. (1966) “Mechanics of Local Scour.” Colorado State University, Civil Engineering Dept., Fort Collins, Colorado, Pub. No. CER66-HWS22.

Sheppard, D. M. (2004). "An Overlooked Local Sediment Scour Mechanism." Proceedings of the 83rd Meeting of the Transportation Research Board, Washington, D.C., January 11-15, 2004 and published in the *J. of the Transportation Research Board, Transportation Research Record,* No. 1890, pp107-111.

Sheppard, D. Max, Mufeed Odeh and Tom Glasser (2004),”Large Scale Clearwater Local Pier Scour Experiments”, J. Hydr. Engrg., ASCE, 130, No. 10, 957-963.

Sheppard, D. Max, Mufeed Odeh and Tom Glasser (2002), “Large Scale Clearwater Local Pier Scour Experiments”, Coastal Engineering Technical Report No. 131, Civil and Coastal Engr. Dept., Univ. of FL, Gainesville, Florida, March 2002, pp 296.

Sheppard, D. Max, Jeffrey Sheldon, Eric Smith, and Mufeed Odeh. (2000) “Hydraulic Modeling and Scour Analysis for the San Francisco-Oakland Bay Bridge,” Proceedings for the 2000 Joint Conference on Water Resources Engineering and Water Resources Planning and Management Conference, Minneapolis, MN, July 30-August 2, 2000.

Sheppard, D. Max, Mufeed Odeh, Tom Glasser, and Athanasios Pritsivelis. (2000) “Clearwater Local Scour Experiments with Large Circular Piles,” Proceedings for the 2000 Joint Conference on Water Resources Engineering and Water Resources Planning and Management Conference, Minneapolis, MN, July 30-August 2, 2000.

Sheppard, D. Max, Mufeed Odeh, Athanasios Pritsivelis, and Tom Glasser. (2000) “Clearwater Local Scour Experiments in a Large Flume.” Proceedings for the 2000 Joint Conference on Water Resources Engineering and Water Resources Planning and Management Conference, Minneapolis, MN, July 30-August 2, 2000.

Sheppard, D. Max. (2000) “A Method for Scaling Local Sediment Scour Depths from Model to Prototype,” Proceedings for the 2000 Joint Conference on Water Resources Engineering and Water Resources Planning and Management Conference, Minneapolis, MN, July 30-August 2, 2000.

Sheppard, D. Max. (2000) “Physical Model Local Scour Studies of the Woodrow Wilson Bridge Piers,” Proceedings for the 2000 Joint Conference on Water Resources

Engineering and Water Resources Planning and Management Conference, Minneapolis, MN, July 30-August 2, 2000.

Sheppard, D. Max, and Sterling Jones. (2000) "Local Scour at Complex Piers," Proceedings for the 2000 Joint Conference on Water Resources Engineering and Water Resources Planning and Management Conference, Minneapolis, MN, July 30-August 2, 2000.

Sheppard, D.M., Zhao, G., and Ontowirjo, B. (1999) "Local Scour Near Single Piles in Steady Currents." Stream Stability and Scour At Highway Bridges, Compendium of Papers, *ASCE Water Resources Engineering Conferences 1991 to 1998,* Edited by E.V. Richardson and P.F. Lagasse.

Sheppard, D.M., and Jones, J.S. (1998) "Scour at complex pier geometries." *Compendium of scour papers from ASCE Water Resources Conferences*, Eds. E.V. Richardson and P.F. Lagasse, ASCE, New York.

Sheppard, D.M. (1997) "Conditions of maximum local scour." Report No. UFL/COEL-97/006, Coastal and Oceanographic Engineering Department, University of Florida, Gainesville, FL.

Sheppard, D.M., Zhao, G., and Ontowirjo, B. (1995) "Local scour near single piles in steady currents." *ASCE Conference Proceedings: The First International Conference on Water Resources Engineering*, San Antonio, TX.

Sheppard, D.M., and Ontowirjo, B. (1994) "A local sediment scour prediction equation for circular piles." Report No. UFL/COEL-TR/101, Coastal and Oceanographic Engineering Department, University of Florida, Gainesville, FL.

Shields, A. (1936) "Anwendung der Aehnlichkeitsmechanik und der turbulenz forschung auf die geschiebebewegung." Mitt. Preuss. Versuchanstalt Wesserbau Schiffbau, Berlin, Germany.

Sleath, J.F. (1984) *Sea Bed Mechanics*. John Wiley & Sons, New York.

Snamenskaya, N.S. (1969) "Morphological principle of modelling of river-bed processes." *Science Council of Japan*, vol. 5-1, Tokyo, Japan.

Tison, L.J. (1940) "Erosion autour des piles de ponts en riviere." *Annales des Travaux Publics de Belgique*, 41(6), 813-817.

Tsubaki, T. and Shinohara, K. (1959) "On the Characteristics of Sand Waves Formed upon the Beds of Open Channels and Rivers." Reports of research Institute for Applied Mechanics, Vol. VII, No. 25

U.S. Department of Transportation (1995) "Evaluating scour at bridges." Hydraulic Engineering Circular No. 18, Pub. No. FHWA-IP-90-017. FHWA, Washington DC.

U.S. Army Corps of Engineers. 2002. Coastal Engineering Manual. Engineer Manual 1110-2-1100, U.S. Army Corps of Engineers, Washington, D.C. (in 6 volumes).

van Rijn, Leo C. (1993) "Principles of Sediment Transport in Rivers, Estuaries and Coastal Seas," Aqua Publications, PO Box 9896, 1006 AN Amsterdam, The Netherlands.

Venkatadri, C. (1965) "Scour around bridge piers and abutments." *Irrigation Power*, January, 35-42.

White W. R. (1973) "Scour around bridge piers in steep streams." *Proc. 16th IAHR Congress*, Vol. 2, Sao Paulo, Brazil, 279-284.